

UNIVERSIDAD DE LA LAGUNA

DOCTORAL THESIS PROJECT

Optoelectrical Dynamics of Ion Channels and Subcellular Calcium Nanodomains

Author:
Roger Gimeno Llobet

Supervisor:
Teresa Giráldez Fernández

Co-Supervisor:
Diego Álvarez de la Rosa

*A thesis submitted in fulfillment of the requirements
for the degree of Doctor*

in the

Dept. Biomedical Sciences (section Physiology)
Faculty of Medicine

October 24, 2018

Este documento incorpora firma electrónica, y es copia auténtica de un documento electrónico archivado por la ULL según la Ley 39/2015.
Su autenticidad puede ser contrastada en la siguiente dirección <https://sede.ull.es/validacion/>

Identificador del documento: 1627512

Código de verificación: kOIBgUMu

Firmado por: Roger Gimeno Llobet UNIVERSIDAD DE LA LAGUNA	Fecha: 25/10/2018 11:00:30
Diego Álvarez de la Rosa Rodríguez UNIVERSIDAD DE LA LAGUNA	25/10/2018 11:52:58
Teresa Giráldez Fernández UNIVERSIDAD DE LA LAGUNA	25/10/2018 11:54:04
Ernesto Pereda de Pablo UNIVERSIDAD DE LA LAGUNA	29/10/2018 13:01:03



Este documento incorpora firma electrónica, y es copia auténtica de un documento electrónico archivado por la ULL según la Ley 39/2015.
Su autenticidad puede ser contrastada en la siguiente dirección <https://sede.ull.es/validacion/>

Identificador del documento: 1627512

Código de verificación: kOIBgUMu

Firmado por:	Fecha:
Roger Gimeno Llobet UNIVERSIDAD DE LA LAGUNA	25/10/2018 11:00:30
Diego Álvarez de la Rosa Rodríguez UNIVERSIDAD DE LA LAGUNA	25/10/2018 11:52:58
Teresa Giráldez Fernández UNIVERSIDAD DE LA LAGUNA	25/10/2018 11:54:04
Ernesto Pereda de Pablo UNIVERSIDAD DE LA LAGUNA	29/10/2018 13:01:03

Declaration of Authorship

Teresa Giráldez (PhD) and Diego Álvarez de la Rosa (PhD)
Dept. Biomedical Sciences (section Physiology)
Faculty of Medicine, University of La Laguna

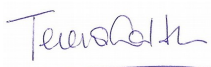
Certifican:

Que *Roger Gimeno Llobet* ha realizado bajo su dirección la tesis titulada: "Opto-electrical Dynamics of Ion Channels and Subcellular Calcium Nanodomains", que presenta para optar al grado de Doctor por la Universidad de La Laguna.

Para que conste y surta los efectos oportunos , firmamos el presente certificado en La Laguna a 21 de octubre de 2018.

Signed:
Dra. Teresa Giráldez Fernández

Signed:
Dr. Diego Álvarez de la Rosa



Este documento incorpora firma electrónica, y es copia auténtica de un documento electrónico archivado por la ULL según la Ley 39/2015.
Su autenticidad puede ser contrastada en la siguiente dirección <https://sede.ull.es/validacion/>

Identificador del documento: 1627512

Código de verificación: KOIBgUMu

Firmado por: Roger Gimeno Llobet UNIVERSIDAD DE LA LAGUNA	Fecha: 25/10/2018 11:00:30
Diego Álvarez de la Rosa Rodríguez UNIVERSIDAD DE LA LAGUNA	25/10/2018 11:52:58
Teresa Giráldez Fernández UNIVERSIDAD DE LA LAGUNA	25/10/2018 11:54:04
Ernesto Pereda de Pablo UNIVERSIDAD DE LA LAGUNA	29/10/2018 13:01:03



Este documento incorpora firma electrónica, y es copia auténtica de un documento electrónico archivado por la ULL según la Ley 39/2015.
Su autenticidad puede ser contrastada en la siguiente dirección <https://sede.ull.es/validacion/>

Identificador del documento: 1627512

Código de verificación: kOIBgUMu

Firmado por:	Fecha:
Roger Gimeno Llobet UNIVERSIDAD DE LA LAGUNA	25/10/2018 11:00:30
Diego Álvarez de la Rosa Rodríguez UNIVERSIDAD DE LA LAGUNA	25/10/2018 11:52:58
Teresa Giráldez Fernández UNIVERSIDAD DE LA LAGUNA	25/10/2018 11:54:04
Ernesto Pereda de Pablo UNIVERSIDAD DE LA LAGUNA	29/10/2018 13:01:03

UNIVERSIDAD DE LA LAGUNA

Abstract

Faculty of Medicine
Dept. Biomedical Sciences (section Physiology)

Doctor of Philosophy

Optoelectrical Dynamics of Ion Channels and Subcellular Calcium Nanodomains

by Roger GIMENO LLOBET

Neuronal networks are dynamic, with molecular components diffusing and rearranging in specific cellular subdomains on timescales from milliseconds to hours. Among all intracellular messengers, Ca^{2+} ions generate versatile intracellular signals that control key functions in all types of neurons. Countless investigations have used highly invasive electrophysiology or non-dynamic biochemical approaches to study synapses and networks. Optogenetic approaches, combined with imaging techniques, are revolutionary tools to excite specific live cells and detect the activity of signaling molecules in populations of neurons. However, refinement of current optical methods is needed, due to the lack of molecular or spatial specificity. This refinement is particularly important for imaging Ca^{2+} in neurons, since Ca^{2+} signals exert their highly specific functions in well-defined cellular subcompartments. Coupling of Ca^{2+} signaling to membrane voltage occurs in Ca^{2+} nanodomains where Ca^{2+} influx through voltage-gated Ca^{2+} channels is located within 20-50 nm of BK K^+ channels. Upon Ca^{2+} entry, BK open in response to additive effects of Ca^{2+} and voltage to limit neuronal excitability. Nevertheless, much remains to be known about this process, since currently no sensors located specifically to these regions are available. Developing probes that provide bright readouts *in vivo* combined with extremely fast and high spatial resolution imaging systems is crucial to progress towards our knowledge about neuronal networking.

Este documento incorpora firma electrónica, y es copia auténtica de un documento electrónico archivado por la ULL según la Ley 39/2015.
Su autenticidad puede ser contrastada en la siguiente dirección <https://sede.ull.es/validacion/>

Identificador del documento: 1627512

Código de verificación: kOIBgUMu

Firmado por:	Fecha:
Roger Gimeno Llobet UNIVERSIDAD DE LA LAGUNA	25/10/2018 11:00:30
Diego Álvarez de la Rosa Rodríguez UNIVERSIDAD DE LA LAGUNA	25/10/2018 11:52:58
Teresa Giráldez Fernández UNIVERSIDAD DE LA LAGUNA	25/10/2018 11:54:04
Ernesto Pereda de Pablo UNIVERSIDAD DE LA LAGUNA	29/10/2018 13:01:03



Este documento incorpora firma electrónica, y es copia auténtica de un documento electrónico archivado por la ULL según la Ley 39/2015.
Su autenticidad puede ser contrastada en la siguiente dirección <https://sede.ull.es/validacion/>

Identificador del documento: 1627512

Código de verificación: kOIBgUMu

Firmado por:	Fecha:
Roger Gimeno Llobet UNIVERSIDAD DE LA LAGUNA	25/10/2018 11:00:30
Diego Álvarez de la Rosa Rodríguez UNIVERSIDAD DE LA LAGUNA	25/10/2018 11:52:58
Teresa Giráldez Fernández UNIVERSIDAD DE LA LAGUNA	25/10/2018 11:54:04
Ernesto Pereda de Pablo UNIVERSIDAD DE LA LAGUNA	29/10/2018 13:01:03

Acknowledgements

En primer lugar quiero agradecer a mi directora y tutora la Dra. Teresa Giráldez Fernández y a mi co-director el Dr. Diego Álvarez de la Rosa todo el apoyo, paciencia y buenos consejos que he recibido durante mi tesis. El entusiasmo por su trabajo es contagioso.

Agradecer también el apoyo de mis compañeros en el laboratorio. A la Dra. Rafaela González por su paciencia en mis primeros pasos en un laboratorio de biología molecular. Al Dr. Alejandro Cerrada, por su apoyo y su aportación a esta tesis con el desarrollo del sensor BK667cpG y los experimentos de superresolución. Al Dr. David Bartolomé, por su ayuda y aportaciones en los experimentos de electrofisiología de *whole cell*, *patch-clamp fluorometry* y con la cpGFP soluble. Al Dr. Aravind Kshatri, por sus aportaciones en experimentos de electrofisiología. Al doctorando Alberto Jesús González, por sus aportaciones en los experimentos de *patch-clamp fluorometry*. A la Dra. Belinda Rivero, por su ayuda en la generación de la construcción cpGFP soluble, los mutantes del poro y la optimización de los *linkers* BK-cpGFP. Al Dr. Fernando Lahoz y a la estudiante de máster Marta Urgellés, por su aportación en los experimentos de tiempo de vida de las construcciones del *gating ring*. Al Dr Andrew Plested (FMP, Berlín), por facilitarnos el plásmido con la cpGFP.

A mi tribunal de seguimiento de tesis, formado por los doctores Tomás Gonzáles, Ángel Acebes, Pedro Barroso y Leticia González. Gracias por todos los comentarios y apoyo recibido cada año.

Finalmente a mi familia, por todo su apoyo. A mi pareja, Macu, por el esfuerzo y apoyo incondicional. Y a Gara, que aunque tus gritos no ayudaban, tenerte aquí es una alegría diaria.

A la meva mare...

Este documento incorpora firma electrónica, y es copia auténtica de un documento electrónico archivado por la ULL según la Ley 39/2015.
Su autenticidad puede ser contrastada en la siguiente dirección <https://sede.ull.es/validacion/>

Identificador del documento: 1627512

Código de verificación: KOIBgUMu

Firmado por: Roger Gimeno Llobet UNIVERSIDAD DE LA LAGUNA	Fecha: 25/10/2018 11:00:30
Diego Álvarez de la Rosa Rodríguez UNIVERSIDAD DE LA LAGUNA	25/10/2018 11:52:58
Teresa Giráldez Fernández UNIVERSIDAD DE LA LAGUNA	25/10/2018 11:54:04
Ernesto Pereda de Pablo UNIVERSIDAD DE LA LAGUNA	29/10/2018 13:01:03



Este documento incorpora firma electrónica, y es copia auténtica de un documento electrónico archivado por la ULL según la Ley 39/2015.
Su autenticidad puede ser contrastada en la siguiente dirección <https://sede.ull.es/validacion/>

Identificador del documento: 1627512

Código de verificación: kOIBgUMu

Firmado por:	Fecha:
Roger Gimeno Llobet UNIVERSIDAD DE LA LAGUNA	25/10/2018 11:00:30
Diego Álvarez de la Rosa Rodríguez UNIVERSIDAD DE LA LAGUNA	25/10/2018 11:52:58
Teresa Giráldez Fernández UNIVERSIDAD DE LA LAGUNA	25/10/2018 11:54:04
Ernesto Pereda de Pablo UNIVERSIDAD DE LA LAGUNA	29/10/2018 13:01:03

Contents

Abstract	v
Acknowledgements	vii
1 Introduction	1
1.1 Large conductance voltage- and calcium- activated potassium channels (BK; KCa1.1; slo1)	1
1.2 Role of BK channels in neuronal function	2
1.3 Ca ²⁺ homeostasis	4
1.4 Physiological activation of BK in Ca ²⁺ nanodomains	4
1.5 Knowledge gap	6
1.6 Fluorescence	6
1.6.1 Jablonsky diagram	7
1.6.2 Förster Resonance Energy Transfer (FRET)	8
1.6.3 Fluorescence Lifetime	9
1.6.4 Fluorescence Proteins	11
1.7 Ca ²⁺ sensors	11
1.7.1 Chemical calcium indicators	13
1.7.2 Genetically encoded calcium indicators	14
FRET-based GECIs	14
Single fluorophore-based GECIs	15
Aequorin	18
1.8 BK-FRET as Ca ²⁺ sensors	19
1.8.1 Optimization of BK-FRET for Ca ²⁺ sensing in nanodomains	19
1.8.2 Patch-clamp fluorometry studies in <i>Xenopus laevis</i> oocytes	19
1.8.3 Limitations	19
2 Hypothesis and Objectives	21
2.1 Hypothesis	21
2.2 Principal objective	21
2.3 Specific objectives	21
2.3.1 Generation	21
2.3.2 Characterization	21
2.3.3 Optimization	21
2.3.4 Validation	22
2.3.5 Extension	22
3 Materials and Methods	23
3.1 Cell culture and transfection	23
3.2 Molecular biology	23
3.2.1 BK-cpGFP subcloning	23
3.2.2 Generation of BK Ca ²⁺ mutants	24
3.2.3 Generation of BK Pore mutants	25

Este documento incorpora firma electrónica, y es copia auténtica de un documento electrónico archivado por la ULL según la Ley 39/2015.
 Su autenticidad puede ser contrastada en la siguiente dirección <https://sede.ull.es/validacion/>

Identificador del documento: 1627512

Código de verificación: KOIBgUMu

Firmado por: Roger Gimeno Llobet UNIVERSIDAD DE LA LAGUNA	Fecha: 25/10/2018 11:00:30
Diego Álvarez de la Rosa Rodríguez UNIVERSIDAD DE LA LAGUNA	25/10/2018 11:52:58
Teresa Giráldez Fernández UNIVERSIDAD DE LA LAGUNA	25/10/2018 11:54:04
Ernesto Pereda de Pablo UNIVERSIDAD DE LA LAGUNA	29/10/2018 13:01:03

x

3.2.4	Generation of BK isolated gating ring constructs	25
3.3	BK-CpGFP characterization	26
3.4	Ionomycin-mediated Ca ²⁺ loading	28
	Imaging	28
	Data analysis	28
3.5	Ca ²⁺ - and pH-titrations	29
	Generation of microsomes	29
	Imaging	29
	Ca ²⁺ titrations	29
	pH titrations	29
	Data analysis	30
3.6	Patch-clamp fluorometry	30
3.7	BK-cpGFP linker optimization	31
	NSP optimization	31
	VVC optimization	31
3.8	Whole cell patch-clamp and fluorometry	32
3.9	Direct stochastic optical reconstruction microscopy	33
	Sample preparation	33
	Imaging (dSTORM)	33
	dSTORM data analysis	34
3.10	Isolated gating ring	34
	FRET measurements using the acceptor photobleaching technique	34
	Fluorescence lifetimes: Time-Correlated Single Photon Counting (TCSPC)	34
3.11	BK cryo-EM structure analysis	35
4	Results	37
4.1	BK-cpGFP constructs emission spectra and channel function	37
4.2	Effect of ionomycin-mediated cell Ca ²⁺ loading on BK-cpGFP emission	39
4.3	BK Ca ²⁺ -binding mutants	42
4.4	BK-cpGFP: Ca ²⁺ affinity and pH dependence	44
4.5	Patch-clamp fluorometry (PCF) recordings of BK-cpGFP signals	45
4.6	Generation of BK-cpGFP pore mutants	46
4.7	Whole cell electrophysiology and fluorimetric recordings	48
4.8	Sensitivity of BK-cpG sensors to different cellular Ca ²⁺ sources	48
4.9	Expression of BK-cpG sensors in Ca ²⁺ nanodomains	51
	4.9.1 Development of new scripts for dSTORM data analysis	51
	4.9.2 Controls for analysis scripts	58
	control1: Simple configuration	58
	control2: Rotation of a channel	59
	4.9.3 BK860cpG construct colocalize with Cav2.1 channels in heterologous expression systems	59
4.10	Distance analysis for generation of additional BK-cpGFP Ca ²⁺ sensors	62
4.11	The gating ring as a transferable Ca ²⁺ -sensitive molecular module	63
	4.11.1 FRET efficiency - Acceptor Photobleaching studies of isolated fluorescent gating rings	64
	4.11.2 Lifetime measurement: Time-Correlated Single Photon Counting (TCSPC)	68
5	Discussion	71

Este documento incorpora firma electrónica, y es copia auténtica de un documento electrónico archivado por la ULL según la Ley 39/2015.
 Su autenticidad puede ser contrastada en la siguiente dirección <https://sede.ull.es/validacion/>

Identificador del documento: 1627512

Código de verificación: kOIBgUMu

Firmado por: Roger Gimeno Llobet UNIVERSIDAD DE LA LAGUNA	Fecha: 25/10/2018 11:00:30
Diego Álvarez de la Rosa Rodríguez UNIVERSIDAD DE LA LAGUNA	25/10/2018 11:52:58
Teresa Giráldez Fernández UNIVERSIDAD DE LA LAGUNA	25/10/2018 11:54:04
Ernesto Pereda de Pablo UNIVERSIDAD DE LA LAGUNA	29/10/2018 13:01:03

	xi
6 Conclusions	81
A NND program code	83
B Clusters program code	87
Bibliography	93

Este documento incorpora firma electrónica, y es copia auténtica de un documento electrónico archivado por la ULL según la Ley 39/2015.
Su autenticidad puede ser contrastada en la siguiente dirección <https://sede.ull.es/validacion/>

Identificador del documento: 1627512

Código de verificación: kOIBgUMu

Firmado por: Roger Gimeno Llobet UNIVERSIDAD DE LA LAGUNA	Fecha: 25/10/2018 11:00:30
Diego Álvarez de la Rosa Rodríguez UNIVERSIDAD DE LA LAGUNA	25/10/2018 11:52:58
Teresa Giráldez Fernández UNIVERSIDAD DE LA LAGUNA	25/10/2018 11:54:04
Ernesto Pereda de Pablo UNIVERSIDAD DE LA LAGUNA	29/10/2018 13:01:03



Este documento incorpora firma electrónica, y es copia auténtica de un documento electrónico archivado por la ULL según la Ley 39/2015.
Su autenticidad puede ser contrastada en la siguiente dirección <https://sede.ull.es/validacion/>

Identificador del documento: 1627512

Código de verificación: kOIBgUMu

Firmado por:	Fecha:
Roger Gimeno Llobet UNIVERSIDAD DE LA LAGUNA	25/10/2018 11:00:30
Diego Álvarez de la Rosa Rodríguez UNIVERSIDAD DE LA LAGUNA	25/10/2018 11:52:58
Teresa Giráldez Fernández UNIVERSIDAD DE LA LAGUNA	25/10/2018 11:54:04
Ernesto Pereda de Pablo UNIVERSIDAD DE LA LAGUNA	29/10/2018 13:01:03

List of Figures

1.1	BK channel	2
1.2	Neuron and calcium homeostasis	3
1.3	Calcium Nanodomains	5
1.4	Quinine	7
1.5	Jablonsky diagram	8
1.6	FRET	9
1.7	Jablonsky diagram FRET	10
1.8	GFP	11
1.9	CCI	13
1.10	CCI: Fura-2	14
1.11	GECIs	16
1.12	Aequorin	18
1.13	BK-FRET	20
3.1	BK-cpG sequence	24
3.2	Multi-site directed mutagenesis	25
3.3	Gating ring sequences	26
3.4	pH calibration	30
3.5	BK-cpGFP linker optimization	32
4.1	BK-cpG spectra and channel function	38
4.2	Ionomycin-mediated experiments	40
4.3	Soluble cpGFP control	41
4.4	Ca ²⁺ -binding mutants	43
4.5	Ca ²⁺ - and pH- dependence	45
4.6	PCF	46
4.7	Pore mutants	47
4.8	Whole cell experiments	49
4.9	Carbacholl experiments	50
4.10	STORM concepts	52
4.11	Flowchart NND	53
4.12	Flowchart Clusters	55
4.13	Scheme Clusters script 1	56
4.14	Scheme Clusters script 2	57
4.15	Control 1 scripts	58
4.16	Control 2 scripts	60
4.17	STORM data from BK-cpG and Cav	61
4.18	BK965cpG: Structure analysis	63
4.19	Gating ring FRET AB	65
4.20	Gating ring FRET AB with ionomycin	67
4.21	Gating ring fluorescence lifetimes	69
A.1	Nearest Neighbor Distance program (page1/2)	84

Este documento incorpora firma electrónica, y es copia auténtica de un documento electrónico archivado por la ULL según la Ley 39/2015.
 Su autenticidad puede ser contrastada en la siguiente dirección <https://sede.ull.es/validacion/>

Identificador del documento: 1627512

Código de verificación: KOIBgUMu

Firmado por: Roger Gimeno Llobet UNIVERSIDAD DE LA LAGUNA	Fecha: 25/10/2018 11:00:30
Diego Álvarez de la Rosa Rodríguez UNIVERSIDAD DE LA LAGUNA	25/10/2018 11:52:58
Teresa Giráldez Fernández UNIVERSIDAD DE LA LAGUNA	25/10/2018 11:54:04
Ernesto Pereda de Pablo UNIVERSIDAD DE LA LAGUNA	29/10/2018 13:01:03

xiv

A.2 Nearest Neighbor Distance program (page2/2)	85
B.1 Clusters program (page1/4)	88
B.2 Clusters program (page2/4)	89
B.3 Clusters program (page3/4)	90
B.4 Clusters program (page4/4)	91

Este documento incorpora firma electrónica, y es copia auténtica de un documento electrónico archivado por la ULL según la Ley 39/2015.
Su autenticidad puede ser contrastada en la siguiente dirección <https://sede.ull.es/validacion/>

Identificador del documento: 1627512

Código de verificación: kOIBgUMu

Firmado por: Roger Gimeno Llobet UNIVERSIDAD DE LA LAGUNA	Fecha: 25/10/2018 11:00:30
Diego Álvarez de la Rosa Rodríguez UNIVERSIDAD DE LA LAGUNA	25/10/2018 11:52:58
Teresa Giráldez Fernández UNIVERSIDAD DE LA LAGUNA	25/10/2018 11:54:04
Ernesto Pereda de Pablo UNIVERSIDAD DE LA LAGUNA	29/10/2018 13:01:03

List of Tables

3.1	Oligonucleotides used in the study.	27
3.2	Saline and media used in the study.	28
4.1	Characterization of the fluorescence variation in response to ionomycin of the constructs used in this study. Data is mean \pm SEM.	41
4.2	Characterization of the fluorescence variation in response to ionomycin of the Ca ²⁺ mutant constructs of BK667cpG and BK860cpG. Data is mean \pm SEM.	44
4.3	<i>In vitro</i> characteristics of constructs BK667cpG, BK860cpG and Lck-GCaMP3.	45
4.4	$\Delta F/F$ and Ratio between ionomycin and carbachol peaks. Data is mean \pm SEM.	51
4.5	Gating ring constructs of fluorescent BK-FRET pairs.	64
4.6	FRET efficiencies (in %) of gating ring constructs and negative control C/Y applying Acceptor Photobleaching technique before and after (IM) addition of ionomycin. n= 8.	68
4.7	Multi-exponential analysis of fluorescence intensity decays.	69

Este documento incorpora firma electrónica, y es copia auténtica de un documento electrónico archivado por la ULL según la Ley 39/2015.
 Su autenticidad puede ser contrastada en la siguiente dirección <https://sede.ull.es/validacion/>

Identificador del documento: 1627512

Código de verificación: KOIBgUMu

Firmado por: Roger Gimeno Llobet UNIVERSIDAD DE LA LAGUNA	Fecha: 25/10/2018 11:00:30
Diego Álvarez de la Rosa Rodríguez UNIVERSIDAD DE LA LAGUNA	25/10/2018 11:52:58
Teresa Giráldez Fernández UNIVERSIDAD DE LA LAGUNA	25/10/2018 11:54:04
Ernesto Pereda de Pablo UNIVERSIDAD DE LA LAGUNA	29/10/2018 13:01:03



Este documento incorpora firma electrónica, y es copia auténtica de un documento electrónico archivado por la ULL según la Ley 39/2015.
Su autenticidad puede ser contrastada en la siguiente dirección <https://sede.ull.es/validacion/>

Identificador del documento: 1627512

Código de verificación: kOIBgUMu

Firmado por:	Fecha:
Roger Gimeno Llobet UNIVERSIDAD DE LA LAGUNA	25/10/2018 11:00:30
Diego Álvarez de la Rosa Rodríguez UNIVERSIDAD DE LA LAGUNA	25/10/2018 11:52:58
Teresa Giráldez Fernández UNIVERSIDAD DE LA LAGUNA	25/10/2018 11:54:04
Ernesto Pereda de Pablo UNIVERSIDAD DE LA LAGUNA	29/10/2018 13:01:03

List of Abbreviations

VSD	Voltage Sensing Domain
PGD	Pore Gate Domain
RCK	Regulator of Conductance for K ⁺
GFP	Green Fluorescent Protein
cpGFP	circularly permuted Green Fluorescent Protein
CCI	Chemical Calcium Indicators
GECI	Genetically Encoded Calcium Indicators
PCF	Patch-Clamp Fluorometry
[Ca ²⁺]	Ca ²⁺ concentration
SSM	Standard Saline Medium
dSTORM	direct Stochastic Optical Reconstruction Microscopy
NND	Nearest Neighbor Distance
DBSCAN	Density-Based Spatial Clustering of Applications with Noise
TCSPC	Time-Correlated Single Photon Counting

Este documento incorpora firma electrónica, y es copia auténtica de un documento electrónico archivado por la ULL según la Ley 39/2015.
Su autenticidad puede ser contrastada en la siguiente dirección <https://sede.ull.es/validacion/>

Identificador del documento: 1627512

Código de verificación: KOIBgUMu

Firmado por: Roger Gimeno Llobet UNIVERSIDAD DE LA LAGUNA	Fecha: 25/10/2018 11:00:30
Diego Álvarez de la Rosa Rodríguez UNIVERSIDAD DE LA LAGUNA	25/10/2018 11:52:58
Teresa Giráldez Fernández UNIVERSIDAD DE LA LAGUNA	25/10/2018 11:54:04
Ernesto Pereda de Pablo UNIVERSIDAD DE LA LAGUNA	29/10/2018 13:01:03



Este documento incorpora firma electrónica, y es copia auténtica de un documento electrónico archivado por la ULL según la Ley 39/2015.
Su autenticidad puede ser contrastada en la siguiente dirección <https://sede.ull.es/validacion/>

Identificador del documento: 1627512

Código de verificación: kOIBgUMu

Firmado por:	Fecha:
Roger Gimeno Llobet UNIVERSIDAD DE LA LAGUNA	25/10/2018 11:00:30
Diego Álvarez de la Rosa Rodríguez UNIVERSIDAD DE LA LAGUNA	25/10/2018 11:52:58
Teresa Giráldez Fernández UNIVERSIDAD DE LA LAGUNA	25/10/2018 11:54:04
Ernesto Pereda de Pablo UNIVERSIDAD DE LA LAGUNA	29/10/2018 13:01:03

Chapter 1

Introduction

1.1 Large conductance voltage- and calcium- activated potassium channels (BK; KCa1.1; slo1)

Large-conductance voltage- and Ca^{2+} -dependent K^+ (BK) channels are homotetrameric proteins characterized by a large unitary conductance for K^+ and a unique sensitivity to both membrane depolarization and intracellular Ca^{2+} levels. BK channels (from Big K^+), also known as maxi-K (Latorre and Miller, 1983), exhibit the highest known conductance for K^+ , of about 300 pS, close to the diffusion limit (Contreras et al., 2013). The large conductance does not preclude a high K^+ selectivity. This channel is also known as Slo1, because is formed by four α -subunits encoded by the slo1 gene (from slowpoke, the gene coding for BK in *Drosophila*). Each pore-forming alpha subunit (Fig. 1.1A) is composed of three main structural domains: the voltage sensing domain (VSD), the pore-gate domain (PGD) and the cytosolic domain (Cui, Yang, and Lee, 2009) (Fig. 1.1B). The voltage-sensing domain is formed by transmembrane domains S1 to S4. The S4 helix has positively charged residues that drive the segment towards the extracellular side upon membrane depolarization (Contreras et al., 2013). The pore gate domain alters its configuration between open and closed states in order to control the flux of K^+ ions. Finally, the cytosolic domain, called the “gating ring”, senses Ca^{2+} ions through specific Ca^{2+} binding sites. This domain is formed by two non-identical regulators of conductance for K^+ domains (RCK1 and RCK2; (Giraldez and Rothberg, 2017). A high affinity Ca^{2+} binding site, dubbed the “ Ca^{2+} bowl”, is located in the RCK2 domain, and comprises a sequence of five aspartic acid residues. With a series of different mutations, some authors inferred the existence of another Ca^{2+} binding site, located at the RCK1 (reviewed in (Latorre et al., 2017)). Additionally the BK has an extra transmembrane segment, S0, that is necessary in the modulation of channel properties by association of auxiliary β -subunits (Contreras et al., 2013).

Activation of BK channels results from the complex synergy between the Ca^{2+} and voltage sensing domains. The open probability of the channel is modulated allosterically by two stimuli: intracellular Ca^{2+} concentration and membrane potential. Ca^{2+} sensing and membrane potential sensing are independent processes. In other words, the channel can be opened both by the effect of Ca^{2+} at a fixed voltage or by changes of membrane voltage in the absence of Ca^{2+} . It is the combination of both whar enhances the open probability. One of the most successful models to describe this behavior is the Horrigan and Aldrich (HA) kinetic model (Horrigan and Aldrich, 2002). Binding of Ca^{2+} ions in the cytosolic domain or the sensing of voltage by depolarization of the membrane in the voltage sensing domain generate

Este documento incorpora firma electrónica, y es copia auténtica de un documento electrónico archivado por la ULL según la Ley 39/2015.
Su autenticidad puede ser contrastada en la siguiente dirección <https://sede.ull.es/validacion/>

Identificador del documento: 1627512

Código de verificación: kOIBgUMu

Firmado por: Roger Gimeno Llobet UNIVERSIDAD DE LA LAGUNA	Fecha: 25/10/2018 11:00:30
Diego Álvarez de la Rosa Rodríguez UNIVERSIDAD DE LA LAGUNA	25/10/2018 11:52:58
Teresa Giraldez Fernández UNIVERSIDAD DE LA LAGUNA	25/10/2018 11:54:04
Ernesto Pereda de Pablo UNIVERSIDAD DE LA LAGUNA	29/10/2018 13:01:03

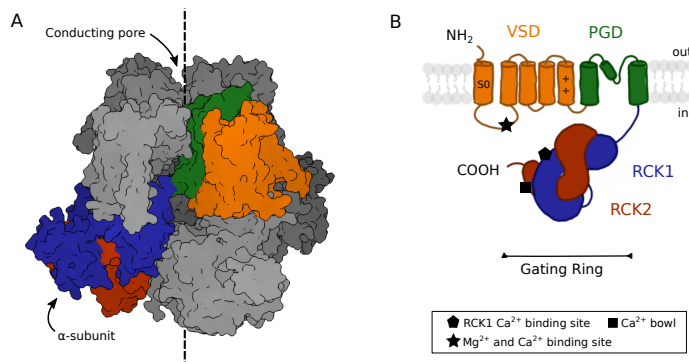


Figure 1.1: BK channel structure. A) BK channel structure (5TJI, (Hite, Tao, and MacKinnon, 2017)) showing the homotetramer of α -subunits (one α -subunit is code-colored). B) Schematic representation of the BK α -subunit. Three main structural domains relative to its function are identified: the voltage sensing domain (VSD), the pore gate domain (PGD) and the cytosolic domain, composed by to regulators of conductance for K^+ (RCK1 and RCK2). The cytosolic domain, called the “gating ring”, senses Ca^{2+} ions, through specific Ca^{2+} binding sites (black shapes).

conformational changes in the protein that are allosterically coupled to the pore gate domain leading to the opening of the gate.

1.2 Role of BK channels in neuronal function

Neuronal networks are dynamical structures, driven by a complex orchestrated activation of molecular components. Understanding the interplay between such components is a fundamental topic in neuroscience. Among all intracellular messengers, Ca^{2+} ions generate versatile intracellular signals that control key functions in all types of neurons. For example, in presynaptic terminals, Ca^{2+} influx triggers exocytosis of neurotransmitter-containing synaptic vesicles. Postsynaptically, a transient rise of the Ca^{2+} level in dendritic spines is essential for the induction of activity-dependent synaptic plasticity. In this context, BK channels couples to the Ca^{2+} signal, taking an essential role in a wide spectrum of processes regarding neuronal activity (Contet et al., 2016).

BK channels are implicated in a large number of processes in the central nervous system (Bock and Stuart, 2016; Contet et al., 2016; Kshatri, Gonzalez-Hernandez, and Giraldez, 2018) (Fig. 1.2A). One fundamental role of BK channels in the nervous system is its implication in neuronal excitability. BK channels located at the soma of variety of neuronal cell types are key players in the repolarization after action potentials (AP) (Bock and Stuart, 2016). In this sense, BK can shape the AP and modify the firing rate. During the AP, local increases of Ca^{2+} concentration caused by the activation of voltage-dependent Ca^{2+} channel (Cav) in combination with membrane depolarization, induce BK activation and outflow of potassium ions. This constitutes a negative feedback mechanism that rapidly hyperpolarizes the membrane. Furthermore, BK channels located at the presynaptic terminals are implicated in the regulation of neurotransmitter release (Contet et al., 2016). In the majority of cases the influence of BK channels in the synaptic transmission is inhibitory (Contet et

Este documento incorpora firma electrónica, y es copia auténtica de un documento electrónico archivado por la ULL según la Ley 39/2015.
 Su autenticidad puede ser contrastada en la siguiente dirección <https://sede.ull.es/validacion/>

Identificador del documento: 1627512

Código de verificación: kOIBgUMu

Firmado por: Roger Gimeno Llobet UNIVERSIDAD DE LA LAGUNA	Fecha: 25/10/2018 11:00:30
Diego Álvarez de la Rosa Rodríguez UNIVERSIDAD DE LA LAGUNA	25/10/2018 11:52:58
Teresa Giráldez Fernández UNIVERSIDAD DE LA LAGUNA	25/10/2018 11:54:04
Ernesto Pereda de Pablo UNIVERSIDAD DE LA LAGUNA	29/10/2018 13:01:03

1.2. Role of BK channels in neuronal function

3

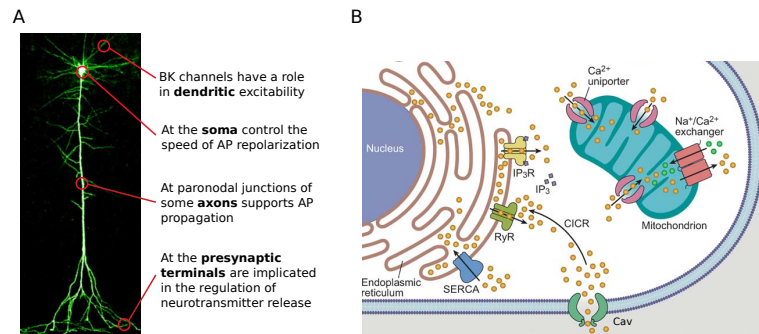


Figure 1.2: A) Role of BK in neuronal function. BK channels localize in the CNS and are implicated in a large number of processes. Coupled to Ca²⁺ effectors, BK channels regulates excitability in dendrites and AP propagation in the soma and along axons, and are involved in the regulation of neurotransmitter release in the presynaptic terminals (Image source: www.cifar.ca, credit: Blake Richards Lab). B) Ca²⁺ homeostasis. Ca²⁺ is increased within the cell from two different sources: extracellular Ca²⁺ mainly by Cav channels and internal reservoirs like endoplasmic reticulum (ER) or mitochondria. The main proteins involved in the efflux of Ca²⁺ ions from the ER are ryanodine receptors (RyRs) and inositol trisphosphate receptors (IP₃-Rs). Ca²⁺ returns to the ER via the sarco/endoplasmic reticulum Ca²⁺-ATPase (SERCA). The general pathways of Ca²⁺ involves the influx of Ca²⁺ by Cav channels that directly activates the Ca²⁺-induced Ca²⁺ release (CICR), the release of Ca²⁺ from internal reservoirs (mediated by RyRs), and IP₃-induced Ca²⁺ release (Figure adapted from ((Dong et al., 2006)).

al., 2016). APs arriving at the presynaptic terminal causes the influx of Ca²⁺ ions through Cav channels. Intracellular Ca²⁺ initiates the exocytosis of vesicles containing neurotransmitters and at the same time couples with membrane depolarization to activate nearby BK channels. Hyperpolarization caused by BK channels normally down-regulates neurotransmitter release. Moreover, Ca²⁺ entry mediated by Cav channels is in fact modulated by the shape of the AP, which, as mentioned previously, is in turn shaped by BK channels (Contet et al., 2016). BK channels have also been shown to have a role in dendritic excitability. In some neuronal types, BK channels are involved in the regulation of the magnitude and duration of dendritic spikes, repolarizing the membrane potential thus preventing the initiation of an AP caused by Ca²⁺ dendritic spikes depolarization (Contet et al., 2016). In murine myelinated cerebellar purkinje cells axons BK channels are localized at paranodal junctions, exhibiting a regulatory mechanism supporting AP propagation (Hirono et al., 2015). During circadian cycles, BK channels in neurons of the suprachiasmatic nucleus dynamically couples to different Ca²⁺ sources; during daytime L-type Ca²⁺ channels are the primary Ca²⁺ effectors, while at nighttime BK activation is due to Ca²⁺ release mediated by ryanodine receptors (RyR) (Whitt, McNally, and Meredith, 2017). Recent studies from our laboratory (Gomez *et al.*, unpublished data) and the Yan laboratory (Zhang et al., 2018) have shown that BK channels are functionally and spatially coupled to NMDA receptors (NMDARs) in different brain regions. In dentate gyrus granule cells, the influx of Ca²⁺ provided by postsynaptic NMDARs after glutamate binding induced BK activation and further regulation of synaptic transmission (Zhang et al., 2018). Work from our laboratory further demonstrates that NMDAR-BK complexes in somatosensory neurons are involved in control of neuronal plasticity (Gomez *et al.*, unpublished data).

Este documento incorpora firma electrónica, y es copia auténtica de un documento electrónico archivado por la ULL según la Ley 39/2015.
 Su autenticidad puede ser contrastada en la siguiente dirección <https://sede.ull.es/validacion/>

Identificador del documento: 1627512

Código de verificación: KOIBgUMu

Firmado por:	Fecha:
Roger Gimeno Llobet UNIVERSIDAD DE LA LAGUNA	25/10/2018 11:00:30
Diego Álvarez de la Rosa Rodríguez UNIVERSIDAD DE LA LAGUNA	25/10/2018 11:52:58
Teresa Giráldez Fernández UNIVERSIDAD DE LA LAGUNA	25/10/2018 11:54:04
Ernesto Pereda de Pablo UNIVERSIDAD DE LA LAGUNA	29/10/2018 13:01:03

1.3 Ca²⁺ homeostasis

Ca²⁺ ions are the ever-present second messengers in cells, involved in a variety of biological functions. Therefore, cytoplasmic Ca²⁺ levels are exquisitely regulated. In general terms, Ca²⁺ is increased within the cell from two sources: extracellular Ca²⁺ and internal reservoirs (i.e. endoplasmic reticulum (ER), sarcoplasmic reticulum (SR) or mitochondria) (Bose, Cieřlar-Pobuda, and Wiechec, 2015). The [Ca²⁺] in the extracellular side is typically 1.2 mM, and the [Ca²⁺] in the cytosol 100 nM. The ER is the main Ca²⁺ store, where its [Ca²⁺] is 500 μM. The main proteins involved in the efflux of Ca²⁺ ions from the ER are ryanodine receptors (RyRs) and inositol trisphosphate receptors (IP3-Rs). Additionally, there is a continue leak of Ca²⁺ ions through the so-called leak channel. Ca²⁺ returns to the ER via the sarco/endoplasmic reticulum Ca²⁺-ATPase (SERCA) (Gleichmann and Mattson, 2011). The spatiotemporal properties of Ca²⁺ signaling are tightly controlled by a myriad of proteins, where their intricate regulatory mechanisms and kinetics make regulation of Ca²⁺ homeostasis a very complex process (Gleichmann and Mattson, 2011). The entry of Ca²⁺ from the extracellular source involves Cav channels, Ca²⁺ release-activated channels (CRAC) and Store-operated Ca²⁺ channels (SOC). CRAC and SOC are channels located in the plasmatic membrane that respond to increased cytosolic [Ca²⁺] caused by depletion of internal stores (mainly ER). The activation of these channels permits the entrance of Ca²⁺ ions from the extracellular side allowing the refill of the internal stores and Ca²⁺ signalling. The general pathways of Ca²⁺ involves the influx of Ca²⁺ by Cav channels that directly activate the Ca²⁺-induced Ca²⁺ release (CICR), the release of Ca²⁺ from internal reservoirs (mediated by RyRs), and IP3-induced Ca²⁺ release (IICR). Some of the concepts are illustrated in Fig. 1.2B. The depletion of Ca²⁺ from the ER initiated by CICR and IICR is rapidly starts a mechanism the stromal interaction molecule 1 (STIM1), localized in the membrane of the ER, drives SOCE by SOC and CRAC activation (Sutherland, Pujic, and Goodhill, 2014; Gleichmann and Mattson, 2011). STIM1 utilizes Ca²⁺ release-activated Ca²⁺ channels1 (ORAI1) to induce the ER Ca²⁺ refilling. Furthermore, there is a another pathway besides STIM1-ORAI1 involving transient receptor potential cation (TRPC) channels, where STIM1 regulates the activation of certain TRPC channels (Hogan and Rao, 2015).

1.4 Physiological activation of BK in Ca²⁺ nanodomains

A key feature of intracellular Ca²⁺ signaling is its complex spatiotemporal organization. The time course, amplitude, and the local action site in well-defined cellular subcompartments, are essential determinants for the function of intracellular Ca²⁺ signals. BK channels interacts with the Ca²⁺ influx via voltage-dependent Ca²⁺ (Cav) channels, in spatially restricted domains called “Ca²⁺ nanodomains”.

Since the Ca²⁺ affinity of BK channels is relatively low (the intracellular concentration of Ca²⁺ required to activate the BK channel is 10 μM), the distance that separates BK channels from Ca²⁺ sources (Cav channels) needs to be minimum. [Ca²⁺] is inversely proportional of the distance between Ca²⁺ sources and Ca²⁺ targets (Eggermann et al., 2012), being the [Ca²⁺] in the center of the nanodomain 100 μM (Fakler and Adelman, 2008). Moreover, the BK response to an action potential (AP) needs to be fast (<1 ms), as rise/decays dynamics after Ca²⁺ influx are of the order of microseconds in a nanodomain (Fakler and Adelman, 2008). Coincidental membrane depolarization (by the incoming AP) and Ca²⁺ increase (from neighboring Cav) open BK channels, leading to K⁺ outflow and constituting a negative feedback on the

Este documento incorpora firma electrónica, y es copia auténtica de un documento electrónico archivado por la ULL según la Ley 39/2015.
 Su autenticidad puede ser contrastada en la siguiente dirección <https://sede.ull.es/validacion/>

Identificador del documento: 1627512

Código de verificación: kOIBgUMu

Firmado por:	Fecha:
Roger Gimeno Llobet UNIVERSIDAD DE LA LAGUNA	25/10/2018 11:00:30
Diego Álvarez de la Rosa Rodríguez UNIVERSIDAD DE LA LAGUNA	25/10/2018 11:52:58
Teresa Giráldez Fernández UNIVERSIDAD DE LA LAGUNA	25/10/2018 11:54:04
Ernesto Pereda de Pablo UNIVERSIDAD DE LA LAGUNA	29/10/2018 13:01:03

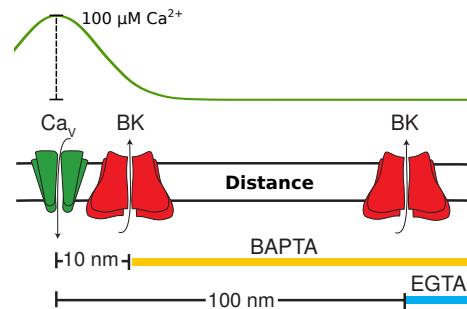


Figure 1.3: Effect of Ca²⁺ chelators BAPTA and EGTA to Ca²⁺ nanodomains. The fast Ca²⁺-binding kinetics of BAPTA in front of EGTA allowed BAPTA to disrupt BK-Cav interactions that are farther than 10 nm. In contrast EGTA is able to buffer Ca²⁺ at 100 nm from the source. (Image From (Vivas et al., 2017)). Upper part: nanodomain signal, where [Ca²⁺] raises up to 100 μM in the mouth of the source.

Ca²⁺ signal regulating neurotransmission (Berkefeld et al., 2006). BAPTA and EGTA Ca²⁺ chelators can be used as biochemical tools to estimate the distance between BK channels and their Ca²⁺ sources (Berkefeld et al., 2006). Both chelators present similar affinities for Ca²⁺ but different association rates (BAPTA > EGTA) (Eggermann et al., 2012). If the distance between both channels within the complexes were 10-50 nm, outward BK-dependent currents would be recorded in the presence of EGTA, but not in BAPTA (Neher, 1998; Augustine, Santamaria, and Tanaka, 2003). If the distance between both channels is larger, Ca²⁺ flowing through the neighboring Ca²⁺ source would be effectively captured by both chelators before reaching BK, and no outward current would be observed (Berkefeld et al., 2006) (Fig. 1.3). In these spatially restricted domains called “Ca²⁺ nanodomains”, BK channels have been proposed to be separated 10-50 nm from Cav channels (Contet et al., 2016). The coupling between Ca²⁺ effectors and Ca²⁺ sensors in a nanodomain present several functional advantages. Synapses in the mammalian CNS employs extensively Ca²⁺ nanodomains for fast neurotransmitter release, as improves the speed and energy efficiency of the process (Eggermann et al., 2012), while maintaining the temporal precision in the information stream (Wang and Augustine, 2015).

Depending on the cellular distribution and subcellular localization, the association of BK channels with diverse Cav partners can lead BK channels to regulate neural activity in different manners. Except the R-type (Cav2.3) channels, all Cav channel subtypes are spatially and functionally coupled to BK channels (Contet et al., 2016). In presynaptic terminals, the influence of fast-activating P/Q- (Cav2.1) and N-type (Cav2.2) on BK channels results on the shortening of the AP duration, and reduces neurotransmitter release (Wu et al., 1999; Kulik et al., 2004). In the dendrites and soma, the slow-activating L- (Cav1.2 and Cav1.3) and T-type (Cav3.2) channels trigger BK channels regulating AP propagation (Engbers et al., 2013; Obermair et al., 2004). In cerebellar neurons, activation of BK channels by T-type channels reduces firing evoked in the synapses (Engbers et al., 2013). In hippocampal CA1 pyramidal neurons, N-type and BK channels are forming complexes, but not with L-type channels (Marrion and Tavalin, 1998). In cortical pyramidal neurons, association of

Este documento incorpora firma electrónica, y es copia auténtica de un documento electrónico archivado por la ULL según la Ley 39/2015.
 Su autenticidad puede ser contrastada en la siguiente dirección <https://sede.ull.es/validacion/>

Identificador del documento: 1627512

Código de verificación: kOIBgUMu

Firmado por:	Fecha:
Roger Gimeno Llobet UNIVERSIDAD DE LA LAGUNA	25/10/2018 11:00:30
Diego Álvarez de la Rosa Rodríguez UNIVERSIDAD DE LA LAGUNA	25/10/2018 11:52:58
Teresa Giráldez Fernández UNIVERSIDAD DE LA LAGUNA	25/10/2018 11:54:04
Ernesto Pereda de Pablo UNIVERSIDAD DE LA LAGUNA	29/10/2018 13:01:03

N- and L-type channels with BK channels are found, both having an important role in BK activation (Sun, Gu, and Haddad, 2003). In chromaffin cells, although N-type channels and BK channels are spatially associated, L- and P/Q-type channels have a larger influence in BK activation (Prakriya and Lingle, 1999).

1.5 Knowledge gap

Despite the well-established relevance of Ca^{2+} nanodomains for function of many types of excitable cells, many questions remain about coupling of BK to Cav channels within the complexes, regarding structural and functional aspects (Vivas et al., 2017; Eggermann et al., 2012). The core molecular determinants of BK in the nanodomain context (i.e. β -subunits that modulated properties of the channel) have been elucidated in some cases, but not all. The spatial distribution and protein stoichiometry in BK-Cav complexes are still not clear (Vivas et al., 2017). Apart from the localized BK-Cav complexes, Ca^{2+} effectors can transiently change its position, altering BK-Cav complexes composition (Fakler and Adelman, 2008). The study of these additional interactions between BK channels and effectors will unravel the function of larger-scale Ca^{2+} signaling networks (Fakler and Adelman, 2008). Other actors and characteristics of the signaling process remain unknown. In practice, it is not straightforward to correlate Ca^{2+} signals to selective physiological responses associated to them (Augustine, Santamaria, and Tanaka, 2003). Important considerations have to be taken into account when studying Ca^{2+} signaling in nanodomains. In order to consider fluorescent Ca^{2+} indicators for nanodomain imaging studies, it is crucial that such indicators achieve the proper temporal and spatial resolution. Some indicators diffuse intracellularly, thus reporting space-averaged $[\text{Ca}^{2+}]$ and lacking the high spatial resolution required to report Ca^{2+} signals constrained to the nanodomain (Tadross, Tsien, and Yue, 2013). Furthermore, Ca^{2+} signals from nanodomains are at the edge of the detection limit for conventional light microscopy, as fluorescent signals from nanodomains should be localized in areas of less than $1 \mu\text{m}$ (Augustine, Santamaria, and Tanaka, 2003). Additionally, temporal resolution is also crucial, as indicators must work in the millisecond to microsecond range to detect the fast Ca^{2+} signals. Finally, one important consideration to be taken into account regarding the use of Ca^{2+} indicators to study nanodomains is their potential as Ca^{2+} buffers. If the indicators are potent buffers, the dynamics of Ca^{2+} in nanodomains may be affected, altering the measured signals (Augustine, Santamaria, and Tanaka, 2003).

In summary, there is an evident need to develop and deploy new tools to study Ca^{2+} dynamics in nanodomains, which will undoubtedly provide unprecedented insights on the cellular and molecular mechanisms underlying the processes related to Ca^{2+} nanodomains function.

1.6 Fluorescence

In 1845 Herschel first observed an unusual optical phenomenon that he described as “an extremely vivid and beautiful celestial blue color” while watching a glass full of water and quinine under the sunlight. Since then, the technology and uses of fluorescence have progressed enormously (Lakowicz, 2011). Fluorescence technology is now used in a wide range of disciplines, taking an important role in the biological sciences. Quinine was the first discovered fluorophore (Fig. 1.4A).

Este documento incorpora firma electrónica, y es copia auténtica de un documento electrónico archivado por la ULL según la Ley 39/2015.
 Su autenticidad puede ser contrastada en la siguiente dirección <https://sede.ull.es/validacion/>

Identificador del documento: 1627512

Código de verificación: kOIBgUMu

Firmado por:	Fecha:
Roger Gimeno Llobet UNIVERSIDAD DE LA LAGUNA	25/10/2018 11:00:30
Diego Álvarez de la Rosa Rodríguez UNIVERSIDAD DE LA LAGUNA	25/10/2018 11:52:58
Teresa Giráldez Fernández UNIVERSIDAD DE LA LAGUNA	25/10/2018 11:54:04
Ernesto Pereda de Pablo UNIVERSIDAD DE LA LAGUNA	29/10/2018 13:01:03

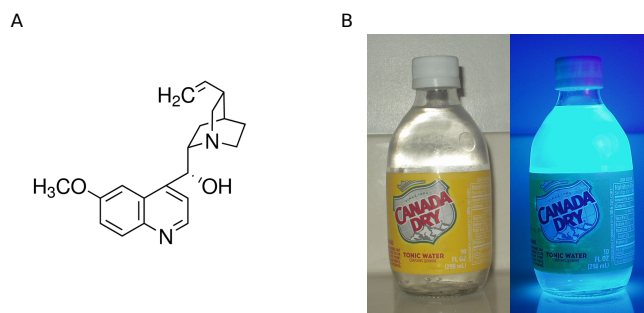


Figure 1.4: A) Chemical structure of quinine. Fluorescence is related to aromatic groups. B) Fluorescence of Tonic water (containing quinine) when illuminated with UV light.

The physical-chemical principle underlying fluorescence resides in the fact that aromatic molecules can be excited with electromagnetic radiation. The excited electron rapidly returns to the ground state emitting a photon (fluorescence). Emitted photons usually have lower energy (longer wavelength) than excitation photons. The average time between excitation and emission, termed fluorescent lifetime (τ), is in the order of 10^{-9} s and is intrinsic to the fluorophore. In the case of Quinine firstly observed by Herschel, ultraviolet light from the Sun excites the molecule, which emits blue light when the molecule returns to the ground state (**Fig. 1.4B**). Aromatic molecules can be excited with electromagnetic radiation. In the phenomenon of fluorescence, the excited electron rapidly returns to the ground state emitting a photon. Emitted photons usually have lower energy (longer wavelength) than excitation photons. The average time between excitation and emission, termed fluorescent lifetime (τ), is in the order of 10^{-9} s and is intrinsic to the fluorophore.

1.6.1 Jablonsky diagram

To illustrate the processes that take place between absorption and emission of a photon in fluorescent substances, Jablonsky diagrams are widely used. An example of a typical absorption-emission process of a fluorophore represented in a Jablonski diagram can be seen in **Fig. 1.5**. Following light absorption, an electron is excited from the ground state (S_0) to a higher energy state (S_1). For the molecule to be excited, only certain wavelengths of light can be absorbed, related to the energy levels of the molecule. The transitions between states are pictured as vertical lines. One pathway to dissipate that energy is through vibrational relaxation, a non-radiative process, indicated in the diagram as a dashed arrow descending across vibrational levels. Another way is the emission of a fluorescence photon, illustrated as a vertical line pointing to the ground state S_0 . The energy lost in the vibrational relaxation causes the emitted photon to have a lower energy and hence a higher wavelength than the absorbed photon. This aspect of the fluorescence phenomenon, called Stokes shift, is the reason why Herschel described as a "beautiful celestial blue color" the sunlit solution containing quinine.

Este documento incorpora firma electrónica, y es copia auténtica de un documento electrónico archivado por la ULL según la Ley 39/2015.
 Su autenticidad puede ser contrastada en la siguiente dirección <https://sede.ull.es/validacion/>

Identificador del documento: 1627512

Código de verificación: KOIBgUMu

Firmado por:	Fecha:
Roger Gimeno Llobet UNIVERSIDAD DE LA LAGUNA	25/10/2018 11:00:30
Diego Álvarez de la Rosa Rodríguez UNIVERSIDAD DE LA LAGUNA	25/10/2018 11:52:58
Teresa Giráldez Fernández UNIVERSIDAD DE LA LAGUNA	25/10/2018 11:54:04
Ernesto Pereda de Pablo UNIVERSIDAD DE LA LAGUNA	29/10/2018 13:01:03

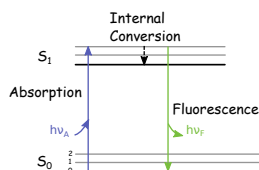


Figure 1.5: Jablonsky diagram showing excitation of a molecule from S_0 to S_1 state by absorption of a photon, relaxation by internal conversion and return to the ground state by emission of a fluorescence photon.

1.6.2 Förster Resonance Energy Transfer (FRET)

In the variety of processes that could drive an excited molecule to its ground state, one is especially useful for the inter/intra-molecular protein study. This process is Förster Resonance Energy Transfer (FRET), also known as fluorescence resonance energy transfer or simply resonance energy transfer (RET). FRET is caused by a non-radiative process (it does not involve the emission and absorption of photons) that takes place when two dipolar molecules with similar resonance frequencies exchange energy when coupled in a dipole-dipole interaction. The transfer of energy occurs between a molecule being in the excited state (called the donor, D) and a molecule in the ground state (called the acceptor, A). For FRET to occur, some conditions must be met:

- Molecules must be in a distance range of about 1 to 10 nm.
- Emission spectrum of the donor must overlap with absorption spectrum of the acceptor (Fig. 1.6A).
- The relative orientation of the dipole moments of donor and acceptor must not be perpendicular.

The most relevant physical property of FRET, of special relevance for the study of molecular protein interactions, is that the efficiency of the energy transfer (E) is inversely proportional to the sixth power of the distance between molecules, and is related to the Förster distance (R_0) by

$$E = \frac{1}{1 + \left(\frac{r}{R_0}\right)^6} \quad (1.1)$$

where r is the distance between donor and acceptor. The dependence of the energy transfer efficiency on distance can be seen in Fig. 1.6B. Because E is inversely proportional to the sixth power of r , small changes in r are acutely reflected in the transfer efficiency, converting FRET measurements into a “spectroscopic ruler” (Stryer, 1978). As shown in Fig. 1.6B, R_0 is the distance at which the energy transfer is 50%, and E quickly fall to zero when r is greater than R_0 . Distances cannot be measured outside the range $r = 0.5R_0$ to $r = 2R_0$. R_0 can be predicted from the spectral properties of donor and acceptor molecules. The related properties can be seen in equation

Este documento incorpora firma electrónica, y es copia auténtica de un documento electrónico archivado por la ULL según la Ley 39/2015.
 Su autenticidad puede ser contrastada en la siguiente dirección <https://sede.ull.es/validacion/>

Identificador del documento: 1627512

Código de verificación: kOIBgUMu

Firmado por:	Fecha:
Roger Gimeno Llobet UNIVERSIDAD DE LA LAGUNA	25/10/2018 11:00:30
Diego Álvarez de la Rosa Rodríguez UNIVERSIDAD DE LA LAGUNA	25/10/2018 11:52:58
Teresa Giráldez Fernández UNIVERSIDAD DE LA LAGUNA	25/10/2018 11:54:04
Ernesto Pereda de Pablo UNIVERSIDAD DE LA LAGUNA	29/10/2018 13:01:03

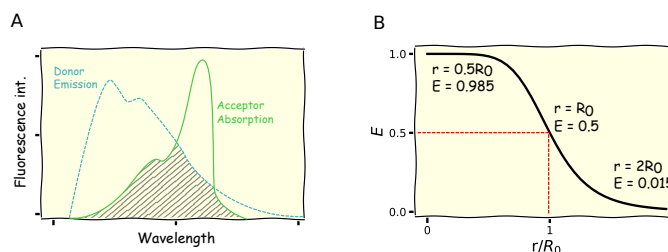


Figure 1.6: A) Spectral overlap (shaded area) between emission spectrum of donor and absorption spectrum of acceptor molecules. B) Dependence of the energy transfer efficiency on distance between molecules. Small changes in r are acutely reflected in the transfer efficiency. Distances cannot be measured outside the range $r = 0.5R_0$ to $r = 2R_0$.

$$R_0 = 9.78 \times 10^3 (\kappa^2 n^{-4} Q_D J(\lambda))^{1/6} \quad (1.2)$$

where κ^2 is the dipole orientation factor, n is the refractive index of the medium, Q_D is the quantum yield of the donor and $J(\lambda)$ is the overlap integral computing the spectral overlap between donor emission and acceptor excitation. It is commonly assumed that $\kappa^2 = 2/3$, a value corresponding to random orientation of donor and acceptor molecules by rotational diffusion.

FRET efficiency can be calculated experimentally by measuring the fluorescence intensity of the donor when the acceptor is out of the energy transfer range (F_D) or is within the range (F_{DA}). F_D and F_{DA} states for fluorescence of the donor only and fluorescence of the donor in the presence of acceptor respectively. The common way of measuring E is with the ratio:

$$E = 1 - \frac{F_{DA}}{F_D} \quad (1.3)$$

If we are measuring lifetimes of donor instead of fluorescence, E can be calculated as:

$$E = 1 - \frac{\tau_{DA}}{\tau_D} \quad (1.4)$$

where τ_D and τ_{DA} are the lifetimes of the donor molecule under same conditions as before.

1.6.3 Fluorescence Lifetime

The fluorescence lifetime corresponds to the time that a fluorophore remains in its excited state before returning to the ground state by emitting a fluorescence photon (Fig. 1.7A). Since emission is a random process, every excited fluorophore can emit a

Este documento incorpora firma electrónica, y es copia auténtica de un documento electrónico archivado por la ULL según la Ley 39/2015.
 Su autenticidad puede ser contrastada en la siguiente dirección <https://sede.ull.es/validacion/>

Identificador del documento: 1627512

Código de verificación: KOIBgUMu

Firmado por: Roger Gimeno Llobet UNIVERSIDAD DE LA LAGUNA	Fecha: 25/10/2018 11:00:30
Diego Álvarez de la Rosa Rodríguez UNIVERSIDAD DE LA LAGUNA	25/10/2018 11:52:58
Teresa Giráldez Fernández UNIVERSIDAD DE LA LAGUNA	25/10/2018 11:54:04
Ernesto Pereda de Pablo UNIVERSIDAD DE LA LAGUNA	29/10/2018 13:01:03

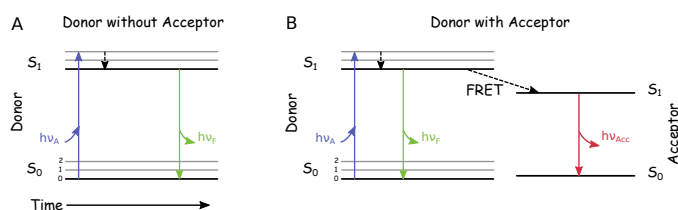


Figure 1.7: A) The fluorescence lifetime is a measure of how long a fluorophore remains on average in its excited state before returning to the ground state by emitting a fluorescence photon. B) Donor fluorescence and energy transfer are competing processes; when FRET is occurring, the emission of the donor takes place at shorter lifetimes.

photon with the same probability. Lifetime, thus, is a statistical average corresponding to the amount of time the fluorophore remained in its excited state. Therefore, a time distribution is observed, which can be described by an exponential function corresponding to the decay of the excited state population.

$$n(t) = n_0 \exp(-t/\tau) \quad (1.5)$$

where $n(t)$ are the excited molecules at a given time t , n_0 the initial amount of excited molecules and τ the fluorescence lifetime. Since fluorescence intensity is proportional to the number of excited molecules, **Eq. 1.5** can be rewritten as

$$I(t) = I_0 \exp(-t/\tau) \quad (1.6)$$

where $I(t)$ is the fluorescence intensity at time t , I_0 the initial intensity.

The decay of a excited molecule is described by a rate constant, Γ . Other non-radiative processes occur to drive the excited molecule to the ground state. Being Knr the rate of non-radiative decay, lifetime is described as,

$$\tau = \frac{1}{\Gamma + Knr} \quad (1.7)$$

Lifetime of a fluorophore thus, will vary if a non-radiative process to decay from the excited state is present. If conditions are met (see above), the excited fluorophores may undergo FRET to come to the relaxed state (**Fig. 1.7B**). When the donor molecule is not under the influence of the acceptor molecule, $\Gamma \gg Knr$. In the presence of the acceptor molecule, the new pathway to decay increases rate Knr , shortening the lifetime of the excited donor. Therefore, fluorescence lifetime measurements can be used experimentally to evaluate changes in protein environment or protein-protein interactions (Lakowicz, 2011).

Este documento incorpora firma electrónica, y es copia auténtica de un documento electrónico archivado por la ULL según la Ley 39/2015.
 Su autenticidad puede ser contrastada en la siguiente dirección <https://sede.ull.es/validacion/>

Identificador del documento: 1627512

Código de verificación: kOIBgUMu

Firmado por: Roger Gimeno Llobet UNIVERSIDAD DE LA LAGUNA	Fecha: 25/10/2018 11:00:30
Diego Álvarez de la Rosa Rodríguez UNIVERSIDAD DE LA LAGUNA	25/10/2018 11:52:58
Teresa Giráldez Fernández UNIVERSIDAD DE LA LAGUNA	25/10/2018 11:54:04
Ernesto Pereda de Pablo UNIVERSIDAD DE LA LAGUNA	29/10/2018 13:01:03

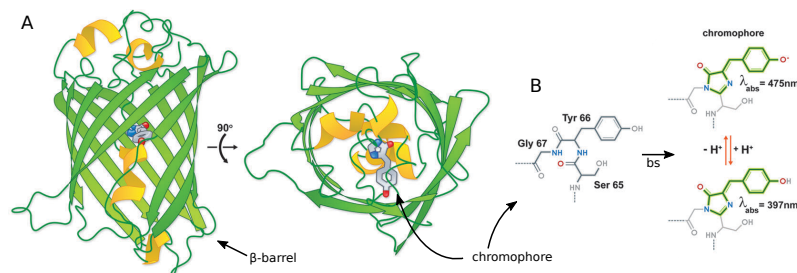


Figure 1.8: GFP structure. A) Protein structure (PDB: 1EMA) where the β -barrel is represented as 11 β -sheets and the internal chromophore shown in stick representation (figure adapted from (Frommer, Davidson, and Campbell, 2009)). B) GFP chromophore unfolded/denatured conformation (left) and final fluorescent conformation (right), where the absorption wavelength is shown for the deprotonated/protonated species. The black arrow "bs" synthesizes the mechanism for intramolecular biosynthesis consisting in cyclization of the main chain, dehydration and an oxidation (figure adapted from (Frommer, Davidson, and Campbell, 2009)).

1.6.4 Fluorescence Proteins

The discovery of the green fluorescent protein (GFP) from the bioluminescent jellyfish *Aequorea Victoria* in the early 1960s (Shimomura, Johnson, and Saiga, 1962) has transformed cell biology by providing an extensive library of probes that allowed to non-invasively studying all kind of biological processes (Ai, 2015). The key factor of such useful tool resides in its particular structure: a cylinder-like shell constituted by 11-stranded β -sheet polypeptide (β -barrel) that shields from the environment a internal fluorophore, generated spontaneously in an autocatalytic process and formed of a serine, a tyrosine and a glycine (Frommer, Davidson, and Campbell, 2009). The protein and the chromophore structure are shown in Fig. 1.8. The robust folding of the GFP has made possible to attach it to target proteins and express the fused proteins into cells (Tsien, 1998). The engineering of the GFP has raised a myriad of fluorescent proteins with improvements in its intrinsic characteristics (i.e. efficient temperature-dependent folding) and variations in its spectral properties, creating a palette of color variants that enhanced the large number of potential applications (Frommer, Davidson, and Campbell, 2009).

1.7 Ca²⁺ sensors

As described in previous sections, Ca²⁺ is an intracellular second messenger of great physiological relevance (Clapham, 2007). Therefore, development of chemical tools to measure intracellular Ca²⁺ concentration has been crucial to advance our knowledge about a large variety of physiological processes, including neuronal function (Clapham, 2007). Available tools for Ca²⁺ imaging mainly consist of two classes of Ca²⁺ indicators: Chemical Calcium Indicators (CCI) and Genetically Encoded Calcium Indicators (GECI). CCI are chemically engineered fluorophores with a broad range of Ca²⁺ affinities, that have to be loaded into cells according to well established experimental protocols. On the other hand, Genetically Encoded Calcium

Este documento incorpora firma electrónica, y es copia auténtica de un documento electrónico archivado por la ULL según la Ley 39/2015.
 Su autenticidad puede ser contrastada en la siguiente dirección <https://sede.ull.es/validacion/>

Identificador del documento: 1627512

Código de verificación: KOIBgUMu

Firmado por: Roger Gimeno Llobet UNIVERSIDAD DE LA LAGUNA	Fecha: 25/10/2018 11:00:30
Diego Álvarez de la Rosa Rodríguez UNIVERSIDAD DE LA LAGUNA	25/10/2018 11:52:58
Teresa Giráldez Fernández UNIVERSIDAD DE LA LAGUNA	25/10/2018 11:54:04
Ernesto Pereda de Pablo UNIVERSIDAD DE LA LAGUNA	29/10/2018 13:01:03

Indicators (GECI) are genetically encoded fluorophore-containing proteins, which are expressed inside cells using gene transfer techniques such as transfection, virus-mediated transformation or transgenesis. Both CCI and GECI have been successfully used as quantitative calcium sensors *in vitro* and *in vivo*.

One way to categorize Ca^{2+} indicators is according to their Ca^{2+} affinity. This allows the researcher to choose the indicator more convenient to study a particular physiological process.

The dissociation constant (Kd) is an equilibrium constant that relates the concentrations of free Ca^{2+} , chelator and the chelator- Ca^{2+} complexes, and is defined as

$$Kd = \frac{[\text{Ca}^{2+}] \cdot [\text{chelator}]}{[\text{chelator} - \text{Ca}^{2+} \text{ complex}]} \quad (1.8)$$

The Kd is the value in molar units where the fluorescence intensity is halfway between the basal fluorescence and the maximum fluorescence, corresponding to half of the indicator molecules forming chelator- Ca^{2+} complexes. Lower Kd values (in the nM range) correspond to high-affinity Ca^{2+} indicators (the indicator has a high tendency to bind Ca^{2+}). Low-affinity Ca^{2+} indicators show high Kd values (in the μM range or more). Experimentally, high-affinity indicators are generally used to measure $[\text{Ca}^{2+}]$ in the cytosol, whereas low-affinity indicators can be used in subcellular organelles where $[\text{Ca}^{2+}]$ are higher. The optimum working range for an indicator corresponds to $[\text{Ca}^{2+}]$ values between 0.1 and 10 times their Kd .

The absolute concentration of Ca^{2+} is calculated experimentally using the formula

$$[\text{Ca}^{2+}] = Kd \frac{F - F_{min}}{F_{max} - F} \quad (1.9)$$

where the Kd is the dissociation constant, F_{min} is the fluorescence in absence of Ca^{2+} , F_{max} is the maximum fluorescence obtained at saturated Ca^{2+} levels ($[\text{Ca}^{2+}] \gg 10Kd$) and F is the fluorescence at a given time.

If absolute values of $[\text{Ca}^{2+}]$ are not required or some of the parameters in Fig. 1.9 cannot be obtained experimentally (such as F_{min} or F_{max}), the relative fluorescent changes can be related to the changes in the $[\text{Ca}^{2+}]$ by

$$\Delta F/F = \frac{F - F_0}{F_0} = \Delta[\text{Ca}^{2+}] \quad (1.10)$$

where F is the fluorescence at a given time and F_0 is the basal fluorescence before the stimuli that lead the change in the fluorescence.

According to their spectral properties, calcium indicators can be classified in two groups: single wavelength indicators or ratiometric indicators.

Single-wavelength indicators display a considerable change in fluorescence intensity upon Ca^{2+} binding (Fig. 1.9A), without varying their excitation/emission spectra. Usually, the free indicator that is not bound to Ca^{2+} exhibits a very weak fluorescence, increasing the intensity as Ca^{2+} binds to the chelator. However, a major drawback of these indicators is that in some instances, fluorescence intensity changes occur that are not related to changes in Ca^{2+} concentration. These intensity-related artifacts can be due to the bleaching of the fluorophore, variations in probe

Este documento incorpora firma electrónica, y es copia auténtica de un documento electrónico archivado por la ULL según la Ley 39/2015.
 Su autenticidad puede ser contrastada en la siguiente dirección <https://sede.ull.es/validacion/>

Identificador del documento: 1627512

Código de verificación: kOIBgUMu

Firmado por: Roger Gimeno Llobet UNIVERSIDAD DE LA LAGUNA	Fecha: 25/10/2018 11:00:30
Diego Álvarez de la Rosa Rodríguez UNIVERSIDAD DE LA LAGUNA	25/10/2018 11:52:58
Teresa Giráldez Fernández UNIVERSIDAD DE LA LAGUNA	25/10/2018 11:54:04
Ernesto Pereda de Pablo UNIVERSIDAD DE LA LAGUNA	29/10/2018 13:01:03

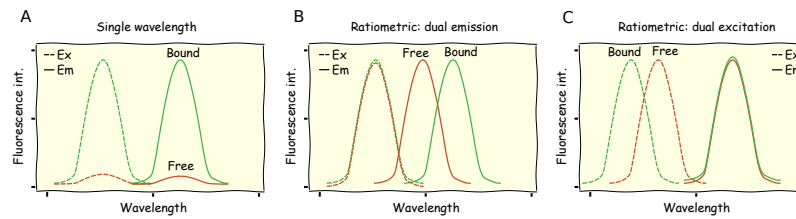


Figure 1.9: Chemical Ca²⁺ indicators A) In single wavelength indicators a change in the fluorescence intensity occur when Ca²⁺ binds to the molecule. In contrast, ratiometric indicators can exhibit an emission spectral shift (B) or an excitation spectral shift (C), after Ca²⁺ binding.

concentration or changes in the acquisition conditions (such as sudden changes of focus or in laser intensity).

Ratiometric indicators undergo Ca²⁺-dependent shifts in their emission or excitation spectra (Fig. 1.9B and C). This behavior allows accurate quantification of Ca²⁺ concentration by correcting intensity-related artifacts. The ratio between the two fluorescence intensities is, in principle, independent of variations in sensor distribution and concentration, and artifacts in the fluorescence intensity will affect both channels in the same manner and can be removed.

The two classifications described above are applicable to both CCI and GECl. The following sections describe specific characteristics of CCI and GECl.

1.7.1 Chemical calcium indicators

As mentioned above, CCI are fluorescent molecules with the ability to chelate Ca²⁺ ions. The majority are based on the Ca²⁺-specific aminopolycarboxylic acid BAPTA (1,2-bis(o-aminophenoxy)ethane-N,N,N',N'-tetraacetic acid) (Fig. 1.10A). This chelator, first reported by Tsien *et al.* in 1980 (Tsien, 1980), shows faster binding kinetics and less pH dependence than ethylene glycol-N,N,N',N'-tetraacetic acid (EGTA, another Ca²⁺ chelator which is used in a wide range of biological experimental conditions). Additionally, BAPTA shows higher selectivity for Ca²⁺ ions over Mg²⁺ ions, which are present in the cytosol more than 4 orders of magnitude higher compared to Ca²⁺. After Ca²⁺ binding, the CCI exhibit a change in the fluorescent properties, either the fluorescence intensity or the excitation/emission wavelengths (i.e. Fura-2, Fig. 1.10B).

The main advantages of CCI are the broad range of Ca²⁺ affinities available and the fast binding kinetics, allowing the recording of events with high temporal resolution. The main drawbacks include: 1) their low spatial resolution; 2) some CCI exert a Ca²⁺ buffering effect, particularly those with larger Ca²⁺ affinities; 3) since these indicators are generally highly charged molecules, they do not efficiently cross the plasma membrane. To address this problem, indicators are normally introduced in the cytosol by microinjection or making them permeant by masking the charged carboxylic groups by forming acetoxymethyl (AM) esters (Whitaker, 2010). Once in the cell, the ester bonds are cleaved by endogenous esterase enzymes, leaving the indicator trapped inside the cell. If the incubation times are not optimized, the indicator may permeate into intracellular organelles such as the endoplasmic reticulum (ER) or mitochondria. The resting Ca²⁺ concentration inside ER (250-600 μM) is

Este documento incorpora firma electrónica, y es copia auténtica de un documento electrónico archivado por la ULL según la Ley 39/2015.
 Su autenticidad puede ser contrastada en la siguiente dirección <https://sede.ull.es/validacion/>

Identificador del documento: 1627512

Código de verificación: KOIBgUMu

Firmado por: Roger Gimeno Llobet UNIVERSIDAD DE LA LAGUNA	Fecha: 25/10/2018 11:00:30
Diego Álvarez de la Rosa Rodríguez UNIVERSIDAD DE LA LAGUNA	25/10/2018 11:52:58
Teresa Giráldez Fernández UNIVERSIDAD DE LA LAGUNA	25/10/2018 11:54:04
Ernesto Pereda de Pablo UNIVERSIDAD DE LA LAGUNA	29/10/2018 13:01:03

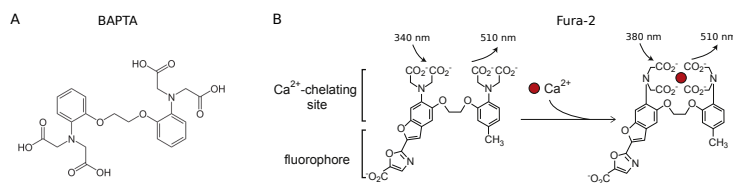


Figure 1.10: A) Chemical structure of BAPTA. The four carboxylic acid functional groups are responsible of Ca^{2+} binding (source: *Wikimedia Commons*). B) Chemical Ca^{2+} indicator Fura-2. The excitation wavelength changes from 340 nm (free Ca^{2+}) to 380 nm (Ca^{2+} bound). The emission is unalterable at 510 nm (figure adapted from (Grienberger and Konnerth, 2012).

higher than the cytosol, hence the signal from the indicator inside the ER can mask the signal from the indicator in the surroundings.

1.7.2 Genetically encoded calcium indicators

As mentioned above, GECIs are based on genetically encoded proteins including a fluorophore and Ca^{2+} -binding domains. The general principle is that changes in the conformation of these Ca^{2+} -sensing domains after Ca^{2+} binding alters the fluorescent properties of the linked fluorophores.

The initial GECIs included FRET-based GECIs (Miyawaki et al., 1997) or single fluorophore chimeras (Baird, Zacharias, and Tsien, 1999). Since then, GECIs have been optimized enormously, improving signal strength, pH- and Ca^{2+} -sensitivity, expression efficiency or expanding the colored variants palette (Rose et al., 2014; Whitaker, 2010).

FRET-based GECIs

FRET-based recombinant Ca^{2+} sensors were the first to appear in the GECI family. In 1997, Tsien described a construct concatenating *Xenopus laevis* calmodulin and the myosin light chain kinase calmodulin binding peptide, M13, flanked by two variants of the GFP (Miyawaki et al., 1997). Comparison of constructs with different FRET pairs (cameleon-1 with BFP/GFP, cameleon-2 with EBFP/EGFP¹ revealed that the construct with ECFP/EYFP (Yellow cameleon-2) showed the best expression, SNR ratio and brightness. However, these benefits were at expenses of lower FRET change and higher pH sensitivity. Calmodulin has two binding sites, with apparent dissociation constants (K_d) of 70 nM in the high-affinity site and 11 μM in the low-affinity site. Mutations in either high-affinity site or low-affinity site led to new variants of cameleon-GECIs cameleon-3 ($K_d = 4.4 \mu\text{M}$) and cameleon-4 (K_d s of 83 nM and 700 μM). To overcome the problem with the pH sensitivity, two mutations (V68L and Q69K) in the EYFP lowered the pKa from 6.9 to 6.1. Indicators Yellow cameleon-2.1 and 3.1 (YC2.1 and YC3.1) benefited from these mutations, suppressing the pH sensitivity above 6.9. K_d s were 100 nM and 4.3 μM for YC2.1 and 1.5 μM for YC3.1. The substitution of the mutated EYFP with an improved version called citrine (more resistant to quenching and photobleaching, and with lower pKa) rendered cameleons YC2.3 and YC3.3. Changes in the dipole-dipole

¹E in EGFP variants states for enhanced and it is an improved version of the fluorescent protein.

Este documento incorpora firma electrónica, y es copia auténtica de un documento electrónico archivado por la ULL según la Ley 39/2015.
 Su autenticidad puede ser contrastada en la siguiente dirección <https://sede.ull.es/validacion/>

Identificador del documento: 1627512

Código de verificación: KOIBgUMu

Firmado por: Roger Gimeno Llobet UNIVERSIDAD DE LA LAGUNA	Fecha: 25/10/2018 11:00:30
Diego Álvarez de la Rosa Rodríguez UNIVERSIDAD DE LA LAGUNA	25/10/2018 11:52:58
Teresa Giráldez Fernández UNIVERSIDAD DE LA LAGUNA	25/10/2018 11:54:04
Ernesto Pereda de Pablo UNIVERSIDAD DE LA LAGUNA	29/10/2018 13:01:03

orientation between ECFP and EYFP in order to maximize FRET efficiency were achieved by changing the EYFP with a circularly permuted Venus (cpv)². Indicators with the cpv were denoted as the YCX.60 series, where YC2.60 had a *K_d* of 40 nM, YC3.60 had a *K_d* of 0.25 μM, and YC4.60 had *K_d*s of 58 nM and 14.4 μM. A schematic representation of YC3.60 can be seen in Fig. 1.11A. The properties displayed *in vitro* by calmodulin-based indicators are not always reflected in *in vivo* experiments (Whitaker, 2010). This may be due to calmodulin binding to a wide variety of target proteins (i.e. NMDA receptors or potassium channels). In order to overcome this drawback, troponin C (TNC) has been used. Even though TNC has a very similar structure to that of calmodulin (the EF hand motifs are conserved, but the linker between motifs is larger in TNC), it has a very specific cellular function. The first approach was to concatenate TNC with CFP and citrine. This new sensor mechanism led to the TN-X GECIs series. TN-L15, where TNC was truncated at residue 14 of the N-terminal had a *K_d* of 470 nM. TN-XL, with a circularly permuted citrine, showed a *K_d* of 2.5 μM and a very fast response time.

Single fluorophore-based GECIs

Camgaroos

In camgaroos, calmodulin is inserted between residues 145 and 146 of the β-barrel of a EYFP. Upon Ca²⁺ binding, calmodulin undergoes structural rearrangements that alter the environment of the fluorophore, causing an increase in fluorescence intensity. Camgaroo-1 had a *K_d* of 7 μM. Camgaroo-2 had an improved basal fluorescence, while its Ca²⁺ binding properties remained almost the same (Whitaker, 2010).

Circularly-permuted GFP based GECIs

A remarkable fact, first described by Baird *et al.* (Baird, Zacharias, and Tsien, 1999) is that the rigid β-barrel structure of GFP variants contains sites that tolerate circular permutations. In a circular permutation, the former N- and C-termini of the protein are fused together and a new N- and C-termini created in another part of the structure. In the case of a GFP, a breakpoint between residues 145 and 146 made the fluorophore of the circularly permuted GFP (cpGFP) more accessible to protons, thus changing its fluorescence properties (Fig. 1.11B). Allosteric coupling between a variety of different ligand binding domains (LBD) and cpGFP has been exploited to generate a variety of biosensors, which can be optimized by changing the insertion place in the LBD of interest and the longitude of linkers between the LBD and the cpGFP (Nadler *et al.*, 2016). The following sections present Ca²⁺ sensors that have been developed based on the concept of fusing Ca²⁺-binding protein domains circularly permuted fluorescent proteins.

Pericams

The concatenation of calmodulin, M13 and a circularly permuted EYFP (cpEYFP) started a family of cpYFP-based Ca²⁺ indicators named pericams (Nagai *et al.*, 2001). Flash pericam, a single wavelength indicator, was optimized from the first pericam, increasing its fluorescence change upon Ca²⁺ binding (*K_d* of 0.7 μM). The protonated form of YFP is non-fluorescent, but mutation of residue 203 results in the ability of the protonated fluorophore to emit fluorescence. Introduction of this mutation in

²Venus is a yellow fluorescent protein that improved EYFP maturation, brightness and environmental sensitivity.

Este documento incorpora firma electrónica, y es copia auténtica de un documento electrónico archivado por la ULL según la Ley 39/2015.
 Su autenticidad puede ser contrastada en la siguiente dirección <https://sede.ull.es/validacion/>

Identificador del documento: 1627512

Código de verificación: kOIBgUMu

Firmado por:	Fecha:
Roger Gimeno Llobet UNIVERSIDAD DE LA LAGUNA	25/10/2018 11:00:30
Diego Álvarez de la Rosa Rodríguez UNIVERSIDAD DE LA LAGUNA	25/10/2018 11:52:58
Teresa Giráldez Fernández UNIVERSIDAD DE LA LAGUNA	25/10/2018 11:54:04
Ernesto Pereda de Pablo UNIVERSIDAD DE LA LAGUNA	29/10/2018 13:01:03

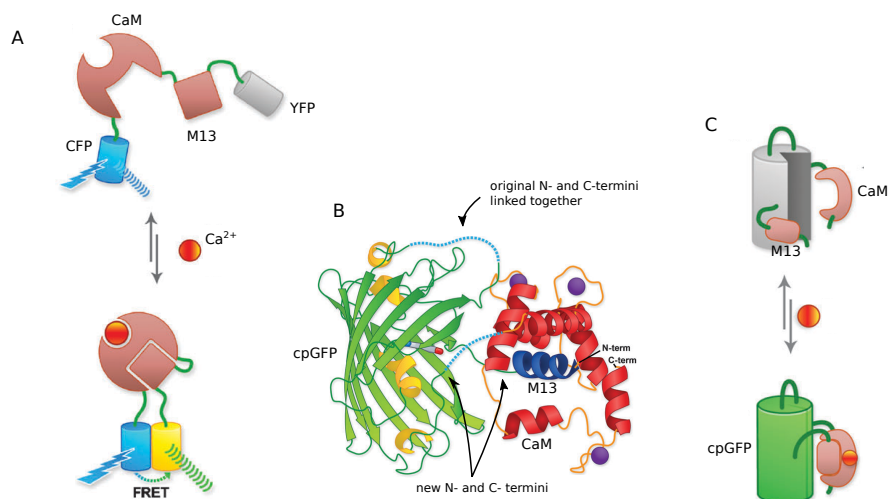


Figure 1.11: Genetically encoded Ca^{2+} indicators (GECIs). A) Schematic representation of Yellow Cameleon (YC). YC is a ratiometric Ca^{2+} indicator that consists of a concatenate of calmodulin (CaM), the myosin light chain kinase calmodulin binding peptide (M13), and the GFP variants CFP and YFP that forms a FRET pair. Without Ca^{2+} present, excitation of CFP causes emission of CFP only. After Ca^{2+} binding the structure collapse closing together the CFP and the YFP and causing FRET. Now excitation of CFP causes YFP emission and decreased CFP emission. B) GCaMP X-ray crystal structure, showing a circularly permuted GFP (cpGFP) linked to CaM and M13. In a cpGFP, the original N- and C-termini of the former GFP are fused together, and new N- and C-termini are created in the β -barrel structure. These new termini are linked to the proteins of interest (in this case to CaM and M13). C) Schematic representation of GCaMP. CaM and M13 are linked to a cpGFP. When Ca^{2+} is not bound, CaM and M13 are in a respective position that permits the contact of the inner chromophore with the environment. In this situation the chromophore is protonated and not fluorescent. After Ca^{2+} binding CaM and M13 moves closer causing the isolation of the chromophore from the environment and permitting the fluorescence. Figure adapted from (Frommer, Davidson, and Campbell, 2009).

Este documento incorpora firma electrónica, y es copia auténtica de un documento electrónico archivado por la ULL según la Ley 39/2015.
 Su autenticidad puede ser contrastada en la siguiente dirección <https://sede.ull.es/validacion/>

Identificador del documento: 1627512

Código de verificación: KOIBgUMU

Firmado por: Roger Gimeno Llobet UNIVERSIDAD DE LA LAGUNA	Fecha: 25/10/2018 11:00:30
Diego Álvarez de la Rosa Rodríguez UNIVERSIDAD DE LA LAGUNA	25/10/2018 11:52:58
Teresa Giráldez Fernández UNIVERSIDAD DE LA LAGUNA	25/10/2018 11:54:04
Ernesto Pereda de Pablo UNIVERSIDAD DE LA LAGUNA	29/10/2018 13:01:03

the flash pericam lead to the indicator ratiometric pericam, which excitation spectrum changed between de Ca²⁺-bound and unbound forms (*K_d* of 1.7 μM). Further mutagenesis of ratiometric pericam led to inverse pericam, where the fluorescence intensity decreased after Ca²⁺ binding (*K_d* of 0.2 μM).

GCaMP

This family of sensors has become the most popular among the single fluorophores Ca²⁺ indicators. Instead of using cpEYFP like pericams, GCaMPs employ cpGFP. The first GCaMP (Nakai, Ohkura, and Imoto, 2001) exhibited an improved signal-to-noise ratio if compared with the existing indicators at that moment. However, protein folding required temperatures below 37°C, and the signal was strongly dependent of pH (as with camgaroos and pericams). The apparent *K_d* for Ca²⁺ was 0.24 μM. Two point mutations that were known to enhance the temperature-related folding of GFP led to GCaMP1.6 (Ohkura et al., 2005). Although these mutations did not improve folding with temperature, they increased the brightness considerably. The next member of the family, GCaMP2 (Tallini et al., 2006) was ~200 times brighter than its predecessor, but with a similar fold-change between Ca²⁺-bound and unbound states. The apparent affinity for Ca²⁺ was 0.84 μM. Interestingly, the thermal stability at 37°C was dependent of a plasmid leader sequence (RSET) that was added to facilitate purification, linked to the M13 domain in the N-terminal. The new indicator was structured as RSET-M13-cpGFP-calmodulin. To improve Ca²⁺ sensitivity, mutations in the calmodulin and the cpGFP were performed (Tian et al., 2009). The resulting construct, GCaMP3, exhibit increased basal fluorescence, increased dynamic range and higher Ca²⁺ affinity (*K_d* = 0.66 μM). GCaMP crystal structures guided targeted library mutagenesis on calmodulin, M13, and the linkers between the cpGFP and these domains. A battery of indicators, GCaMP5 5A, 5D, 5G and 5K (Akerboom et al., 2012), improved GCaMP3 in many aspects. Due to the distinct properties of each GCaMP5 (apparent *K_d* for 5A is 307 nM, for 5D is 730 nM, for 5G is 460 nM and for 5K is 189 nM) the election of which member of the GCaMP5 family to use should vary depending of the application. A new set of GCaMP sensors, GCaMP6 family (Chen et al., 2013) improved the existing sensors mainly by exhibiting higher sensitivity (higher than some commonly used chemical indicators such OGB1-AM). The authors focused mutagenesis approaches at the cpGFP-calmodulin interface and additional sites on the M13-calmodulin interface and calmodulin. GCaMP6f displayed faster (f) kinetics and a medium-high Ca²⁺ affinity (*K_d* = 375 nM), GCaMP6m displayed intermediate (m) kinetics and a high Ca²⁺ affinity (*K_d* = 164 nM) and GCaMP6s displayed slower (s) kinetics and a high Ca²⁺ affinity (*K_d* = 144 nM) (Rose et al., 2014). In order to study Ca²⁺-related events near the plasma membrane, a series of new constructs with a membrane-tethering domain Lck (light chain kinase) were developed (Shigetomi et al., 2010; Shigetomi, Kracun, and Khakh, 2010; Shigetomi, Patel, and Khakh, 2016). While Lck-GCaMP2 exhibited a *K_d* of 168 nM similar to the reported values for GCaMP2 (Tallini et al., 2006), Lck-GCaMP3 exhibited a *K_d* of 153 nM, higher than the 660 nM reported for GCaMP3 (Tian et al., 2009)³. More recently, a battery of new GCaMP sensors, jGCaMP7, was developed in the Janelia Research Campus (Douglas S Kim, unpublished). The jGCaMP7 family has improved GCaMP6 performance, with higher sensitivity and faster kinetics. A schematic representation of a GCaMP indicator can be

³This difference can arise from the experimental procedures carried out to measure the apparent Ca²⁺ affinity. While all the *K_d* reported in the text were measured *in vitro*, on purified proteins, Lck-GCaMP *K_d*s were measured *in vivo* permeabilizing cells with detergent.

Este documento incorpora firma electrónica, y es copia auténtica de un documento electrónico archivado por la ULL según la Ley 39/2015.
 Su autenticidad puede ser contrastada en la siguiente dirección <https://sede.ull.es/validacion/>

Identificador del documento: 1627512

Código de verificación: kOIBgUMu

Firmado por:	Fecha:
Roger Gimeno Llobet UNIVERSIDAD DE LA LAGUNA	25/10/2018 11:00:30
Diego Álvarez de la Rosa Rodríguez UNIVERSIDAD DE LA LAGUNA	25/10/2018 11:52:58
Teresa Giráldez Fernández UNIVERSIDAD DE LA LAGUNA	25/10/2018 11:54:04
Ernesto Pereda de Pablo UNIVERSIDAD DE LA LAGUNA	29/10/2018 13:01:03

seen in Fig. 1.11C.

Aequorin

The bioluminescent Ca^{2+} indicator aequorin was first isolated from the luminescent jellyfish *Aequorea victoria* by Shimomura *et al.* in 1962 (Shimomura, Johnson, and Saiga, 1962). Aequorin is composed of two units, the apoprotein apoaequorin (enzyme) and the prosthetic group coelenterazine (substrate). The active form of aequorin is generated by oxygen and the binding of apoaequorin and coelenterazine. Ca^{2+} ions binds to three specific binding sites and the protein undergoes a conformational change, converting via oxidation coelenterazine into excited coelenteramide. When coelenteramide relaxes to its ground state it emits a fluorescence photon of blue light (465 nm) (Grienberger and Konnerth, 2012). This process can be seen in Fig. 1.12. Curiously, the jellyfish *Aequorea victoria* is capable to emit green light by the association of aequorin with the green fluorescent protein (GFP), which acts as the acceptor molecule of the FRET pair aequorea-GFP. Aequorins have been extensively used to measure Ca^{2+} concentration in a wide range of biological systems (Webb and Miller, 2012; Webb, Karplus, and Miller, 2015) and have significant advantages, like a high signal-to-noise ratio, a wide dynamic range (suited to measure $[\text{Ca}^{2+}]$ from 0.5 to 10 μM , where most Ca^{2+} indicators are saturated), a low Ca^{2+} buffering effect and the possibility of targeting it to specific intracellular compartments. On the other hand, the major disadvantage is a low light emission, which makes it difficult to obtain a good signal when imaging small domains with low concentration of the indicator. Another drawback is the need to add coelenterazine separately when aequorin is transfected. Originally, aequorin was isolated from the jellyfish and placed inside the cells by microinjection, but after aequorin cDNA was cloned, constructs encoding recombinant aequorin were employed (Brini *et al.*, 1995).

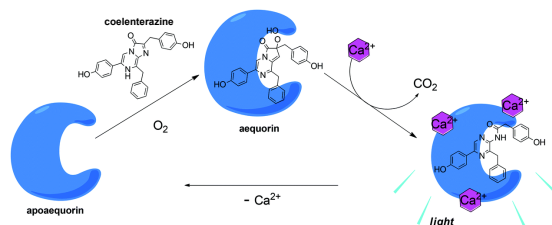


Figure 1.12: Aequorin is composed of two units, apoaequorin (enzyme) and the prosthetic group coelenterazine (substrate). The active form of aequorin (middle) is generated by oxygen and the binding of apoaequorin and coelenterazine. Ca^{2+} ions binds to three specific binding sites and the protein undergoes a conformational change, converting via oxidation coelenterazine into excited coelenteramide. When coelenteramide relaxes to its ground state it emits a fluorescence photon of blue light (465 nm). Figure adapted from (Jiang, Du, and Li, 2016).

Este documento incorpora firma electrónica, y es copia auténtica de un documento electrónico archivado por la ULL según la Ley 39/2015.
 Su autenticidad puede ser contrastada en la siguiente dirección <https://sede.ull.es/validacion/>

Identificador del documento: 1627512

Código de verificación: KOIBgUMU

Firmado por: Roger Gimeno Llobet UNIVERSIDAD DE LA LAGUNA	Fecha: 25/10/2018 11:00:30
Diego Álvarez de la Rosa Rodríguez UNIVERSIDAD DE LA LAGUNA	25/10/2018 11:52:58
Teresa Giráldez Fernández UNIVERSIDAD DE LA LAGUNA	25/10/2018 11:54:04
Ernesto Pereda de Pablo UNIVERSIDAD DE LA LAGUNA	29/10/2018 13:01:03

1.8 BK-FRET as Ca²⁺ sensors

1.8.1 Optimization of BK-FRET for Ca²⁺ sensing in nanodomains

As mentioned in previous sections the study of Ca²⁺ signaling in excitable cells is a fundamental topic in neuroscience. Of significant interest is to understand the intricate dynamics of Ca²⁺ in subcellular nanodomains, and the molecular mechanisms involved. BK channels are spatially and functionally coupled to Ca²⁺ sources in the nanodomain context, thus are perfect candidates as reporters of changes in [Ca²⁺] restricted to nanodomains. Our group has been studying intensively the complex structural rearrangements that BK channel undergo with Ca²⁺ sensing. To this end simultaneous studies of function and structural changes have been possible with the incorporation of state-of-the-art techniques such as patch clamp fluorometry (PCF), a technique that simultaneously combines electrophysiological and fluorimetric recordings. Previous work has been focused in randomly generate fluorescent tagged BK channels with insertions of GFP variants in specific sites of the protein. This genetic high-throughput approach made it possible to obtain a library of 20 fluorescent BK channel constructs, with GFP variants inserted in different locations of the gating ring that did not alter channels function (Giraldez, Hughes, and Sigworth, 2005)(Fig. 1.13A and B). The fluorescent proteins inserted were the cyan and yellow fluorescent proteins (CFP and YFP), an extensively used FRET pair.

1.8.2 Patch-clamp fluorometry studies in *Xenopus laevis* oocytes

Three of these constructs have been studied using PCF in membrane patches of *Xenopus* oocytes (Miranda et al., 2013). The employed constructs had insertion of fluorescent proteins in: 1) the 667 position, situated in the linker between the RCK1 and RCK2 (BK-667CY); 2) in the 860 position, near the Ca²⁺ bowl in the RCK2 domain (BK-860CY), and 3) in the 901 position, adjacent to the Ca²⁺ bowl (BK-901CY). Heterotetramers containing α -subunits tagged with CFP or YFP at equivalent positions in different subunits within the tetramer were co-expressed in the oocytes, and FRET signals and K⁺ currents were simultaneously recorded from excised inside-out patches, while the membrane voltage and the [Ca²⁺] were modified. After voltage and [Ca²⁺] variations, the relative movement of the fluorophores was calculated as variations in the FRET efficiency. The BK-FRET constructs reported BK activity induced by voltage and Ca²⁺ binding (BK-667CY), or only Ca²⁺ binding (BK-860CY) (Fig. 1.13C). Construct BK-901CY only showed small differences in FRET values while varying [Ca²⁺] (Miranda et al., 2013; Miranda, Giraldez, and Holmgren, 2016).

1.8.3 Limitations

Extension of this experimental approach to mammalian cells has various limitations. First of all, excised patches are much smaller, thus containing lower number of channels which results in diminished fluorescence and current signals. While electrophysiology is a powerful technique able to detect small currents with precision, weak fluorescence signals could be a problem. Moreover, FRET changes usually have limited signal variations (Tian et al., 2009), being a problem when signal-to-noise ratio is low. In addition to the signal limitation is the required dual transfection of CFP- and YFP-tagged subunits. Transfection of a single tagged-subunit would be more convenient. This issue will be considered in more detail in **Chapter 4: Section 4.1**.

Este documento incorpora firma electrónica, y es copia auténtica de un documento electrónico archivado por la ULL según la Ley 39/2015.
 Su autenticidad puede ser contrastada en la siguiente dirección <https://sede.ull.es/validacion/>

Identificador del documento: 1627512

Código de verificación: kOIBgUMu

Firmado por:	Fecha:
Roger Gimeno Llobet UNIVERSIDAD DE LA LAGUNA	25/10/2018 11:00:30
Diego Álvarez de la Rosa Rodríguez UNIVERSIDAD DE LA LAGUNA	25/10/2018 11:52:58
Teresa Giráldez Fernández UNIVERSIDAD DE LA LAGUNA	25/10/2018 11:54:04
Ernesto Pereda de Pablo UNIVERSIDAD DE LA LAGUNA	29/10/2018 13:01:03

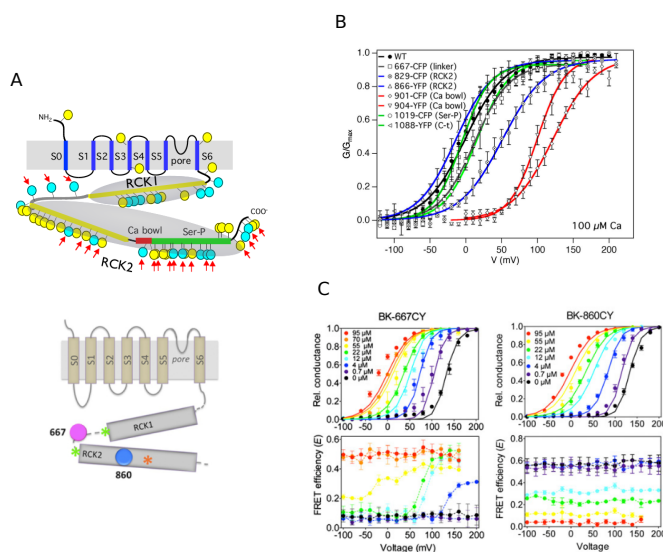


Figure 1.13: BK-FRET. A) (up) Library of fluorescent BK channels available in our laboratory. Yellow and blue circles indicates YFP and CFP insertions in specific sites. Red arrows indicate constructs that are expressed in the membrane following an immunostaining protocol (Giraldez, Hughes, and Sigworth, 2005). (bottom) Insertion sites of constructs that were characterized (Miranda et al., 2013); magenta dot indicates 667 site (BK-667) and blue dot 860 site (BK-860), near the Ca²⁺ bowl (orange asterisk). B) Normalized G-V curves shown for wild-type BK (WT, black) and seven representative insertions; 829, 901 and 904 insertions exhibited altered G-V curves. C) G-V curves (upper panels) and FRET efficiency (E-V) curves (lower panels) were determined simultaneously from patches at various [Ca²⁺]. BK-667CY construct (left) reported Ca²⁺ and voltage changes, while BK-860CY construct (right) reported Ca²⁺ changes. Data are code-colored according to [Ca²⁺]. Figures from (Giraldez, Hughes, and Sigworth, 2005; Miranda et al., 2013).

Este documento incorpora firma electrónica, y es copia auténtica de un documento electrónico archivado por la ULL según la Ley 39/2015.
 Su autenticidad puede ser contrastada en la siguiente dirección <https://sede.ull.es/validacion/>

Identificador del documento: 1627512

Código de verificación: kOIBgUMu

Firmado por: Roger Gimeno Llobet UNIVERSIDAD DE LA LAGUNA	Fecha: 25/10/2018 11:00:30
Diego Álvarez de la Rosa Rodríguez UNIVERSIDAD DE LA LAGUNA	25/10/2018 11:52:58
Teresa Giráldez Fernández UNIVERSIDAD DE LA LAGUNA	25/10/2018 11:54:04
Ernesto Pereda de Pablo UNIVERSIDAD DE LA LAGUNA	29/10/2018 13:01:03

Chapter 2

Hypothesis and Objectives

2.1 Hypothesis

BK channels are physiological Ca^{2+} sensors that can be optimized with molecular biology techniques to measure specific Ca^{2+} signals from subcellular nanodomains.

2.2 Principal objective

The main goal of our study is the development of a battery of Ca^{2+} sensors based on the BK channel in order to study BK-Cav complexes formed in Ca^{2+} nanodomains to obtain novel information with unprecedented spatial and temporal resolution.

2.3 Specific objectives

2.3.1 Generation

- Generate sensors based on BK-FRET constructs employing variants of the green fluorescent protein (GFP)

2.3.2 Characterization

- Spectral characteristics
- Ca^{2+} dependence (pCa)
- pH dependence (pKa)
- Generation and characterization of mutants affecting Ca^{2+} and voltage sensitivity fluorescent protein (GFP)

2.3.3 Optimization

- Expression and detection systems
- Non-conducting sensors
- Modification of the connecting linker sequences between BK channel and the circularly permuted GFP (cpGFP)

Este documento incorpora firma electrónica, y es copia auténtica de un documento electrónico archivado por la ULL según la Ley 39/2015.
Su autenticidad puede ser contrastada en la siguiente dirección <https://sede.ull.es/validacion/>

Identificador del documento: 1627512

Código de verificación: KOIBgUMu

Firmado por: Roger Gimeno Llobet UNIVERSIDAD DE LA LAGUNA	Fecha: 25/10/2018 11:00:30
Diego Álvarez de la Rosa Rodríguez UNIVERSIDAD DE LA LAGUNA	25/10/2018 11:52:58
Teresa Giráldez Fernández UNIVERSIDAD DE LA LAGUNA	25/10/2018 11:54:04
Ernesto Pereda de Pablo UNIVERSIDAD DE LA LAGUNA	29/10/2018 13:01:03

2.3.4 Validation

- Sensor performance in the physiological context (heterologous systems/neurons)
- Formation of complexes between BK-based sensors and voltage-dependent Ca^{2+} channels (Cav)
- Development of analysis systems to process superresolution data

2.3.5 Extension

- Study of the characteristics of isolated gating ring as a transferable sensor module (i.e. coupled to other proteins of interest)

Este documento incorpora firma electrónica, y es copia auténtica de un documento electrónico archivado por la ULL según la Ley 39/2015.
Su autenticidad puede ser contrastada en la siguiente dirección <https://sede.ull.es/validacion/>

Identificador del documento: 1627512

Código de verificación: KOIBgUMu

Firmado por: Roger Gimeno Llobet UNIVERSIDAD DE LA LAGUNA	Fecha: 25/10/2018 11:00:30
Diego Álvarez de la Rosa Rodríguez UNIVERSIDAD DE LA LAGUNA	25/10/2018 11:52:58
Teresa Giráldez Fernández UNIVERSIDAD DE LA LAGUNA	25/10/2018 11:54:04
Ernesto Pereda de Pablo UNIVERSIDAD DE LA LAGUNA	29/10/2018 13:01:03

Chapter 3

Materials and Methods

3.1 Cell culture and transfection

HEK293T cells (purchased from the American Type Culture Collection #CRL-1573) or HeLa cells were maintained in Dulbecco's Modified Eagle Medium (DMEM) supplemented with 10% fetal bovine serum and 1% penicillin/streptomycin at 37°C and 5% CO₂. Cells were split twice a week as follows. The confluent cells were incubated with pre-warmed Trypsin (Sigma Aldrich). Detached cells were collected with 6 mL of DMEM, transferred into a 15 mL Falcon tube and centrifuged at 1500 rpm for 5 min. The cell pellet was resuspended in 6 mL of DMEM and a 1:5 dilution of cells plated in new flasks with fresh medium. Transient transfections of pcDNA3.1(+) and pBNJ13.1 expression plasmids were performed using jetPRIME (Polyplus transfection), 24h after splitting the cells. The transfection medium was changed after 6-12h of transfection. The procedure for transfection and plasmid DNA, buffer and reagent quantities were as described in manufacturer's manual.

3.2 Molecular biology

3.2.1 BK-cpGFP subcloning

To generate the construct with the circularly permuted Green Fluorescent Protein (cpGFP) insertion BK667cpG, construct BK667C was digested with *AscI* (New England Biolabs) and the plasmid backbone isolated by gel electrophoresis and purified. To prepare the insert, the cpGFP was amplified by PCR using forward primer F-cpGFP and reverse primer R-cpGFP (Table 3.1) and construct GluA2_391cpGFP, where the cpGFP was bound to the glutamate receptor, as template (courtesy of Dr. Andrew Plested, FMP, Berlin, Germany). PCR products were then resolved by agarose gel electrophoresis, purified and digested with *AscI* restriction enzyme. Ligation with the vector backbone BK667 using the Quick Ligation Kit (NEB) produced an expression vector encoding the BK channel with an in-frame cpGFP insertion in the 667 site, BK667cpG. To generate the BK860cpG, constructs BK860Y and BK667cpG were digested with *AscI* to obtain the vector and the insert respectively. The products of the digestion were isolated by gel electrophoresis, purified and ligated using the Quick Ligation Kit from New England Biolabs. Positive subclones were confirmed by sequencing. Sequence of the BK channel showing the insertion sites can be seen in Fig. 3.1.

Este documento incorpora firma electrónica, y es copia auténtica de un documento electrónico archivado por la ULL según la Ley 39/2015.
Su autenticidad puede ser contrastada en la siguiente dirección <https://sede.ull.es/validacion/>

Identificador del documento: 1627512

Código de verificación: KOIBgUMu

Firmado por: Roger Gimeno Llobet UNIVERSIDAD DE LA LAGUNA	Fecha: 25/10/2018 11:00:30
Diego Álvarez de la Rosa Rodríguez UNIVERSIDAD DE LA LAGUNA	25/10/2018 11:52:58
Teresa Giráldez Fernández UNIVERSIDAD DE LA LAGUNA	25/10/2018 11:54:04
Ernesto Pereda de Pablo UNIVERSIDAD DE LA LAGUNA	29/10/2018 13:01:03

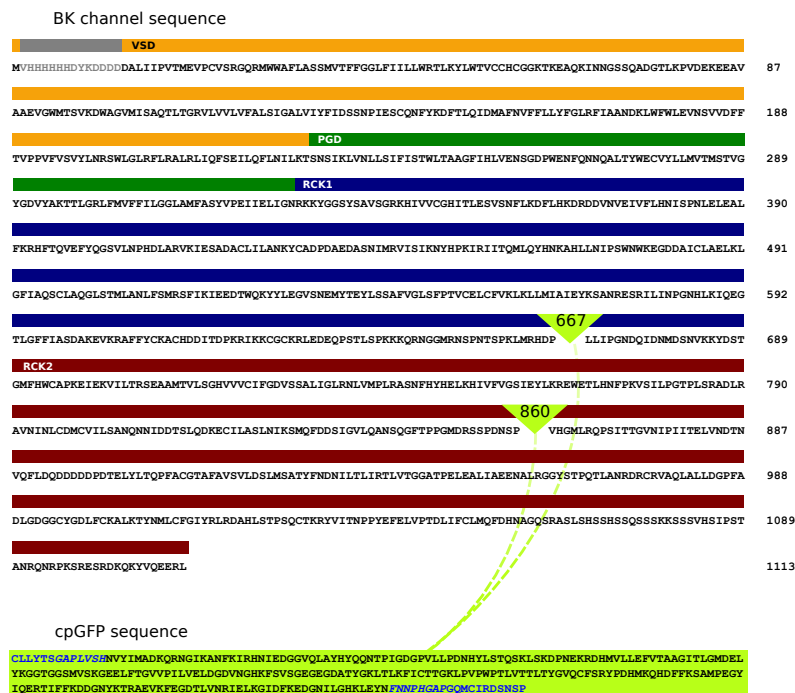


Figure 3.1: Sequence for BK667cpG and BK860cpG constructs, where the same cpGFP sequence (fluorescent green) is inserted in the 667 position or the 860 position (blue aminoacids in the cpGFP sequence are linkers). The secondary structure elements are indicated as color bars in the sequence; the voltage sensing domain (orange), the pore gate domain (green), the RCK1 domain (blue) and the RCK2 domain (red). The grey region at the beginning of the BK sequence are a His Tag and a Flag, and are not counted in the amino acid numbering.

3.2.2 Generation of BK Ca²⁺ mutants

The single Ca²⁺ mutants D99A, D362/7A and 5D5A of constructs BK667cpG and BK80cpG were created using QuikChange multi site-directed mutagenesis kit (Agilent Genomics). Forward primer F-D99A and the reverse primer R-D99A were used to generate constructs BK667cpG-D99A and BK860cpG-D99A, forward primer F-D362/7A and the reverse primer R-D362/7A were used to generate constructs BK667cpG-D362/7A and BK860cpG-D362/7A, and forward primer F-5D5A and the reverse primer R-5D5A were used to generate constructs BK667cpG-5D5A and BK860cpG-5D5A. Sequences of all primers are showed in **Table 3.1**. To generate the constructs containing the three mutations D99A, D362/7A and 5D5A (identified as triple mutants or TM), three round of PCR combining forward primer of the first mutation with reverse primer of the following mutation were performed (**Fig. 3.2**), as described in (Liang et al., 2012). The PCR products were ligated with In-fusion HD cloning from Takara. Positive subclones were confirmed by sequencing.

Este documento incorpora firma electrónica, y es copia auténtica de un documento electrónico archivado por la ULL según la Ley 39/2015. Su autenticidad puede ser contrastada en la siguiente dirección https://sede.ull.es/validacion/	
Identificador del documento: 1627512	Código de verificación: kOIBgUMu
Firmado por: Roger Gimeno Llobet UNIVERSIDAD DE LA LAGUNA	Fecha: 25/10/2018 11:00:30
Diego Álvarez de la Rosa Rodríguez UNIVERSIDAD DE LA LAGUNA	25/10/2018 11:52:58
Teresa Giráldez Fernández UNIVERSIDAD DE LA LAGUNA	25/10/2018 11:54:04
Ernesto Pereda de Pablo UNIVERSIDAD DE LA LAGUNA	29/10/2018 13:01:03

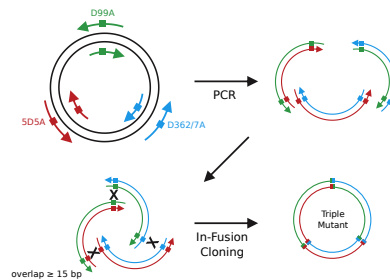


Figure 3.2: Multi-site directed mutagenesis. For constructs containing the three mutations D99A, D362/7A and 5D5A three round of PCR combining forward primer of the first mutation with reverse primer of the following mutation were performed. PCR products were ligated with In-fusion HD cloning. Image modified from (Liang et al., 2012).

3.2.3 Generation of BK Pore mutants

Pore mutant F315A, which uncouples voltage sensing from the pore domain, was introduced in constructs BK667cpG and BK80cpG using QuikChange multi site-directed mutagenesis kit (Agilent Genomics). Forward primer F-F315A and the reverse primer R-F315A (Table 3.1) were used to generate constructs BK667cpG-F315A and BK860cpG-F315A. PCR products were ligated with In-fusion HD cloning from Takara. Positive subclones were confirmed by sequencing.

3.2.4 Generation of BK isolated gating ring constructs

Plasmids expressing the isolated gating ring of BK channels were generated from constructs BK667C, BK667Y, BK860C and BK860Y. These constructs, obtained in previous work by Giraldez *et al.* (Giraldez, Hughes, and Sigworth, 2005), are based on the BK channel with CFP (C) or YFP (Y) insertions in specific sites of the channel (667 and 860 amino acidic positions), achieved using a transposon-based insertion technique. We generated a total of eight gating ring constructs, two variants of the gating ring length for each original construct. The two variants of the gating ring lengths were selected from (Wu et al., 2010; Javaherian et al., 2011). Resulting constructs were BKgr667C_j, BKgr667C_o, BKgr667Y_j, BKgr667Y_o, BKgr860C_j, BKgr860C_o, BKgr860Y_j and BKgr860Y_o. The added _j and _o at the end of each construct specifies the length of the gating ring, and stands for Jiang's (Wu et al., 2010) based gating ring (_j) and Olcese's (Javaherian et al., 2011) based gating ring (_o). Length of _j constructs is 2991 bp and length of _o constructs is 2835 bp. Forward primer F-BKgr1 and reverse primer R-BKgr1 amplified the gating ring of Olcese's based constructs. Forward primer F-BKgr1 and reverse primer R-BKgr2 amplified the gating ring of Jiang's based constructs. All primers had the restriction sites NotI at 3' and HindIII at 5'. Primer sequences can be seen in Table 3.1. Mammalian expression vector pcDNA3.1(+) (Invitrogen) was double digested with NotI and HindIII restriction enzymes. For the gating rings PCR was performed using a proof-reading thermostable DNA polymerase, PfuII Ultra (Agilent) following the manufacturer instructions. Plasmid fragments and PCR products were then resolved by agarose gel electrophoresis and purified with a commercial Kit (GE

Este documento incorpora firma electrónica, y es copia auténtica de un documento electrónico archivado por la ULL según la Ley 39/2015.
 Su autenticidad puede ser contrastada en la siguiente dirección <https://sede.ull.es/validacion/>

Identificador del documento: 1627512

Código de verificación: kOIBgUMu

Firmado por: Roger Gimeno Llobet UNIVERSIDAD DE LA LAGUNA	Fecha: 25/10/2018 11:00:30
Diego Álvarez de la Rosa Rodríguez UNIVERSIDAD DE LA LAGUNA	25/10/2018 11:52:58
Teresa Giráldez Fernández UNIVERSIDAD DE LA LAGUNA	25/10/2018 11:54:04
Ernesto Pereda de Pablo UNIVERSIDAD DE LA LAGUNA	29/10/2018 13:01:03

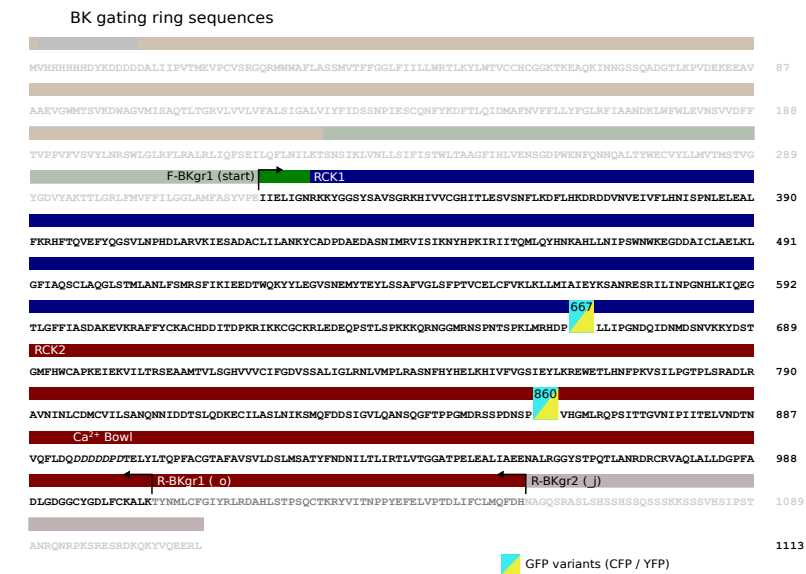


Figure 3.3: Secondary structure of the human BK. The gating ring constructs BKgr667/860/C/Y_o starts at amino acids IIE and ends at amino acids ALK. The other gating ring constructs BKgr667/860C/Y_j starts at the same amino acids and ends at amino acids FDH. F-BKgr1, R-BKgr1 and R-BKgr2 are the primers utilized and can be seen in Table 3.1.

Healthcare Life Sciences). The purified PCR fragments containing the gating rings were digested with NotI and HindIII (New England Biolabs) restriction enzymes and cloned into the pcDNA3.1(+) backbone with Fast-link DNA ligation kit (Epicentre). A volume of 2.5 μ l of the reaction was transformed into TOP10 competent cells. A volume of 50 μ l of the culture was spread in a LB agar plate with 100 microgr/ml ampicillin. Colonies were picked and the plasmids obtained by MINIpiprep (Macherey-Nagel) sent to sequencing. Sequence of the BK gating ring constructs showing the different lengths can be seen in Fig. 3.3.

3.3 BK-CpGFP characterization

To obtain the emission spectrum of cpGFP-based constructs, 24h after transfection, HEK293T cells grown in 8 well LAB-TEK chamber slides were bathed with Standard Saline Medium (SSM, Table 3.2) and imaged in a Leica SP8 confocal microscope equipped with a objective 63x Plan APO 1.4 NA oil. Wavelength profiles were obtained with the module lambda-scan, where excitation wavelength was 488 nm and the detection window set from 498 to 600 nm.

To obtain the G-V curves and representative currents for BK-cpG constructs and for wild-type BK, After 24h of transfection, cells grown in glass bottom dishes (Ibidi) were bathed with intracellular solution (IS, Table 3.2). Samples were imaged on a NIKON Eclipse Ti-U microscopy, equipped with a Lumencor Spectra X LED with a 470 nm line, a 20x dry NA 0.40 objective, ET-EGFP (Chroma) filter cube and a iXon

Este documento incorpora firma electrónica, y es copia auténtica de un documento electrónico archivado por la ULL según la Ley 39/2015.
 Su autenticidad puede ser contrastada en la siguiente dirección <https://sede.ull.es/validacion/>

Identificador del documento: 1627512

Código de verificación: kOIBgUMu

Firmado por: Roger Gimeno Llobet UNIVERSIDAD DE LA LAGUNA	Fecha: 25/10/2018 11:00:30
Diego Álvarez de la Rosa Rodríguez UNIVERSIDAD DE LA LAGUNA	25/10/2018 11:52:58
Teresa Giráldez Fernández UNIVERSIDAD DE LA LAGUNA	25/10/2018 11:54:04
Ernesto Pereda de Pablo UNIVERSIDAD DE LA LAGUNA	29/10/2018 13:01:03

3.3. BK-CpGFP characterization

27

Table 3.1: Oligonucleotides used in the study.

Name	Sequence
F-cpGFP	TCATGGCGCGCCTCTGGTGAGCCAC
R-cpGFP	TCAGGGCGCGCCAAGGGGTTGTTAAA
F-D99A	ACCTCCGTGAAGGCCTGGGCGGGG
R-D99A	CCCCCGCCAGGCCTTCACGGAGGT
F-D362/7A	TTCCTGAAGGCTTTTCTGCACAAGGCTCGGGATGACGTC
R-D362/7A	GACGTCATCCCGAGCCTTGTGCAGAAAAGCCTTCAGGAA
F-5D5A	GTTCAGTTTTTGGACCAAGCCGCTGCTGCTGCCCTGATACAGAAGTGTAC
R-5D5A	GTACAGTTCGTATCAGGGGCAGCAGCAGCGGCTTGGTCCAAAAACTGAAC
F-F315A	GGACTGGCCATGGCTGCCAGCTACGTC
R-F315A	GACGTAGCTGGCAGCCATGGCCAGTCC
F-BKgr1	CCTAAGCTTGCCACCATGATCATAGAGTTAATAGGAAACCGC
R-BKgr1	TTAGCGGCCGCTCATTTCAGAGCTTGCAGAACAGATC
R-BKgr2	TTAGCGGCCGCTCAGTGGTCAAAGTGCATTAAGCAG
F-cpGFP_NSP	CCAGATAACAGCCCCCTGGTGAGCCACAACGTCTATATC
R-cpGFP_NSP	GTGCACTGGGCTGTTGGGGTTGTTAAAGTTGTACTCC
F-cpGFP_VVC	CCAGATAACAGCCCCVVCVVCVVCCTGGTGAGCCACAACGTCTATATC
R-cpGFP_VVC	TAACATCCCGTGCACVVCVVCVVCVCGGGGTTGTTAAAGTTGTACTCC
F-5'BK	GTACCATGGTGCATCACCATCACCATCACG
R-5'BK	GGGGCTGTTATCTGGAGAGGATC
F-3'BK_NSP	AACAGCCCAGTGCACGGGATGTTACG
F-3'BK_VHG	GTGCACGGGATGTTACGTCAACC
R-3'BK	AGCTTTCAAATGCTTCGCAATAC
F-pBNJ13	AGCATTTGAAAAGCTTACTAGTGATGCATATTCTATAG
R-pBNJ13	TGGTGATGCACCATGGTACCTGCAGGCGTACCTTC

Este documento incorpora firma electrónica, y es copia auténtica de un documento electrónico archivado por la ULL según la Ley 39/2015.
 Su autenticidad puede ser contrastada en la siguiente dirección <https://sede.ull.es/validacion/>

Identificador del documento: 1627512

Código de verificación: KOIBgUMu

Firmado por: Roger Gimeno Llobet UNIVERSIDAD DE LA LAGUNA	Fecha: 25/10/2018 11:00:30
Diego Álvarez de la Rosa Rodríguez UNIVERSIDAD DE LA LAGUNA	25/10/2018 11:52:58
Teresa Giráldez Fernández UNIVERSIDAD DE LA LAGUNA	25/10/2018 11:54:04
Ernesto Pereda de Pablo UNIVERSIDAD DE LA LAGUNA	29/10/2018 13:01:03

Table 3.2: Saline and media used in the study.

Name	Composition (mM)
Standard Saline Medium	145 NaCl, 1 KCl, 1 MgCl ₂ , 10 Glucose, 10 HEPES, 5 Ca ²⁺ (pH7.4)
Intracellular Solution	80 KMeSO ₃ , 60 N-Methylglucamine-MeSO ₃ , 2 KCl, 20 HEPES, 1 H-EDTA* (pH7.4)
Pipette Solution	135 KCl, 3.5 MgCl ₂ , 2 Na ₂ ATP, 5 HEPES, 0.1 EGTA (pH7.4)
Lysis Buffer Microsomes	Intracellular Solution + 1.7% Sucrose (pH7.4)
Imaging Buffer	100 B-mercaptoethylamine (MEA), 0.56 mg/ml glucose oxidase, 34 µg/ml catalase, 50 Tris-HCl, 10 NaCl, 10% glucose (w/v) (pH8)

In the Intracellular solution, when $[Ca^{2+}] < 100 \mu M$ H-EDTA is present; for $[Ca^{2+}] \geq 100$ no H-EDTA is added to the solution.

Ultra 888 EMCCD camera (Andor). Inside-out patches were excised from fluorescent cells and recorded using a patch clamp setup, consisting of an Axopatch 200B amplifier and a Clampex software (Molecular Devices) to acquire the data, and a Digidata 1550A with 1-channel HumSilencer (Molecular Devices) to digitalize the records. Pipette solution is described in Table 3.2. All electrophysiology data was analyzed with pCLAMP 10.6 software (Molecular Devices).

All data was processed with custom-made Python scripts to plot the figures.

3.4 Ionomycin-mediated Ca²⁺ loading

Imaging

24h after transfection, cells grown in 8 well LAB-TEK chamber slides were bathed with Standard Saline Medium (SSM, Table 3.2). The samples were imaged on a NIKON Eclipse Ti-S microscopy equipped with a Nikon LU-NV Laser Unit, a S Plan Fluor 20x dry NA 0.45 objective, a ET-EGFP (Chroma) filter cube and a Hamamatsu ORCA-Flash 4.0 CMOS camera. Images in 12-bit format with 1 Hz scanning frequency were collected during a time-lapse. After about 1 minute from start, and after verifying that the baseline fluorescence was stable, 15 µM ionomycin (Sigma-Aldrich) was added into the well.

Experiments with carbachol has been performed as described, but sequential applications of 100 µM carbachol (Sigma-Aldrich), 15 µM ionomycin (Sigma-Aldrich) and 1 mM H-EDTA (Sigma-Aldrich) were added to the cells.

Data analysis

Nikon *nd2* files were imported into Fiji (ImageJ2, NIH) with the Bioformats plugin. Cells in the field were selected as Regions Of Interest (ROI), and the fluorescence intensity of ROIs over the time course was obtained with the Time Series Analyzer V3 plugin and saved in a *txt* file. The data from the *txt* file was then analyzed with a custom-build Python¹ program, in order to extract information relative to the changes in the fluorescence intensity ($\Delta F/F$, τ , $t_{1/2}$), perform statistical analysis

¹The programming language Python can be (and is frequently) used for scientific applications employing external libraries, mainly Numpy, Scipy and Matplotlib.

Este documento incorpora firma electrónica, y es copia auténtica de un documento electrónico archivado por la ULL según la Ley 39/2015.
 Su autenticidad puede ser contrastada en la siguiente dirección <https://sede.ull.es/validacion/>

Identificador del documento: 1627512

Código de verificación: KOIBgUMu

Firmado por:	Fecha:
Roger Gimeno Llobet UNIVERSIDAD DE LA LAGUNA	25/10/2018 11:00:30
Diego Álvarez de la Rosa Rodríguez UNIVERSIDAD DE LA LAGUNA	25/10/2018 11:52:58
Teresa Giráldez Fernández UNIVERSIDAD DE LA LAGUNA	25/10/2018 11:54:04
Ernesto Pereda de Pablo UNIVERSIDAD DE LA LAGUNA	29/10/2018 13:01:03

3.5. Ca²⁺- and pH-titrations

29

and plot the results. Statistical analyses are also performed with Prism (Graphpad Software).

To determine the characteristics of the fluorescence response, the fluorescence intensity profiles over time of the selected ROIs were analyzed fitting the profiles to a sigmoid function of the form:

$$y(x) = \frac{y_{max} - y_{min}}{1 + \exp(-(x - t_{1/2})/\tau)} + y_{min} \quad (3.1)$$

where y_{max} and y_{min} are the maximum and minimum fluorescence intensity values, τ is the slope of the curve and $t_{1/2}$ the time where the fluorescence intensity is halfway between y_{min} and y_{max} .

Constructs displaying a biphasic shape in the fluorescence response were analyzed fitting a sigmoid in each phase. The same information as before was extracted and identified with a subscript 1 or a subscript 2 to denote the first or the second phase respectively.

3.5 Ca²⁺- and pH-titrations

Generation of microsomes

After 24h-48h of transfection, HEK2913T cells grown in P-6 plates were washed twice with PBS, scraped, and centrifuged at 1000 G during 5 minutes. Pellet was resuspended in lysis buffer (Table 3.2) and 1 mM H-EDTA or 100 μ M Ca²⁺ if it was for Ca²⁺ titration or pH titration respectively) and homogenized with a syringe and a 25g needle. The homogenate solution was adjusted to 8% sucrose and centrifuged at 1000 G during 10 minutes. Finally the supernatant containing microsomes was recovered.

Imaging

The solution containing microsomes was imaged in a fluorescence spectrophotometer (Cary Eclipse, Agilent). A volume of 3 ml was added from each condition to fluorimeter cuvettes. In order to permeate all microsomes to Ca²⁺ an H⁺ ions, 5 min before the experiment 15 μ M ionomycin was added to the cuvette. Excitation was set to 488 nm, and detection range to 510 \pm 5 nm.

Ca²⁺ titrations

For Ca²⁺ titration experiments, different Ca²⁺ concentrations ranging from Ca²⁺ free to 1 mM Ca²⁺ were calculated using MaxChelator program (web.stanford.edu). Calculated amounts of Ca²⁺ were added to the cuvette from a 0.1 M Ca²⁺ stock (Calcium Standard, Orion ionplus Application Solution, Thermo Fisher).

pH titrations

pH titrations were performed by adding fixed amounts of NaOH. The solutions containing the microsomes were previously brought to an acidic pH of 4.30 with HCl.

Este documento incorpora firma electrónica, y es copia auténtica de un documento electrónico archivado por la ULL según la Ley 39/2015.
 Su autenticidad puede ser contrastada en la siguiente dirección <https://sede.ull.es/validacion/>

Identificador del documento: 1627512

Código de verificación: kOIBgUMu

Firmado por:	Fecha:
Roger Gimeno Llobet UNIVERSIDAD DE LA LAGUNA	25/10/2018 11:00:30
Diego Álvarez de la Rosa Rodríguez UNIVERSIDAD DE LA LAGUNA	25/10/2018 11:52:58
Teresa Giráldez Fernández UNIVERSIDAD DE LA LAGUNA	25/10/2018 11:54:04
Ernesto Pereda de Pablo UNIVERSIDAD DE LA LAGUNA	29/10/2018 13:01:03

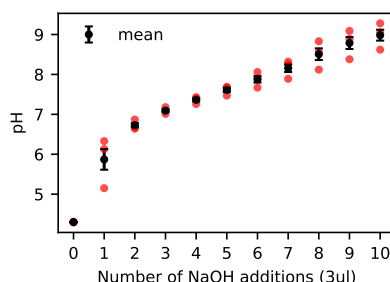


Figure 3.4: Calibration of pH with a pH-meter ; NaOH additions for pH-titration curves. We used three samples with the same conditions as for the experiments (red dots) to calculate the average pH values after each NaOH application.

With sequential additions of NaOH the solutions were progressively brought from 4.30 to 8.5-9. Extra samples were prepared in order to calculate the change in pH by the addition of 3 μ l of 1M NaOH before the experiment in the fluorimeter. With these replica samples the process was the same as in the experimental samples, but instead of measuring fluorescence intensity the pH was measured using a pH-meter (SevenEasy, Mettler Toledo) (Fig. 3.4). After three independent measurements, data was averaged and used as the change in pH for each addition of NaOH.

Data analysis

Data was processed from txt files created by the Cary Eclipse module Kinetics. Each file contained time and fluorescence intensity. The fluorescence was paired with the calculated $[Ca^{2+}]$ or pH. The resulting distribution of data points was then fitted to a sigmoidal dose-response equation

$$y(x) = \frac{T - B}{1 + 10^{(\log_{10}(Kd) - x)n_H}} + B \quad (3.2)$$

where T and B are the top and bottom intensity values, Kd is the x value when the response is halfway between bottom and top and n_H is the Hill slope and describes the steepness of the curve. This analysis was performed using custom scripts written in Python3. For pH-titrations, the fluorescent changes registered in the fluorimeter were represented in a plot in function of the pH changes previously calculated with the pH-meter.

3.6 Patch-clamp fluorometry

After 24h of transfection, cells grown in glass bottom dishes (Ibidi) were bathed with intracellular solution (IS, Table 3.2). Samples were imaged on a NIKON Eclipse Ti-U microscopy, equipped with a Lumencor Spectra X LED with a 470 nm line, a 20x dry NA 0.40 objective, ET-EGFP (Chroma) filter cube and a iXon Ultra 888 EM-CCD camera (Andor). Inside-out patches were excised from fluorescent cells and recorded using a patch clamp setup, consisting of an Axopatch 200B amplifier and

Este documento incorpora firma electrónica, y es copia auténtica de un documento electrónico archivado por la ULL según la Ley 39/2015.
 Su autenticidad puede ser contrastada en la siguiente dirección <https://sede.ull.es/validacion/>

Identificador del documento: 1627512

Código de verificación: kOIBgUMu

Firmado por:	Fecha:
Roger Gimeno Llobet UNIVERSIDAD DE LA LAGUNA	25/10/2018 11:00:30
Diego Álvarez de la Rosa Rodríguez UNIVERSIDAD DE LA LAGUNA	25/10/2018 11:52:58
Teresa Giráldez Fernández UNIVERSIDAD DE LA LAGUNA	25/10/2018 11:54:04
Ernesto Pereda de Pablo UNIVERSIDAD DE LA LAGUNA	29/10/2018 13:01:03

3.7. BK-cpGFP linker optimization

31

a Clampex software (Molecular Devices) to acquire the data, and a Digidata 1550A with 1-channel HumSilencer (Molecular Devices) to digitalize the records. Pipette solutions is described in **Table 3.2**. Images of the membrane patch at the tip of the pipette were collected in 8 bit format with 1 Hz scanning frequency. The recordings were synchronized with the amplifier using remote control through Digidata TTL-Outputs (Tansistor-Transistor Logic), allowing simultaneous register of current and fluorescence. All electrophysiology data was analyzed with pCLAMP 10.6 software (Molecular Devices). Fluorescence data was analyzed with ImageJ Time Series Analyzer V3 plugin.

3.7 BK-cpGFP linker optimization

As explained in the introduction, allosteric coupling between cpGFP and the biosensor (in this case the BK channel) resulting in a change in fluorescence emission can be improved by altering linker sequences between both modules (Nadler et al., 2016). The BK860cpG sensors were therefore optimized by varying the length and/or amino acid composition of the linkers between BK and cpGFP.

NSP optimization

The first optimization performed was to shorten the linkers between the BK and the cpGFP (**Fig. 3.5 middle**). Forward primer F-cpGFP_NSP and reverse primer R-cpGFP_NSP (**Table 3.1**) were used to amplify the cpGFP of construct BK667cpG construct. BK was amplified from BK860cpG plasmid with forward primer F-5'BK and reverse primer R-5'BK and forward primer F-3'BK_NSP and reverse primer R-3'BK. The backbone pBNJ13.1 was amplified with forward primer F-pBNJ13 and reverse primer R-pBNJ13. The purified PCR fragments were cloned together with In-fusion (Clontech); all fragments overlapped 15 bd. A volume of 2.5 μ l of the reaction was transformed into TOP10 competent cells. All the culture volume was spread in a LB agar plate with ampicillin. Colonies were picked and the plasmid obtained by MINIpiprep (Macherey-Nagel) sent to sequence.

VVC optimization

The other optimization performed on BK860cpG sensor was the substitution of the original linkers for three random amino acids encoded by the degenerate codon VVC (where V=A/C/G) repeated three times between the cpGFP and the BK (**Fig. 3.5 bottom**). The forward primer F-cpGFP_VVC and the reverse primer R-cpGFP_VVC (**Table 3.1**) were designed introducing three repetitions of the degenerate VVC codons on both 5'- and 3'- ends of the amplified cpGFP template (Nadler et al., 2016). The overlapping BK and cpGFP fragments were obtained, cloned and transformed as in NSP optimization, except for the fragment of BK from 860 position to end of BK, that was amplified with forward primer F-3'BK_VHG and reverse primer R-3'BK (**Table 3.1**). To randomly screen all the possible combinations, all the culture volume was spread in LB agar plates with ampicillin. All colonies were picked, plasmids were purified by MINIpiprep, and transfected into HEK293T cells in 96-well plates. To determine the change in fluorescence $\Delta F/F$, the 96-well plates were screened using a Perkin Elmer Victor X multi-well plate reader before and after adding ionomycin

Este documento incorpora firma electrónica, y es copia auténtica de un documento electrónico archivado por la ULL según la Ley 39/2015.
 Su autenticidad puede ser contrastada en la siguiente dirección <https://sede.ull.es/validacion/>

Identificador del documento: 1627512

Código de verificación: kOIBgUMu

Firmado por:	Fecha:
Roger Gimeno Llobet UNIVERSIDAD DE LA LAGUNA	25/10/2018 11:00:30
Diego Álvarez de la Rosa Rodríguez UNIVERSIDAD DE LA LAGUNA	25/10/2018 11:52:58
Teresa Giráldez Fernández UNIVERSIDAD DE LA LAGUNA	25/10/2018 11:54:04
Ernesto Pereda de Pablo UNIVERSIDAD DE LA LAGUNA	29/10/2018 13:01:03

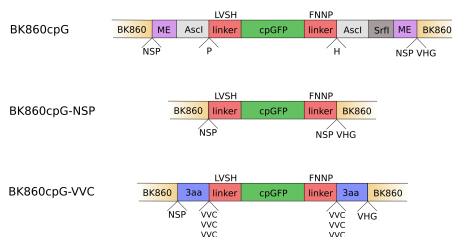


Figure 3.5: In the BK860cpG (upper sequence), the linker peptide sequences between BK channel (orange) and the cpGFP (green) are a mosaic end (ME, purple) and an Ascl or Ascl/SrfI restriction sites (grey). The linkers LVSH and FNNP (red) are the original linkers of the cpGFP. Optimization BK860cpG-NSP (middle sequence): all the sequence between BK channel and the original linkers are removed. Optimization BK860cpG-VVC (bottom sequence): Between the BK channel and the cpGFP are inserted three random amino acids.

to each well. The constructs with higher $\Delta F/F$ were sequenced and used for further characterization.

3.8 Whole cell patch-clamp and fluorometry

HEK293 cells were grown on poly-L-lysine coated coverslips and 24 to 48 h after transfection whole cell currents (voltage-clamp configuration) or membrane potential (current-clamp configuration) were recorded at room temperature (25°C) using an Axopatch 200B amplifier. Cells were perfused with an extracellular solution (Standard Saline Medium, **Table 3.2**). Patch recording pipettes (3–6M Ω) were filled with Pipette solution (**Table 3.2**). The data were sampled at 5 kHz with a Digidata 1550A with 1-channel HumSilencer A/D converter (Molecular Devices) and filtered at 2 kHz. HEK293 cells were voltage clamped at –60 mV and cells with a series resistance >20M Ω or with more than 20% changes in series resistance during the experiment were discarded. Data was recorded with pCLAMP 10.6 software (Molecular Devices). Simultaneously, and synchronized with the electrophysiology recordings through Digidata TTL-Outputs, cell fluorescence was imaged (3.3 Hz scanning frequency) on a NIKON Eclipse Ti-U microscopy, equipped with a Lumencor Spectra X LED with a 470 nm line, a 40x dry NA 0.65 objective, ET-EGFP (Chroma) filter cube and a iXon Ultra 888 EMCCD camera (Andor). Micro-Manager Open Source Microscopy Software was used for fluorescence data acquisition. All electrophysiology data was analyzed with pCLAMP 10.6 software (Molecular Devices). Fluorescence data was analyzed with ImageJ Time Series Analyzer V3 plugin.

Este documento incorpora firma electrónica, y es copia auténtica de un documento electrónico archivado por la ULL según la Ley 39/2015.
 Su autenticidad puede ser contrastada en la siguiente dirección <https://sede.ull.es/validacion/>

Identificador del documento: 1627512

Código de verificación: kOIBgUMU

Firmado por: Roger Gimeno Llobet UNIVERSIDAD DE LA LAGUNA	Fecha: 25/10/2018 11:00:30
Diego Álvarez de la Rosa Rodríguez UNIVERSIDAD DE LA LAGUNA	25/10/2018 11:52:58
Teresa Giráldez Fernández UNIVERSIDAD DE LA LAGUNA	25/10/2018 11:54:04
Ernesto Pereda de Pablo UNIVERSIDAD DE LA LAGUNA	29/10/2018 13:01:03

3.9 Direct stochastic optical reconstruction microscopy

Sample preparation

We used the following primary antibodies: mouse anti-BK (ab99046), rabbit anti-Cav2.1 α (ab32642) and anti-Cav2.3 α (ab63705) from Abcam (Cambridge, United Kingdom). Secondary antibodies were goat anti-rabbit conjugated to Alexa Fluor 647 (A21245) or Alexa Fluor 488 (A11008), and goat anti-mouse conjugated to Alexa Fluor 647 (A32728) or Alexa Fluor 488 (A11001) from Invitrogen (Oregon, US). Specificity of the primary antibodies was assessed by transfecting or not cDNA in HEK293T and subsequent immunocytochemistry. Samples that were not labeled with primary antibody but incubated with secondary antibody were evaluated as non-antigenic controls in validation as well.

All steps during sample preparation were performed at room temperature. Cells transfected with BK or BK860cpG and Cav2.1 or Cav2.2 were fixed for 10 min with 3% paraformaldehyde + 0.1% glutaraldehyde (Electron Microscopy Sciences, EM grade) diluted in PBS. Cells were then reduced with 0.1 % NaBH₄ in PBS for 7 min at room temperature to mitigate cell auto-fluorescence. Next, cells were washed 3 times with PBS (5 min per wash) and then permeabilized with 0.2 % Triton X-100 in PBS for 15 min. Afterwards, cells were blocked for 90 min with 10 % Normal Goat Serum (NGS) supplemented with 0.05 % Triton X-100 in PBS and subsequently incubated with primary antibodies diluted in 5 % NGS + 0.05 % Triton X-100 in PBS for 60 min. Samples were washed 5 times with 1 % NGS + 0.05 Triton X-100 in PBS for 10 min per wash. After that, cells were incubated with secondary antibodies diluted in 5 % NGS + 0.05 % Triton X-100 in PBS for 60 min. Samples were washed again 5 times with 1 % NGS + 0.05 Triton X-100 in PBS for 10 min per wash and once with PBS for 5 min. Finally, cells were post-fixed with 3 % PFA with 0.1 % glutaraldehyde for 10 min and rinsed 3 times with PBS, 5 minutes per wash. Samples were stored in PBS at 4°C until used.

Imaging (dSTORM)

Before the experiment, Imaging Buffer (Table 3.2) was added to the samples. STORM imaging was performed on a Nikon N-STORM super-resolution system (Nikon Instruments Inc.) with a Nikon Eclipse Ti inverted microscope equipped with a HP Apo TIRF 100x oil NA 1.49 objective (Nikon). Reporter dyes Alexa Fluor-647 and Alexa Fluor-488 were stimulated with the appropriate laser lines. Fluorescence emission was filtered with a 405/488/561/640nm Laser Quad Band filter cube (TRF89901; Chroma) and collected by an ORCA-Flash4.0 V2 Digital CMOS camera C11440 (Hamamatsu) at a frame rate of 50 Hz (20 ms exposure time). An additional lens was placed into the detection path generating a final pixel size of 80 nm. All images were taken in TIRF (total internal reflection fluorescence) mode to restrict laser illumination to a thin sheet close to the plasma membrane in order to achieve a high signal-to-noise ratio.

A total of 50000 frames (25000 per each channel) was acquired and used to generate the reconstructed images utilizing the NIS-Elements software (Nikon). Image resolution was estimated using a method based on Fourier ring correlation as described elsewhere [26] [27] and was determined to be 42 ± 6 nm for Alexa Fluor 647 and 39 ± 7 nm for Alexa Fluor 488 emitter localizations. Reconstructed images were filtered to remove background localizations, facilitating the display of protein clustering using a density filtering procedure provided by NIS-Elements software.

Este documento incorpora firma electrónica, y es copia auténtica de un documento electrónico archivado por la ULL según la Ley 39/2015.
 Su autenticidad puede ser contrastada en la siguiente dirección <https://sede.ull.es/validacion/>

Identificador del documento: 1627512

Código de verificación: kOIBgUMu

Firmado por:	Fecha:
Roger Gimeno Llobet UNIVERSIDAD DE LA LAGUNA	25/10/2018 11:00:30
Diego Álvarez de la Rosa Rodríguez UNIVERSIDAD DE LA LAGUNA	25/10/2018 11:52:58
Teresa Giráldez Fernández UNIVERSIDAD DE LA LAGUNA	25/10/2018 11:54:04
Ernesto Pereda de Pablo UNIVERSIDAD DE LA LAGUNA	29/10/2018 13:01:03

Briefly, this filtering process permits to define the maximum neighborhood of localization (radius) as well as the minimum number of localizations needed to constitute a cluster (count) in the rendered images. In our experimental conditions, a density filtering of 60 nm radius with a count of 10 molecules was found to fit best the clustering properties of the samples. The single localizations that did not meet the requisites were considered as background noise and were eliminated from the final images.

dSTORM data analysis

Superresolution images obtained by dSTORM were analyzed with custom made scripts developed in Python. The details concerning script function and type of analysis performed is explained in **Chapter 4: Section 4.9.1**.

3.10 Isolated gating ring

FRET measurements using the acceptor photobleaching technique

To obtain FRET efficiencies, transfected HEK293T cells with the gating ring constructs were imaged in a Leica SP8 confocal microscope. Prior to imaging, cells grown in 12 mm cover-slips placed in a P-12 plate were moved to an imaging chamber (Warner Instruments) with Standard Saline Medium (SSM, **Table 3.2**) with 2 mM Ca^{2+} . FRET efficiencies were measured with the Acceptor Photobleaching (AB) technique, with the specific AB software module in the Leica SP8. To bleach the donor molecule (YFP), 8 bleaching steps at 80% power of the 514 nm laser line were performed in a selected region of interest (ROI). The software automatically outputs information of the FRET efficiency and donor and acceptor pre- and post-bleach intensities, as well as a FRET image with a custom look-up table (LUT) ranging from 0% to 100% FRET efficiency. FRET efficiency can be calculated using **Eq. ??**.

Fluorescence lifetimes: Time-Related Single Photon Counting (TCSPC)

A high-performance fluorescence spectrometer (LifeSpec II, Edinburgh Instruments) was used for fluorescence lifetime measurements employing the time-correlated single photon counting (TCSPC) technique. Transfected HEK293T cells with BKgr860CY, ECFP and CGY constructs were grown in P-6 plates. After 24h of transfection, cells were resuspended in Standard Saline Medium (**Table 3.2**) with 2 mM Ca^{2+} , and 2 ml of each construct placed in the spectrometer cuvettes. During the experiment, and because of the absence of a magnetic mixer, several pauses were done to resuspend the cells. For lifetime experiments with BKgr860CY construct, after the lifetime of the donor was measured, 15 μM ionomycin was added to the cuvette, mixed, and then the experiment was performed again. The samples were excited with a 405 nm picosecond pulsed diode laser. The lifetime data were analyzed with the software FAST (Edinburgh Instruments) and with custom-made scripts written in Python. All lifetime decays were fitted to multi-exponential model using the expression,

$$I(t) = a_1 e^{-t/\tau_1} + a_2 e^{-t/\tau_2} \quad (3.3)$$

Este documento incorpora firma electrónica, y es copia auténtica de un documento electrónico archivado por la ULL según la Ley 39/2015.
 Su autenticidad puede ser contrastada en la siguiente dirección <https://sede.ull.es/validacion/>

Identificador del documento: 1627512

Código de verificación: kOIBgUMu

Firmado por:	Fecha:
Roger Gimeno Llobet UNIVERSIDAD DE LA LAGUNA	25/10/2018 11:00:30
Diego Álvarez de la Rosa Rodríguez UNIVERSIDAD DE LA LAGUNA	25/10/2018 11:52:58
Teresa Giráldez Fernández UNIVERSIDAD DE LA LAGUNA	25/10/2018 11:54:04
Ernesto Pereda de Pablo UNIVERSIDAD DE LA LAGUNA	29/10/2018 13:01:03

3.11. BK cryo-EM structure analysis

35

were $I(t)$ is the fluorescence intensity at a given time t , a_1 and a_2 are the initial amplitudes (initial photon counts) of the two exponentials and τ_1 and τ_2 are the lifetimes of the two exponentials. The fractional contribution (f_i) of each exponential $i = 1, 2$ is given by,

$$f_i = a_i \tau_i \quad (3.4)$$

and the average lifetime by,

$$\bar{\tau} = f_1 \tau_1 + f_2 \tau_2 \quad (3.5)$$

The efficiency of the energy transfer can be determined with eq.4. The distance r between donor and acceptor molecules can be calculated by

$$r = R_0 \left(\frac{\tau_D}{\tau_{DA}} - 1 \right)^{-1/6} \quad (3.6)$$

For the FRET pair CFP-YFP the Förster distance is $R_0 = 4.92 \pm 0.10$ nm (Patterson, Piston, and Barisas, 2000).

3.11 BK cryo-EM structure analysis

We used the *Aplysia Californica* BK channel Cryo-EM structures deposited in the Protein Data Bank with accession numbers 5TJ6 and 5TJI (www.rcsb.org), corresponding to the open state of the channel in the presence of 10 mM Ca^{2+} and 10 mM Mg^{2+} , and the closed state of the channel in the presence of 1 mM EDTA. We used the program Chimera (UCSF) to superimpose the two structures, using the match command to specify the atoms of the two structures to pair. The superimposition of the two conformations was aligned by their selectivity filters, pairing V277, G278 and F279 residues. After pairing the new positions of residues, structures were exported to .cif files containing the X, Y and Z positions of all the atoms. The distances between the $\text{C}\alpha$ for each residue between the structures were calculated with a home-made script written in Python.

The resolved residue with the largest distance where we had a GFP variant insertion was in amino acid position 965 (BK965C) was obtained in previous work by Giraldez *et al.* (Giraldez, Hughes, and Sigworth, 2005). We subcloned the cpGFP from construct BK667cpG into construct BK965C as described in **Subsection 3.2.1**. Ca^{2+} loading experiments with ionomycin of construct BK965cpG were carried out as described in **Section 3.4**.

Este documento incorpora firma electrónica, y es copia auténtica de un documento electrónico archivado por la ULL según la Ley 39/2015.
 Su autenticidad puede ser contrastada en la siguiente dirección <https://sede.ull.es/validacion/>

Identificador del documento: 1627512

Código de verificación: kOIBgUMu

Firmado por:	Fecha:
Roger Gimeno Llobet UNIVERSIDAD DE LA LAGUNA	25/10/2018 11:00:30
Diego Álvarez de la Rosa Rodríguez UNIVERSIDAD DE LA LAGUNA	25/10/2018 11:52:58
Teresa Giráldez Fernández UNIVERSIDAD DE LA LAGUNA	25/10/2018 11:54:04
Ernesto Pereda de Pablo UNIVERSIDAD DE LA LAGUNA	29/10/2018 13:01:03



Este documento incorpora firma electrónica, y es copia auténtica de un documento electrónico archivado por la ULL según la Ley 39/2015.
Su autenticidad puede ser contrastada en la siguiente dirección <https://sede.ull.es/validacion/>

Identificador del documento: 1627512

Código de verificación: kOIBgUMu

Firmado por:	Fecha:
Roger Gimeno Llobet UNIVERSIDAD DE LA LAGUNA	25/10/2018 11:00:30
Diego Álvarez de la Rosa Rodríguez UNIVERSIDAD DE LA LAGUNA	25/10/2018 11:52:58
Teresa Giráldez Fernández UNIVERSIDAD DE LA LAGUNA	25/10/2018 11:54:04
Ernesto Pereda de Pablo UNIVERSIDAD DE LA LAGUNA	29/10/2018 13:01:03

Chapter 4

Results

4.1 BK-cpGFP constructs emission spectra and channel function

The requirement of having to transfect two plasmids (a CFP-tagged subunit and a YFP-tagged subunit) has some disadvantages. Particularly, it restricts the experimental conditions to heterologous expression systems. A major concern regarding FRET donor and acceptor fluorophores being in separate subunits is the non-fixed stoichiometry. After transfection of both CFP- and YFP-labeled subunits, the ratio of donor and acceptor expression and tetramerization is no longer fixed, producing different tetramer donor-acceptor compositions and distinct contributions to the measured FRET signal. The transfection stoichiometry used in previous FRET experiments with the CFP- and YFP-labeled BK gating ring subunits was 3:1. In this way, the expressed subunit combination with highest probability is 3CFP:1YFP, followed by 1CFP:3YFP and 2CFP:2YFP; in these conditions, 0CFP:4YFP nor 4CFP:0YFP combinations do not contribute to FRET efficiency (Miranda et al., 2013). Finally, the limited signal intensity produced by these FRET constructs make it difficult to measure rapid variations in the Ca^{2+} concentrations in restricted subcellular domains in which a good temporal and spatial resolution is needed (Tian et al., 2009). To overcome these issues, we generated new fluorescent BK constructs using a circularly permuted Green Fluorescent Protein (cpGFP). It has been demonstrated that Ca^{2+} indicators designed with cpGFP give much larger fluorescent changes than FRET-based Ca^{2+} indicators (Nakai, Ohkura, and Imoto, 2001; Nagai et al., 2001; Tian et al., 2009). As described in Materials and Methods, we inserted a cpGFP into 667 and 860 sites of the BK channel (Fig. 3.1).

Fig. 4.1A shows representative images of the structures with the cpGFP close to each insertion site. The fluorescence emission spectra (Fig. 4.1B) for BK667cpG and BK860cpG showed no differences compared to the GluA2_391cpGFP, the construct where the cpGFP was extracted (courtesy of Dr. Andrew Plested, FMP, Berlin, Germany). This construct consists of an AMPA receptor with an insertion of a cpGFP. Spectra of these constructs was slightly left-shifted compared to Lck-GCaMP3, a cpGFP-based Ca^{2+} probe. All of them are slightly left-shifted compared to the EGFP (Fig. 4.1C).

Fig. 4.1D shows the G-V curves for BK667cpG (solid dots) and BK860cpG (white dots) compared to the wild-type BK (grey shadow) for Ca^{2+} concentrations ranging from free Ca^{2+} to 100 μ M Ca^{2+} (colors from black to red). The representative currents in Ca^{2+} free and 100 μ M Ca^{2+} are shown in Fig. 4.1E. The electrophysiological properties of the constructs with the insertions are very similar to the wild-type channel.

Este documento incorpora firma electrónica, y es copia auténtica de un documento electrónico archivado por la ULL según la Ley 39/2015.
 Su autenticidad puede ser contrastada en la siguiente dirección <https://sede.ull.es/validacion/>

Identificador del documento: 1627512

Código de verificación: KOIBgUMu

Firmado por:	Fecha:
Roger Gimeno Llobet UNIVERSIDAD DE LA LAGUNA	25/10/2018 11:00:30
Diego Álvarez de la Rosa Rodríguez UNIVERSIDAD DE LA LAGUNA	25/10/2018 11:52:58
Teresa Giráldez Fernández UNIVERSIDAD DE LA LAGUNA	25/10/2018 11:54:04
Ernesto Pereda de Pablo UNIVERSIDAD DE LA LAGUNA	29/10/2018 13:01:03

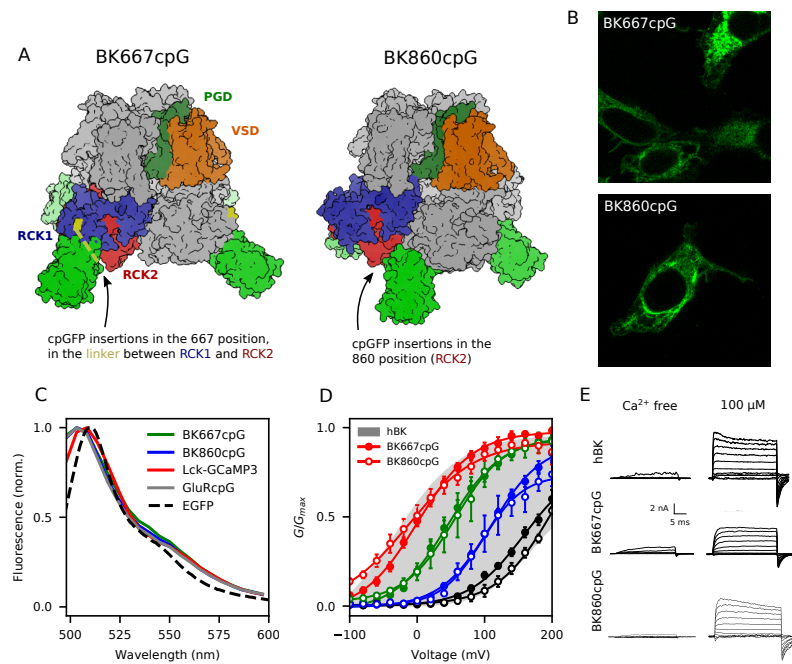


Figure 4.1: Initial characterization of cpGFP based constructs BK667cpG and BK860cpG. (A) BK channel structures (5TJI) where the cpGFP insertions are closer to the 667 and 860 sites. The dashed yellow line between RCK1 and RCK2 in BK667cpG indicated the non-resolved residues that forms the linker between both domains. One subunit of the tetramer is colored with the same code of colors that in fig. 1.1 and 4.1, where PGD: pore gate domain, VSG: voltage sensor domain. (B) Fluorescence images of BK667cpG (top) and BK860cpG (bottom). (C) Emission spectra for constructs BK667cpG (green), BK860cpG (blue), Lck-GCaMP3 (red), GluRcpG (grey) and ECFP (dashed black). All the constructs based on the cpGFP are slightly blue-shifted if compared to ECFP. (D) G-V curves for BK667cpG (solid dots) and BK860cpG (with dots) constructs, as well as for the wild-type BK channel (grey shadow) were determined at various Ca²⁺ concentrations (black lines are Ca²⁺ free, blue are 1 μM Ca²⁺, green are 10 μM Ca²⁺ and red are 100 μM Ca²⁺). (E) Representative currents in Ca²⁺ free and 100 μM Ca²⁺.

Este documento incorpora firma electrónica, y es copia auténtica de un documento electrónico archivado por la ULL según la Ley 39/2015.
 Su autenticidad puede ser contrastada en la siguiente dirección <https://sede.ull.es/validacion/>

Identificador del documento: 1627512

Código de verificación: KOIBgUMU

Firmado por: Roger Gimeno Llobet UNIVERSIDAD DE LA LAGUNA	Fecha: 25/10/2018 11:00:30
Diego Álvarez de la Rosa Rodríguez UNIVERSIDAD DE LA LAGUNA	25/10/2018 11:52:58
Teresa Giráldez Fernández UNIVERSIDAD DE LA LAGUNA	25/10/2018 11:54:04
Ernesto Pereda de Pablo UNIVERSIDAD DE LA LAGUNA	29/10/2018 13:01:03

4.2 Effect of ionomycin-mediated cell Ca^{2+} loading on BK-cpGFP emission

The next step was to characterize the response of our cpGFP-based constructs to a cytosolic Ca^{2+} rise. In these experiments, intracellular $[Ca^{2+}]$ was increased using 15 μM ionomycin, an ionophore that causes the entrance of extracellular Ca^{2+} inside the cell (Erdahl et al., 1994). HEK293T cells transiently expressing BK667cpG or BK860cpG were bathed with a medium containing 5 mM Ca^{2+} , and fluorescence intensity was recorded over time, before and after the drug was added to the bath. In order to compare the responses, we also transfected a construct of the BK channel with the yellow fluorescent variant instead of the cpGFP (BK860Y) as a negative control and the construct from where we obtained the cpGFP, GluA2_391cpGFP.

A diagram of the experimental set-up can be seen in Fig. 4.2A. After 24h of transfection, HEK293T cells grown in coverslips were placed in the imaging chambers with Standard Saline Medium with 5 mM Ca^{2+} (Table 3.2). The basal fluorescence and the fluorescent changes after the addition of ionomycin added 60 s after starting to register were recorded at 1 Hz frequency. Fig. 4.2B shows representative fluorescent images at 0 s, 75 s and 125 s. Fig. 4.2C shows the change in the fluorescence intensity ($\Delta F/F$) with time. After the ionomycin stimuli (black arrow), the increase in fluorescence in the BK860cpG was near 4-fold higher than BK667cpG. As expected, the construct BK860Y (BK channel with a YFP in the 860 position) did not show any significant fluorescent change after addition of ionomycin. BK667cpG showed an increase in the fluorescence intensity similar to GluA2_391cpGFP but significantly smaller than BK860cpG.

Fig. 4.2D shows a comparison of the fluorescent changes between our cpGFP-based constructs BK667cpG and BK860cpG and a cpGFP-based Ca^{2+} probe, Lck-GCaMP3. Lck-GCaMP3 is a construct based on the genetically encoded Ca^{2+} sensor GCaMP3 (Tian et al., 2009) with a membrane-tethering domain, Lck (Shigetomi et al., 2010). It showed a 5-fold increase in fluorescence compared to BK860cpG, as expected with an extremely optimized Ca^{2+} probe.

In order to compare the responses of all constructs, we characterized the fluorescent changes with three parameters: $\Delta F/F$ as the change in fluorescent intensity compared with an initial state previous to the stimuli, τ as the slope and $t_{1/2}$ as the time where the fluorescent response is halfway between the baseline and the maximum, counted from the addition of ionomycin. It is important to note that $t_{1/2}$ does not only reflect the process of change in fluorescence intensity of the cpGFP after the rearrangements of the BK channel when Ca^{2+} binds, but also the time that takes the ionomycin to diffuse in the well and reach the cells. BK860cpG and Lck-GCaMP3 showed a biphasic fluorescence change after the stimuli. The kinetics of these two phases are different and are identified as (subscript 1) and (subscript 2). This behavior has been previously observed in the Ca^{2+} sensor GCaMP (Baird, Zacharias, and Tsien, 1999; Nakai, Ohkura, and Imoto, 2001).

The change in fluorescence $\Delta F/F$ is shown in Fig. 4.2E. BK667cpG exhibited a $\Delta F/F = 0.37 \pm 0.01$ ($n = 21$), similar to construct GluA2_391cpGFP with $\Delta F/F = 0.27 \pm 0.01$ ($n = 27$). BK860cpG showed an improvement in the fluorescent change in response to ionomycin compared to the BK667cpG construct, with a $\Delta F/F = 1.40 \pm 0.12$ ($n = 38$). The GECI Lck-GCaMP3 showed a $\Delta F/F$ of 7.18 ± 0.34 ($n = 29$). Finally, the construct used as a negative control, BK860Y did not show any response to the stimulus, with $\Delta F/F = 0.07 \pm 0.01$ ($n=50$). Fig. 4.2F and G represent the slope of the fluorescent change τ and the response time $t_{1/2}$, with grey shadows indicating

Este documento incorpora firma electrónica, y es copia auténtica de un documento electrónico archivado por la ULL según la Ley 39/2015.
 Su autenticidad puede ser contrastada en la siguiente dirección <https://sede.ull.es/validacion/>

Identificador del documento: 1627512

Código de verificación: kOIBgUMu

Firmado por:	Fecha:
Roger Gimeno Llobet UNIVERSIDAD DE LA LAGUNA	25/10/2018 11:00:30
Diego Álvarez de la Rosa Rodríguez UNIVERSIDAD DE LA LAGUNA	25/10/2018 11:52:58
Teresa Giráldez Fernández UNIVERSIDAD DE LA LAGUNA	25/10/2018 11:54:04
Ernesto Pereda de Pablo UNIVERSIDAD DE LA LAGUNA	29/10/2018 13:01:03

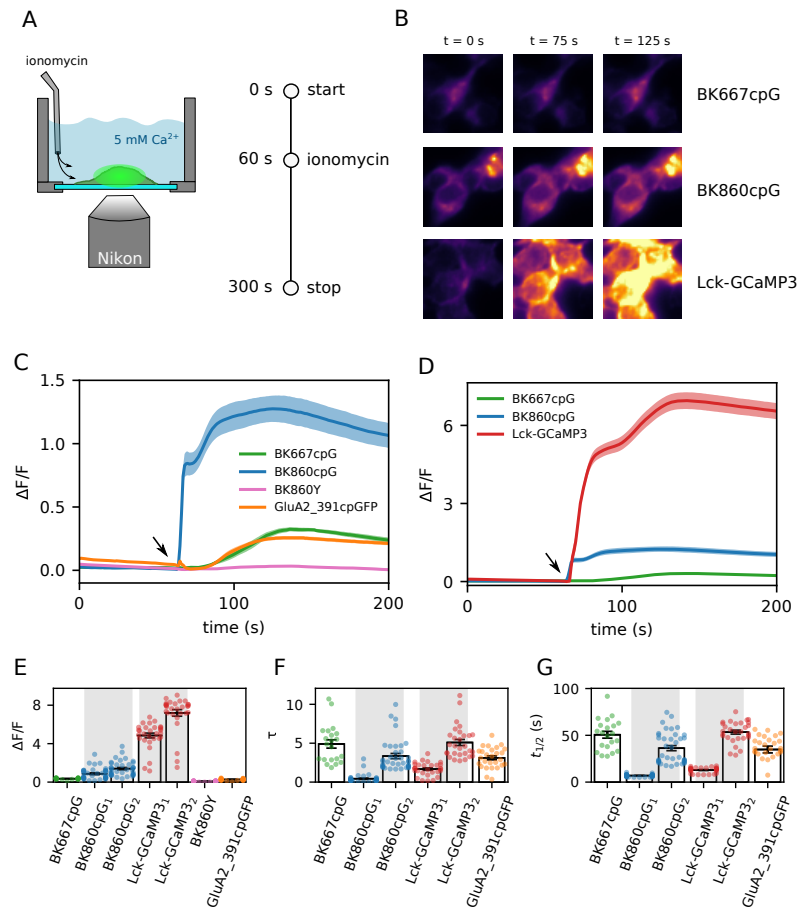


Figure 4.2: Ca^{2+} experiments with ionomycin. (A) Scheme of the experiment. Transfected HEK293T are grown in cover-slips and moved to a imaging chamber with 5 mM Ca^{2+} standard saline medium 24h after transfection to perform the experiment. We started registering the basal fluorescence emission to check stability and bleaching, and at 60 s after the start 15 μM of ionomycin is added directly to the chamber. (B) Representative fluorescent images of BK667cpG, BK860cpG and Lck-GCaMP3 constructs at time 0, 75 and 125 s. The LUT is set to notice changes in the fluorescence intensity. (C) and (D) Fluorescence intensity changes ($\Delta F/F$) with respect to time (black arrows indicates the addition of 15 μM ionomycin). Boxplots of (E) the fluorescent changes ($\Delta F/F$), (F) τ slope of the fluorescent traces and (G) the response time ($t_{1/2}$) from data of Ca^{2+} experiments with ionomycin. Grey shadows indicates the two phases that exhibits fluorescent change in constructs BK860cpG and Lck-GCaMP3, and are denoted in the labels as subscript 1 (first phase) and subscript 2 (second phase). $n = 21$ for BK667cpG, $n = 38$ for BK860cpG, $n = 29$ for Lck-GCaMP3, $n = 50$ for BK860Y and $n = 27$ for GluA2_391cpGFP. Data representing mean \pm SEM. Data are collected of more than three independent experiments.

Este documento incorpora firma electrónica, y es copia auténtica de un documento electrónico archivado por la ULL según la Ley 39/2015.
 Su autenticidad puede ser contrastada en la siguiente dirección <https://sede.ull.es/validacion/>

Identificador del documento: 1627512

Código de verificación: KOIBgUMU

Firmado por: Roger Gimeno Llobet UNIVERSIDAD DE LA LAGUNA	Fecha: 25/10/2018 11:00:30
Diego Álvarez de la Rosa Rodríguez UNIVERSIDAD DE LA LAGUNA	25/10/2018 11:52:58
Teresa Giráldez Fernández UNIVERSIDAD DE LA LAGUNA	25/10/2018 11:54:04
Ernesto Pereda de Pablo UNIVERSIDAD DE LA LAGUNA	29/10/2018 13:01:03

4.2. Effect of ionomycin-mediated cell Ca^{2+} loading on BK-cpGFP emission 41

Table 4.1: Characterization of the fluorescence variation in response to ionomycin of the constructs used in this study. Data is mean \pm SEM.

Constructs	$\Delta F/F$	τ	$t_{1/2}$ (s)	n
BK667cpG	0.35 ± 0.02	4.90 ± 0.54	50.60 ± 3.65	23
BK860cpG (phase1)	0.87 ± 0.10	0.43 ± 0.09	6.91 ± 0.19	40
BK860cpG (phase2)	1.40 ± 0.12	3.35 ± 0.33	36.28 ± 2.71	40
Lck-GCaMP3 (phase1)	4.85 ± 0.25	1.67 ± 0.16	12.90 ± 0.54	31
Lck-GCaMP3 (phase2)	7.20 ± 0.34	5.09 ± 0.39	53.42 ± 2.12	31
BK860Y	0.07 ± 0.01			52
GluA2_391cpGFP	0.26 ± 0.01	3.11 ± 0.25	34.81 ± 3.63	29

the constructs that showed a biphasic fluorescent change. BK860cpG showed faster kinetics in the two phases than Lck-GCaMP3 after the stimulus. It is remarkable the response time of BK860cpG with $t_{1/2}1 = 6.91 \pm 0.19$ s (first phase) and $t_{1/2}2 = 36.28 \pm 2.71$ s (second phase) compared to Lck-GCaMP3, with $t_{1/2}1 = 12.90 \pm 0.54$ s (first phase) and $t_{1/2}2 = 53.42 \pm 2.12$ s (second phase). All values are summarized in **Table 4.1**.

To clarify if part of the increment in the fluorescence intensity that we are observing with the cpGFP-based constructs is due to changes in the environment (direct interaction with elevated $[Ca^{2+}]$, change in pH) and not due to structural rearrangements of the linked proteins we designed a control consisting in the expression of isolated, soluble cpGFP. The isolated cpGFP coding sequence was amplified from construct BK667cpG by PCR. **Fig. 4.3A** shows a map of the isolated cpGFP construct. As expected, this construct was localized in the cytosol (**Fig. 4.3B**). Ca^{2+} -loading experiments with ionomycin using the same conditions as previous experiments (5 mM extracellular Ca^{2+} and 15 μ M ionomycin) caused an increase in the fluorescence intensity comparable with what obtained with constructs BK667cpG and GluA2_391cpGFP (**Fig. 4.3C**). The change in fluorescence intensity after application of ionomycin is $\Delta F/F = 1.19 \pm 0.02$.

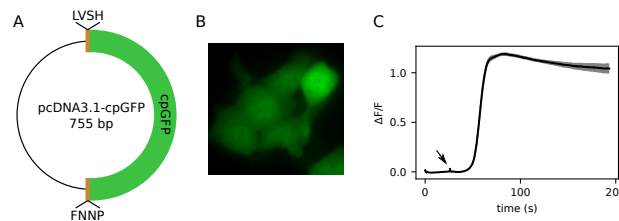


Figure 4.3: Soluble cpGFP control. A) Map of the construct; the cpGFP conserves its original linkers. B) Fluorescence image of transfected HEK293T cells. C) Changes in fluorescence intensity after application of 15 μ M ionomycin (black arrow).

Este documento incorpora firma electrónica, y es copia auténtica de un documento electrónico archivado por la ULL según la Ley 39/2015.
 Su autenticidad puede ser contrastada en la siguiente dirección <https://sede.ull.es/validacion/>

Identificador del documento: 1627512

Código de verificación: KOIBgUMu

Firmado por: Roger Gimeno Llobet UNIVERSIDAD DE LA LAGUNA	Fecha: 25/10/2018 11:00:30
Diego Álvarez de la Rosa Rodríguez UNIVERSIDAD DE LA LAGUNA	25/10/2018 11:52:58
Teresa Giráldez Fernández UNIVERSIDAD DE LA LAGUNA	25/10/2018 11:54:04
Ernesto Pereda de Pablo UNIVERSIDAD DE LA LAGUNA	29/10/2018 13:01:03

4.3 BK Ca²⁺-binding mutants

To confirm that the observed fluorescent response of constructs BK667cpG and BK860cpG is due to the binding of Ca²⁺ in the cytosolic part of the BK channel, we mutated specific Ca²⁺ binding sites as described in the literature (Schreiber and Salkoff, 1997; Schreiber, Yuan, and Salkoff, 1999; Xia, Zeng, and Lingle, 2002; Zhang et al., 2010; Cui, 2010). First we mutated the Mg²⁺ and Ca²⁺ low affinity binding site comprising sites from two intracellular loops within the transmembrane region and the RCK1 domain (Cui, Yang, and Lee, 2009). This binding site can be altered by mutating the aspartate in position 99 to alanine (D99A). Secondly, we mutated the high affinity binding site located at the RCK1 domain. This binding site can be deactivated by mutations of 362 and 367 positions, changing aspartates to alanines (D362/7A). Finally, we mutated the high affinity Ca²⁺ binding site known as the “Ca²⁺ bowl”, between positions 894-988, changing five aspartates to alanines (5D5A). The map of the BK channel showing the positions of all mutations referred here can be seen in Fig. 4.4A. In this study, we generated in total four BK667cpG construct mutants and four BK860cpG construct mutants. Specifically, constructs BK667cpG-D99A and BK860cpG-D99A contain the D99A mutation; constructs BK667cpG-D362/7A and BK860cpG-D362/7A contain mutations D362A and D367A; constructs BK667cpG-5D5A and BK860cpG-5D5A have the Ca²⁺ bowl mutation; finally, constructs BK667cpG-TM and BK860cpG-TM contain all three mutations (TM stands for Triple Mutants).

We carried out ionomycin experiments with all Ca²⁺ mutants. Fig. 4.4B represents fluorescent changes obtained after performing the same protocol shown in preceding section, now with construct BK667cpG and its mutants. In general we observed responses similar to those of BK667cpG in all mutants. In contrast, the mutated constructs of BK860cpG exhibit a notably reduced response after addition of ionomycin (Fig. 4.4C). The change in fluorescence intensity of all mutants is indeed comparable to that of BK667cpG and its mutants. This result is very significant since it is in accordance with the hypothesis that, in the case of the BK860cpG construct, the change in fluorescence intensity corresponds to specific sensing of Ca²⁺ by the BK channel binding sites. In contrast, the changes in fluorescence intensity observed after ionomycin addition in the BK667cpG construct, as well as the various Ca²⁺ binding sites mutations and the AMPAR-cpG construct, may correspond to unspecific effects of Ca²⁺, ionomycin, or other component in our experimental conditions, which are acting either directly on the cpGFP or at other sites within the proteins where it has been inserted, generating small increases in fluorescence intensity.

Data representing $\Delta F/F$, τ and $t_{1/2}$ of all constructs are shown in Fig. 4.4D, E and F, and values are summarized in Table 4.2.

Este documento incorpora firma electrónica, y es copia auténtica de un documento electrónico archivado por la ULL según la Ley 39/2015.
 Su autenticidad puede ser contrastada en la siguiente dirección <https://sede.ull.es/validacion/>

Identificador del documento: 1627512

Código de verificación: kOIBgUMu

Firmado por:	Fecha:
Roger Gimeno Llobet UNIVERSIDAD DE LA LAGUNA	25/10/2018 11:00:30
Diego Álvarez de la Rosa Rodríguez UNIVERSIDAD DE LA LAGUNA	25/10/2018 11:52:58
Teresa Giráldez Fernández UNIVERSIDAD DE LA LAGUNA	25/10/2018 11:54:04
Ernesto Pereda de Pablo UNIVERSIDAD DE LA LAGUNA	29/10/2018 13:01:03

4.3. BK Ca²⁺-binding mutants

43

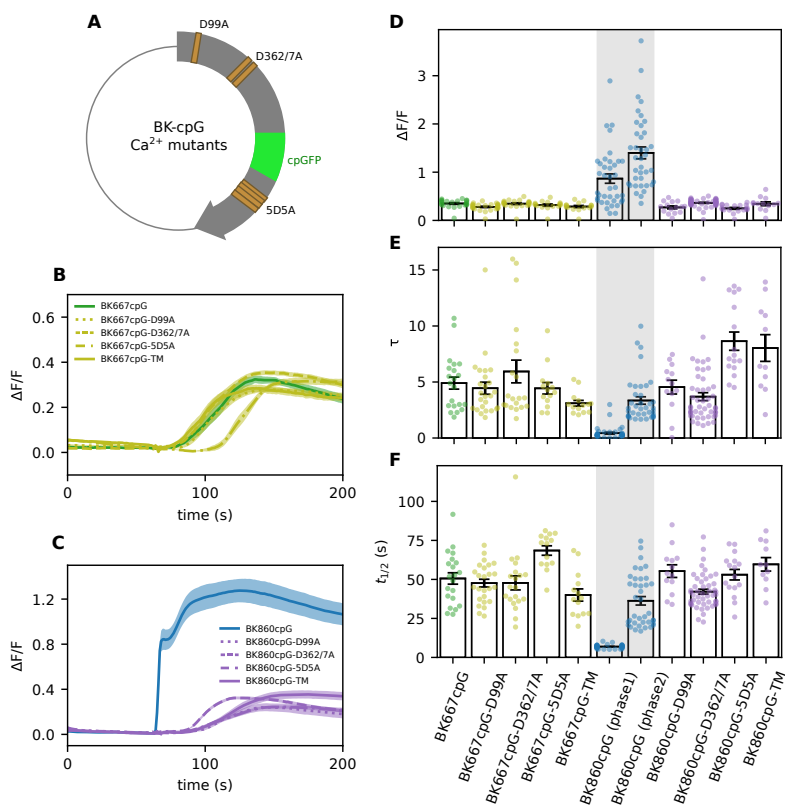


Figure 4: Ca²⁺ experiments with ionomycin with constructs BK667cpG and BK860cpG and its Ca²⁺ binding sites mutants. A) Map of the BK channel showing the positions of the three mutation clusters. Fluorescent changes in response to ionomycin (black arrow) for BK667cpG and its mutants B) and for BK860cpG and its mutants C). Boxplots of fluorescent variations $\Delta F/F$ D), slope τ E) and response time $t_{1/2}$ F) are shown. For BK667cpG (green) $n = 21$, for BK667cpG-D99A (yellow, dotted line in (B)) $n = 20$, for BK667cpG-D362/7A (yellow, dot-dash line in (B)) $n = 10$, for BK667cpG-5D5A (yellow, dashed line in (B)) $n = 14$, for BK667cpG-TM (yellow, solid line in (B)) $n = 7$. For BK860cpG (blue) $n = 38$, for BK860cpG-D99A (purple, dotted line in (C)) $n = 9$, for BK860cpG-D362/7A (purple, dot-dash line in (C)) $n = 16$, for BK860cpG-5D5A (purple, dashed line in (C)) $n = 11$ and for BK860cpG-TM (purple, solid line in (C)) $n = 18$. Data representing mean \pm SEM. Data are collected of more than three independent experiments.

Este documento incorpora firma electrónica, y es copia auténtica de un documento electrónico archivado por la ULL según la Ley 39/2015.
 Su autenticidad puede ser contrastada en la siguiente dirección <https://sede.ull.es/validacion/>

Identificador del documento: 1627512

Código de verificación: KOIBgUMu

Firmado por: Roger Gimeno Llobet UNIVERSIDAD DE LA LAGUNA	Fecha: 25/10/2018 11:00:30
Diego Álvarez de la Rosa Rodríguez UNIVERSIDAD DE LA LAGUNA	25/10/2018 11:52:58
Teresa Giráldez Fernández UNIVERSIDAD DE LA LAGUNA	25/10/2018 11:54:04
Ernesto Pereda de Pablo UNIVERSIDAD DE LA LAGUNA	29/10/2018 13:01:03

Table 4.2: Characterization of the fluorescence variation in response to ionomycin of the Ca²⁺ mutant constructs of BK667cpG and BK860cpG. Data is mean \pm SEM.

Constructs	$\Delta F/F$	τ	$t_{1/2}$ (s)	n
BK667cpG	0.35 \pm 0.02	4.90 \pm 0.54	50.60 \pm 3.65	23
BK667cpG-D99A	0.28 \pm 0.01	4.45 \pm 0.54	47.63 \pm 2.48	27
BK667cpG-D362/7A	0.35 \pm 0.02	5.94 \pm 1.01	47.75 \pm 4.49	22
BK667cpG-5D5A	0.32 \pm 0.02	4.44 \pm 0.51	68.51 \pm 3.02	16
BK667cpG-TM	0.29 \pm 0.02	3.10 \pm 0.25	39.99 \pm 3.92	16
BK860cpG (phase1)	0.87 \pm 0.10	0.43 \pm 0.09	6.91 \pm 0.19	40
BK860cpG (phase2)	1.40 \pm 0.12	3.35 \pm 0.33	36.28 \pm 2.71	40
BK860cpG-D99A	0.27 \pm 0.03	4.54 \pm 0.62	55.31 \pm 4.05	15
BK860cpG-D362/7A	0.36 \pm 0.01	3.69 \pm 0.35	42.13 \pm 1.58	50
BK860cpG-5D5A	0.25 \pm 0.02	8.64 \pm 0.81	53.02 \pm 3.37	18
BK860cpG-TM	0.34 \pm 0.04	8.03 \pm 1.19	59.66 \pm 4.32	13

4.4 BK-cpGFP: Ca²⁺ affinity and pH dependence

Our experiments using ionomycin, including mutations of BK specific Ca²⁺ binding sites, provide solid evidence that construct BK860cpG responds to specific Ca²⁺ binding to the channel by altering the fluorescence intensity of cpGFP. These results led us to the following questions: 1) What is the [Ca²⁺] affinity of the observed fluorescent response? 2) How does the BKcpG constructs fluorescence depend on cytosolic pH?

To this end we designed quantitative dose-response experiments where the Ca²⁺ concentration or the pH were varied. As described in the Methods section, we prepared plasma membrane microsomes from cells transfected with the relevant constructs, which were permeabilized with ionomycin to rapidly equilibrate changes in pH or Ca²⁺ concentration. Fig. 4.5A shows Ca²⁺ titration of BK667cpG, BK860cpG and Lck-GCaMP3 constructs. Data was fitted to monophasic sigmoidals, yielding apparent dissociation constants (*K_d*) for BK667cpG of 427 nM, for BK860cpG *K_d* = 235 nM and for Lck-GCaMP3 *K_d* = 252 nM. Hill slopes (*n_H*) are 7.3 for BK667cpG, 2.1 for BK860cpG and 1.8 for Lck-GCaMP3. The apparent Ca²⁺ affinity and Hill slope values of Lck-GCaMP3 differ from the values obtained in (Shigetomi et al., 2010), where *K_d* = 153 nM and *n_H* = 3.5. It is remarkable that the change in fluorescence for BK667cpG decreases for small Ca²⁺ increments, while for construct BK860cpG increases. Interestingly, opposite direction in the FRET efficiency responses between constructs BK667X and BK860X (X denotes the FRET pair or the cpGFP) have been observed previously (Miranda et al., 2013).

pH titrations (Fig. 4.5B, black curves) revealed similar responses of constructs BK667cpG and BK860cpG, showing a pKa of 7.5. For Lck-GCaMP3 the pKa was 7.8. As described previously (Campbell and Choy, 2001), at low pH the absorbance peak of GFP-like species blue-shifts a around 390 nm. At alkaline environments, the fluorescence increases due to ionization of the chromophore (Nagai et al., 2001). Data presented in fig. 3.6B correspond to 100 μ M Ca²⁺.

For comparative purposes, Fig. 4.5B shows all titration curves with $\Delta F/F$ as a function of pCa or pH (Ca²⁺-titration curves in blue and pH-titration curves in

Este documento incorpora firma electrónica, y es copia auténtica de un documento electrónico archivado por la ULL según la Ley 39/2015.
 Su autenticidad puede ser contrastada en la siguiente dirección <https://sede.ull.es/validacion/>

Identificador del documento: 1627512

Código de verificación: KOIBGUMU

Firmado por:	Fecha:
Roger Gimeno Llobet UNIVERSIDAD DE LA LAGUNA	25/10/2018 11:00:30
Diego Álvarez de la Rosa Rodríguez UNIVERSIDAD DE LA LAGUNA	25/10/2018 11:52:58
Teresa Giráldez Fernández UNIVERSIDAD DE LA LAGUNA	25/10/2018 11:54:04
Ernesto Pereda de Pablo UNIVERSIDAD DE LA LAGUNA	29/10/2018 13:01:03

4.5. Patch-clamp fluorometry (PCF) recordings of BK-cpGFP signals

45

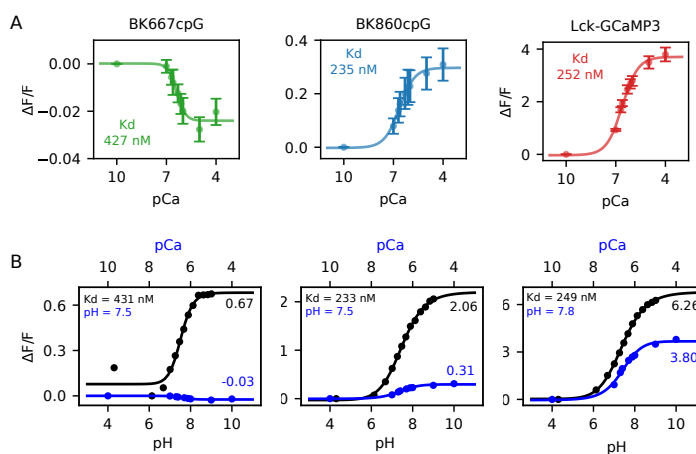


Figure 4.5: Sensibility of constructs BK667cpG (left panels), BK860cpG (middle panels) and the positive control Lck-GCaMP3 (right panels) to Ca^{2+} and pH. A) Ca^{2+} -titration curves; BK667cpG exhibit a small decrease in the fluorescence for increasing $[\text{Ca}^{2+}]$. On the contrary BK860cpG increases the fluorescence with $[\text{Ca}^{2+}]$. B) Comparison of pH-titration curves (black) and Ca^{2+} -titration curves (blue). Changes in the fluorescence intensity ($\Delta\text{F}/\text{F}$) are indicated at the plateau of the curves. Variations in the fluorescence intensity are larger for pH than for $[\text{Ca}^{2+}]$.

Table 4.3: *In vitro* characteristics of constructs BK667cpG, BK860cpG and Lck-GCaMP3.

Constructs	Kd (nM)	Hill coef.	pKa	$\Delta\text{F}/\text{F}$ (Ca^{2+})	$\Delta\text{F}/\text{F}$ (pH)
BK667cpG	427	7.3	7.5	-0.03 ± 0.01	0.67 ± 0.03
BK860cpG	235	2.1	7.5	0.31 ± 0.06	2.06 ± 0.13
Lck-GCaMP3	252	1.8	7.8	3.80 ± 0.26	6.26 ± 0.50

black). In this way it is possible to identify the contribution due to variations of Ca^{2+} and pH to the total fluorescence. Our data show that changes in pH induce larger changes in fluorescence intensity than $[\text{Ca}^{2+}]$. Interestingly, these changes are more pronounced in BK-cpGFP constructs than Lck-GCaMP3. For BK667cpG, the response to incremental $[\text{Ca}^{2+}]$ is a small but consistent decrease of $\Delta\text{F}/\text{F} = -3\%$ in the fluorescence intensity, while there is a larger increase in the fluorescence ($\Delta\text{F}/\text{F} = 67\%$) for increasing pH. BK860cpG exhibited a increase in the fluorescence of $\Delta\text{F}/\text{F} = 31\%$ for increasing $[\text{Ca}^{2+}]$, but a $\Delta\text{F}/\text{F} = 206\%$ increase as pH increased. Lck-GCaMP3 showed a $\Delta\text{F}/\text{F} = 380\%$ increase in fluorescence as $[\text{Ca}^{2+}]$ increased, and a $\Delta\text{F}/\text{F} = 626\%$ increase due to alkalinization. All data is summarized in Table 4.3.

4.5 Patch-clamp fluorometry (PCF) recordings of BK-cpGFP signals

Patch-Clamp Fluorometry (PCF) combines fluorometric and electrophysiological techniques to simultaneously detect conformational fluorescence emission of labeled

Este documento incorpora firma electrónica, y es copia auténtica de un documento electrónico archivado por la ULL según la Ley 39/2015.
 Su autenticidad puede ser contrastada en la siguiente dirección <https://sede.ull.es/validacion/>

Identificador del documento: 1627512

Código de verificación: KOIBgUMu

Firmado por: Roger Gimeno Llobet UNIVERSIDAD DE LA LAGUNA	Fecha: 25/10/2018 11:00:30
Diego Álvarez de la Rosa Rodríguez UNIVERSIDAD DE LA LAGUNA	25/10/2018 11:52:58
Teresa Giráldez Fernández UNIVERSIDAD DE LA LAGUNA	25/10/2018 11:54:04
Ernesto Pereda de Pablo UNIVERSIDAD DE LA LAGUNA	29/10/2018 13:01:03

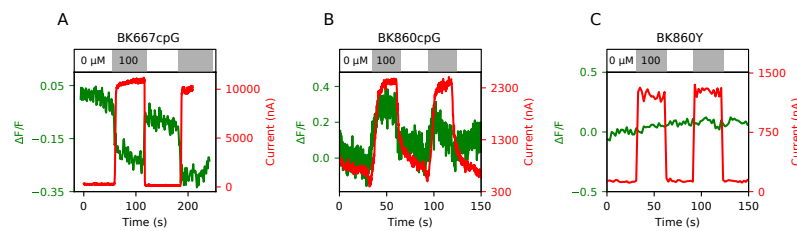


Figure 4.6: Representative patch-clamp fluorimetry (PCF) experiments, showing synchronously fluorimetric and electrophysiological recordings for Ca^{2+} free and $100 \mu\text{M}$ Ca^{2+} . The change in fluorescence intensity ($\Delta\text{F}/\text{F}$, green) and tail currents (red) are shown in the same plot. A) BK667cpG construct exhibited a small decrease in the fluorescence intensity when BK was activated by $100 \mu\text{M}$ Ca^{2+} . B) On the contrary, BK860cpG showed an increase in the fluorescence corresponding to the activation of the channel when $[\text{Ca}^{2+}]$ increased. C) As a negative control we used BK860Y construct; no change in fluorescence intensity was observed when the channels were activated by $100 \mu\text{M}$ Ca^{2+} .

subunits and ionic currents across the membrane. Our laboratory has mastered this technique to study BK conformational changes (Miranda et al., 2013; Miranda, Giraldez, and Holmgren, 2016). In this project, we took advantage of this approach to measure simultaneous changes in the K^+ currents and fluorescence from BK667cpG and BK867cpG sensors. An inside-out patch is excised from a fluorescent cell, allowing the perfusion of different Ca^{2+} concentrations (0 and $100 \mu\text{M}$) directly to the patch with another micropipette, while varying membrane potential and recording current permeating through BK. The membrane potential was varied from a resting value of -60 mV to 100 mV, a potential where all channels will be opened, then to -80 mV, a potential where all channels will be closed and finally to -60 mV again. These step-potential changes are repeated in 150 ms intervals. Current was measured at the peak obtained during the repolarizing pulse, as previously described (Giraldez, Hughes, and Sigworth, 2005). Representative recordings can be seen in Fig. 4.6. Fig. 4.6A shows simultaneous recordings of fluorescence intensity (green) and K^+ current (red) from patches expressing BK667cpG homotetramers. Ca^{2+} concentration was alternatively changed between 0 and $100 \mu\text{M}$. Increased Ca^{2+} concentrations were correlated with activation of the BK and decreased fluorescence intensity values ($\Delta\text{F}/\text{F} = -0.20$). The constant loss of the fluorescence signal can be due to the bleaching of the fluorophore. Fig. 4.6B shows the simultaneous fluorescence and K^+ current recordings for BK860cpG, while changing $[\text{Ca}^{2+}]$ from 0 to $100 \mu\text{M}$. Contrary to BK667cpG, BK860cpG increased the fluorescence at high $[\text{Ca}^{2+}]$ ($\Delta\text{F}/\text{F} = 0.30$). To assess the specificity of the observed signals, construct BK860Y was used as a negative control (Fig. 4.6C). In this case no changes in fluorescence were observed after changing Ca^{2+} concentration.

4.6 Generation of BK-cpGFP pore mutants

In some situations it may be useful to have a non-conducting channel that does not alter the ionic balance of the cell when over-expressed, while reporting changes in intracellular calcium concentration. Therefore, we decided to generate non-conducting variants of our BK-cpG sensors. Mutation of amino acid 315 in the S6 segment has

Este documento incorpora firma electrónica, y es copia auténtica de un documento electrónico archivado por la ULL según la Ley 39/2015.
 Su autenticidad puede ser contrastada en la siguiente dirección <https://sede.ull.es/validacion/>

Identificador del documento: 1627512

Código de verificación: kOIBgUMu

Firmado por: Roger Gimeno Llobet UNIVERSIDAD DE LA LAGUNA	Fecha: 25/10/2018 11:00:30
Diego Álvarez de la Rosa Rodríguez UNIVERSIDAD DE LA LAGUNA	25/10/2018 11:52:58
Teresa Giraldez Fernández UNIVERSIDAD DE LA LAGUNA	25/10/2018 11:54:04
Ernesto Pereda de Pablo UNIVERSIDAD DE LA LAGUNA	29/10/2018 13:01:03

4.6. Generation of BK-cpGFP pore mutants

47

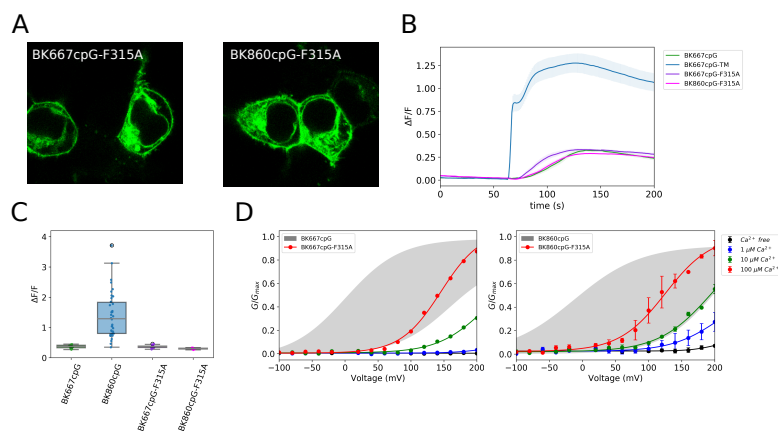


Figure 4.7: Pore mutants (F315A) for BK667cpG and BK860cpG constructs. (A) Fluorescence images of HEK293T cells transfected with pore mutant constructs. We can appreciate a clear distribution of the labeled channels in the membrane. (B) Ca²⁺ experiments with ionomycin. BK860cpG-F315A (pink) did not show the typical response of BK860cpG (blue), but it shows a similar response to the construct BK667cpG (green). (C) Boxplot of fluorescent changes ($\Delta F/F$). (D left) G-V curves for BK667cpG-F315A and BK667cpG (solid dots and grey shadow respectively) and (right) BK860cpG-F315A and BK860cpG (solid dots and grey shadow respectively) constructs. Curves were determined at various Ca²⁺ concentrations (black lines are Ca²⁺ free, blue are 1 μ M Ca²⁺, green are 10 μ M Ca²⁺ and red are 100 μ M Ca²⁺).

been described to produce important effects on gating and K⁺ conductance (Wang and Brenner, 2006; Carrasquel-Ursulaez et al., 2015). F315-mutated BK channels exhibit alterations in voltage and Ca²⁺ sensitivity, producing extremely right-shifted G-V curves (Wu et al., 2009). We mutated phenylalanine in position 315 to alanine (F315A) to generate constructs BK667cpG-F315A and BK860cpG-F315A. When transfected in HEK293T cells, we observed that transfected cells had a predominant fluorescence distribution at the plasma membrane (Fig. 4.7A), when compared with non-mutated BK667cpG and BK860cpG constructs (Fig. 4.7B). A possible explanation for this difference could be due to the fact that over-expressed non-conducting BK channels do not alter membrane resting potential, probably slowing down channel removal from the membrane.

Ionomycin Ca²⁺-loading experiments with these mutants are shown in Fig. 4.7B. BK667cpG-F315A constructs showed similar responses in terms of fluorescent change and shape of the response than non-mutated BK667cpG constructs. Surprisingly, the construct BK860cpG-F315A showed diminished fluorescent responses than non-mutated construct BK860cpG, comparable to those of BK667cpG.

Fig. 4.7C shows the ionomycin-induced changes in fluorescence intensity ($\Delta F/F$) for each construct. Fig. 4.7D shows the G-V relations for BK667cpG-F315A compared to BK667cpG (grey shadow), and BK860cpG-F315A compared to BK860cpG (grey shadow). Both F315A mutants right-shift G-V curves, greatly decreasing the open probability at all [Ca²⁺]. This behavior has been reported previously in BK channels carrying the same F315A mutation (Wang and Brenner, 2006).

Este documento incorpora firma electrónica, y es copia auténtica de un documento electrónico archivado por la ULL según la Ley 39/2015.
 Su autenticidad puede ser contrastada en la siguiente dirección <https://sede.ull.es/validacion/>

Identificador del documento: 1627512

Código de verificación: kOIBgUMu

Firmado por: Roger Gimeno Llobet UNIVERSIDAD DE LA LAGUNA	Fecha: 25/10/2018 11:00:30
Diego Álvarez de la Rosa Rodríguez UNIVERSIDAD DE LA LAGUNA	25/10/2018 11:52:58
Teresa Giráldez Fernández UNIVERSIDAD DE LA LAGUNA	25/10/2018 11:54:04
Ernesto Pereda de Pablo UNIVERSIDAD DE LA LAGUNA	29/10/2018 13:01:03

4.7 Whole cell electrophysiology and fluorimetric recordings

To extract information regarding membrane potential and ions flux from Ca^{2+} experiments with ionomycin we utilized simultaneously electrophysiology and fluorimetric in whole-cell configuration. The parameters remained almost identical as previous experiments; 5 mM cells bathed in 5 mM Ca^{2+} SSM (Table 3.2) and application of 15 μM ionomycin. The only variation was that in this case the intracellular medium was homogenized with the pipette solution (Table 3.2) after the patch was done. Representative experiments showing membrane voltage and currents with simultaneous recordings of fluorescence intensity can be seen in Fig. 4.8. In the voltage clamp configuration (V-Clamp), with holding potential (V_h) at -60 mV, application of ionomycin caused hyperpolarizing currents in both constructs (Fig. 4.8A, solid red curves). These currents are compatible with an efflux of K^+ ions caused by BK activation. Simultaneously, an increase in the fluorescence intensity is observed (Fig. 4.8A, solid black curves). In order to determine if the currents observed were due to activation of BK channels, we used paxiline, a K^+ channel blocker. As seen in Fig. 4.8A (dashed red curves), cells treated with paxiline did not show hyperpolarizing currents after application of ionomycin. Alternatively, depolarizing currents can be seen probably due to the entrance of Ca^{2+} ions by the effect of ionomycin. This suggests that the hyperpolarizing currents observed in experiments without paxiline could be the composition of the outward K^+ currents and the inward Ca^{2+} currents, where the net result was a positive hyperpolarizing current. Fluorescent changes in paxiline experiments were smaller if compared with experiments without paxiline (Fig. 4.8A, dashed black curves).

We also carried out these experiments with our control construct Lck-GCaMP3 (Fig. 4.8A left). The current observed in both without paxiline and with paxiline was a negative depolarizing current, probably due to the Ca^{2+} influx. The changes in the fluorescence intensity were as usual for this construct, showing the biphasic shape. In Fig. 4.8B and C can be seen the changes in the fluorescence intensity and current of BK667cpG, BK860cpG and Lck-GCaMP3 for experiments without and with paxiline.

4.8 Sensitivity of BK-cpG sensors to different cellular Ca^{2+} sources

As described in the introduction, cellular Ca^{2+} signals can originate from various extra- and intracellular sources. An essential step in development of novel Ca^{2+} sensors involves the characterization of sensitivity of such sensors to different Ca^{2+} sources, which will help to determine the spatial specificity of the sensor response. Experiments using ionomycin recapitulate the effect of external Ca^{2+} sources on the sensors signals. Additionally, we validated the response of our sensors BK667cpG and BK860cpG to intracellular Ca^{2+} sources by using carbachol, a non-selective agonist of acetylcholine receptors. Stimulation of HEK293 cells by carbachol evokes a fast increase in the cytoplasmic Ca^{2+} concentration, originated by the release of Ca^{2+} from internal stores (Nakai, Ohkura, and Imoto, 2001; Ohkura et al., 2005). It is important to note that carbachol treatment does not alter internal pH. We transfected HEK293T cells with constructs BK667cpG, BK860cpG. Additionally, we performed experiments using Lck-GCaMP3 as a positive control.

Fig. 4.9A shows fluorescence recordings corresponding to transfected HEK293T cells in response to different treatments. Addition of 100 μM carbachol (CCH), 15

Este documento incorpora firma electrónica, y es copia auténtica de un documento electrónico archivado por la ULL según la Ley 39/2015.
 Su autenticidad puede ser contrastada en la siguiente dirección <https://sede.ull.es/validacion/>

Identificador del documento: 1627512

Código de verificación: KOIBgUMu

Firmado por:	Fecha:
Roger Gimeno Llobet UNIVERSIDAD DE LA LAGUNA	25/10/2018 11:00:30
Diego Álvarez de la Rosa Rodríguez UNIVERSIDAD DE LA LAGUNA	25/10/2018 11:52:58
Teresa Giráldez Fernández UNIVERSIDAD DE LA LAGUNA	25/10/2018 11:54:04
Ernesto Pereda de Pablo UNIVERSIDAD DE LA LAGUNA	29/10/2018 13:01:03

4.8. Sensitivity of BK-cpG sensors to different cellular Ca^{2+} sources

49

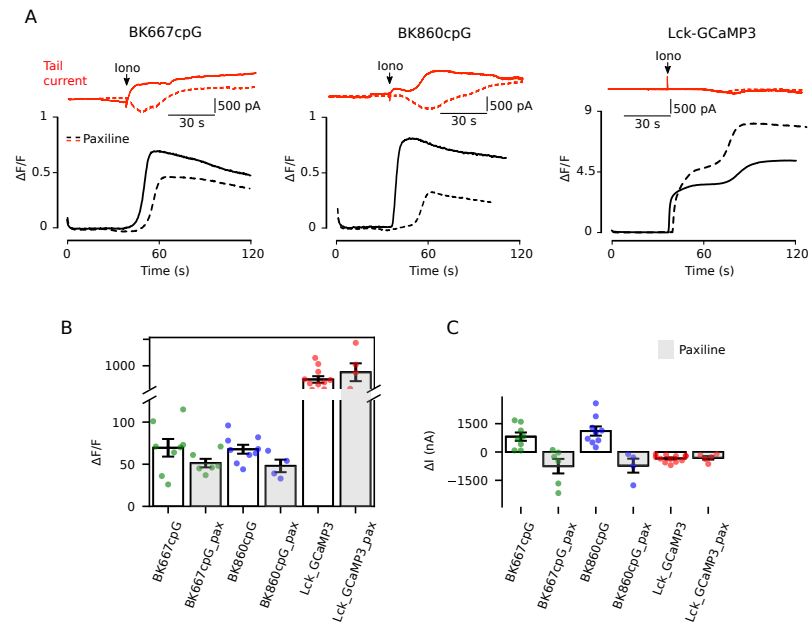


Figure 4.8: Whole-cell electrophysiology with fluorometry recordings of HEK293T cells transfected with BK667cpG, BK860cpG and Lck-GCaMP3. The K⁺ channel blocker paxiline was added in some experiments to determine the role of BK in the currents obtained after application of ionomycin. A) V-Clamp electrophysiological (red) and fluorimetric (black) recordings after addition of ionomycin (Iono). Experiments where 0.5 μ M paxiline was added before the experiment are shown with dashed lines. Holding potential was set to -60 mV. The hyperpolarizing currents observed in BK667cpG and BK860cpG are abolished when paxiline is added, indicating that these currents are due to BK activation. The depolarizing current remaining in paxiline experiments and in Lck-GCaMP3 probably is due to influx of Ca^{2+} from the extracellular medium by the action of ionomycin. B) Changes in fluorescence intensity ($\Delta F/F$) of constructs. Experiments where paxiline was added are shown with grey bars. The blocking of BK constructs by paxiline affects the fluorescence response, diminishing the increase in the fluorescence intensity. C) Change in the current measured (ΔI) after application of ionomycin respect initial current. Positive currents are hyperpolarizing currents. All data in B) and C) is represented as mean \pm SEM, n = 8 for BK667cpG, n = 6 for BK667cpG with paxiline, n = 9 for BK860cpG, n = 4 for BK860cpG with paxiline, n = 11 for Lck-GCaMP3 and n = 5 for Lck-GCaMP3 with paxiline.

Este documento incorpora firma electrónica, y es copia auténtica de un documento electrónico archivado por la ULL según la Ley 39/2015.
 Su autenticidad puede ser contrastada en la siguiente dirección <https://sede.ull.es/validacion/>

Identificador del documento: 1627512

Código de verificación: kOIBgUMu

Firmado por: Roger Gimeno Llobet UNIVERSIDAD DE LA LAGUNA	Fecha: 25/10/2018 11:00:30
Diego Álvarez de la Rosa Rodríguez UNIVERSIDAD DE LA LAGUNA	25/10/2018 11:52:58
Teresa Giráldez Fernández UNIVERSIDAD DE LA LAGUNA	25/10/2018 11:54:04
Ernesto Pereda de Pablo UNIVERSIDAD DE LA LAGUNA	29/10/2018 13:01:03

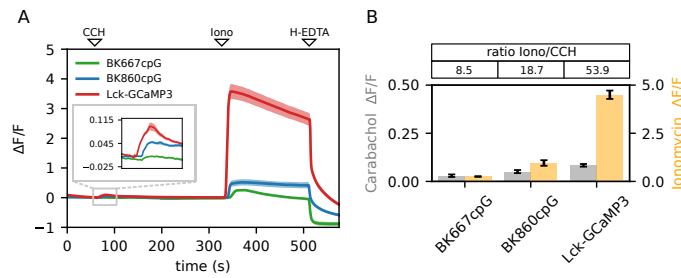


Figure 4.9: Behavior of BK667cpG and BK860cpG constructs to various Ca^{2+} sources. The fluorescent changes of transfected HEK293T cells in response to different drugs are shown in A), where applications of 100 μ M carbachol (CCH), 15 μ M ionomycin (Iono) and 1 mM H-EDTA are indicated as triangles in the top of the plot. The insert shows with more detail the response to CCH. B) Carbachol and ionomycin $\Delta F/F$ values and the ratio Iono/CCH of each construct.

μ M ionomycin (Iono) and 1 mM H-EDTA is indicated with a triangle symbol on top of the plot. Carbachol induced small fluorescence peaks in both BK667cpG and BK860cpG constructs as well as Lck-GCaMP3 (insert in Fig. 4.9A), with $\Delta F/F = 0.03 \pm 0.01$ for BK667cpG, $\Delta F/F = 0.05 \pm 0.01$ for BK860cpG and $\Delta F/F = 0.08 \pm 0.01$ for Lck-GCaMP3. After several minutes, addition of ionomycin caused higher increase in the fluorescence intensity, with $\Delta F/F = 0.25 \pm 0.02$ for BK667cpG, $\Delta F/F = 0.96 \pm 0.14$ for BK860cpG and $\Delta F/F = 4.45 \pm 0.22$ for Lck-GCaMP3. Values obtained for all constructs are lower than that obtained previously with only application of ionomycin. Addition of the chelating agent H-EDTA decreased the fluorescence under basal levels in all constructs.

Fluorescent traces showed in Fig. 4.9A correspond to representative traces of one experimental day. Maximum values of $\Delta F/F$ shown in Fig. 4.9B correspond to averaged values from carbachol and ionomycin experiments performed in three days (note different Y-axis scales). All data is summarized in Table 4.4.

To evaluate the quantitative relationship of recorded signals in all constructs tested, we obtained the fluorescence response ratio between ionomycin and carbachol $\Delta F/F$. Lowest ratio values were observed for construct BK667cpG, which showed the lowest fluorescence change in response to ionomycin. Lck-GCaMP3 $\Delta F/F$ ratio increased considerably, since the response to carbachol remained low whereas the response to ionomycin as the highest. Finally, BK860cpG constructs showed intermediate $\Delta F/F$ ratios. The low increase in fluorescence intensity of Lck-GCaMP3 to carbachol is intriguing, as it has been shown that previous versions¹ of this GECI responded with greater fluorescence changes ($\Delta F/F = 0.8$) to equal quantities of carbachol in HEK cells (Nakai, Ohkura, and Imoto, 2001).

¹Note that the GECI employed in this study (Nakai, Ohkura, and Imoto, 2001), G-CaMP, was not as optimized as the version that we are using, GCaMP3; additionally, data shown here correspond to Lck-GCaMP3, which is localized at the plasma membrane.

Este documento incorpora firma electrónica, y es copia auténtica de un documento electrónico archivado por la ULL según la Ley 39/2015.
 Su autenticidad puede ser contrastada en la siguiente dirección <https://sede.ull.es/validacion/>

Identificador del documento: 1627512

Código de verificación: kOIBgUMu

Firmado por:	Fecha:
Roger Gimeno Llobet UNIVERSIDAD DE LA LAGUNA	25/10/2018 11:00:30
Diego Álvarez de la Rosa Rodríguez UNIVERSIDAD DE LA LAGUNA	25/10/2018 11:52:58
Teresa Giráldez Fernández UNIVERSIDAD DE LA LAGUNA	25/10/2018 11:54:04
Ernesto Pereda de Pablo UNIVERSIDAD DE LA LAGUNA	29/10/2018 13:01:03

Table 4.4: $\Delta F/F$ and Ratio between ionomycin and carbachol peaks. Data is mean \pm SEM.

Constructs	$\Delta F/F$ (CCH)	$\Delta F/F$ (IM)	IM/CCH	n
BK667cpG	0.03 \pm 0.01	0.25 \pm 0.02	8.54 \pm 2.03	18
BK860cpG	0.05 \pm 0.01	0.96 \pm 0.14	18.74 \pm 4.09	19
Lck-GCaMP3	0.08 \pm 0.01	4.45 \pm 0.22	53.89 \pm 5.22	14

4.9 Expression of BK-cpG sensors in Ca²⁺ nanodomains

In this study we have developed a potential Ca²⁺ sensor based on the BK channel, BK860cpG, which produces significant and measurable changes in fluorescence intensity in response to physiological Ca²⁺ concentrations.

The next validation step was to evaluate the ability of BK860cpG sensors to form Ca²⁺ nanodomains with voltage-gated calcium (Cav) channels. Previous results (Berkefeld et al., 2006; Contet et al., 2016), including data obtained in our laboratory using superresolution microscopy², show that wild-type BK channels (without GFP insertions) form complexes with P and Q-type voltage-gated calcium channels (Cav2.1), when co-transfected in heterologous expression systems like HEK293T cells. In this study we used superresolution microscopy to evaluate the ability of BK860cpG sensor to form nanodomains with Cav2.1 channels, as observed with the wild-type BK. We used the superresolution microscopy technique called Stochastic Optical Reconstruction Microscopy (STORM) which we have recently implemented in our laboratory. Direct STORM (dSTORM) relies on the use of conventional carbocyanine dyes that are able to reversibly switch between a fluorescent “on” and a dark “off” state. Control of photoswitching can be achieved by varying thiol and oxygen concentrations of the medium as well as varying laser intensity (Jensen and Crossman, 2014). In this way the number of “on” fluorophores is optimized, being most of fluorophores in the “off” state and permitting the precise localization of individual fluorescent molecules (Fig. 4.10A). Fig. 4.10B shows a simplified Jablonsky diagram of the process. Excited “on” state molecules can relax to its ground state by emitting a fluorescence photon, or can experience intersystem crossing to a dark triplet state. Through redox reactions facilitated by specific medium, the molecule can progress to a dark state, taking from milliseconds to minutes to non-radiatively relax to the ground state by inverse redox reactions (Nahidiazar et al., 2016). After several cycles of “on”, molecule localization, and “off” switching, a subdiffraction limit image can be generated from calculated coordinates of each registered molecule.

4.9.1 Development of new scripts for dSTORM data analysis

STORM data analysis is not straightforward. The images obtained are not conventional fluorescence images. Rather, representations in a 2-D plane of particle coordinates (molecules list) are obtained. Each fluorescent molecule detected has a corrected position in the image plane (X_{wc}, Y_{wc}), whose accuracy is given by quality parameters from the received signal, such as the number of photons obtained. In this study, analysis of STORM data involved the generation of custom-made scripts written in Python, which constituted part of this Doctoral Thesis work.

²Cerrada-Dueñas et al. (2018), manuscripts in preparation.

Este documento incorpora firma electrónica, y es copia auténtica de un documento electrónico archivado por la ULL según la Ley 39/2015.
 Su autenticidad puede ser contrastada en la siguiente dirección <https://sede.ull.es/validacion/>

Identificador del documento: 1627512

Código de verificación: kOIBgUMu

Firmado por:	Fecha:
Roger Gimeno Llobet UNIVERSIDAD DE LA LAGUNA	25/10/2018 11:00:30
Diego Álvarez de la Rosa Rodríguez UNIVERSIDAD DE LA LAGUNA	25/10/2018 11:52:58
Teresa Giráldez Fernández UNIVERSIDAD DE LA LAGUNA	25/10/2018 11:54:04
Ernesto Pereda de Pablo UNIVERSIDAD DE LA LAGUNA	29/10/2018 13:01:03

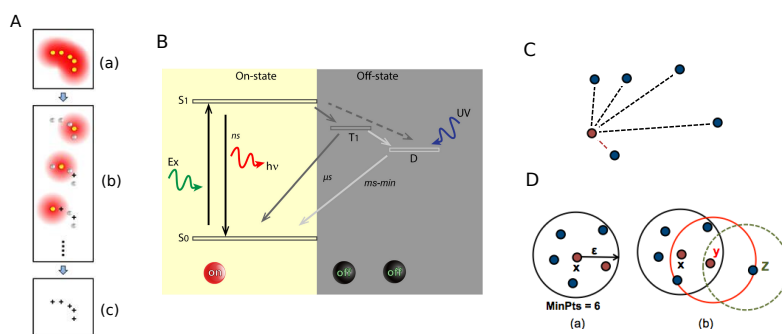


Figure 4.10: Concepts for STROM. A) Scheme illustrating the “on” and “off” and localization cycles; (a) When all molecules are emitting at the same time, individual molecules can not be resolved. (b) Stochastic activation and localization cycles. (c) A superresolution image can be reconstructed from individual localizations (image source: Huang Lab, huanglab.ucsf.edu). B) Jablonsky diagram showing molecular states of fluorophore blinking (image from (Nahidiazar et al., 2016)). C) NND; only the distance of each particle (red dot) to its nearest neighbor (dashed red line) is saved. D) Identification of dense regions by DBSCAN. Any point (x) in the data set that satisfies min_pts is marked as a core point of the cluster. A point will be marked as a border point (y) if the number of neighbors is less than min_pts but is reached by the eps parameter of a core point. Points that do not satisfy these requirements are counted as noise (z).

We developed two different methods to analyze the data. The first analysis method is the Nearest Neighbor Distance (NND), based on the k-Nearest Neighbor (k-NN) algorithm. With this method we can infer the most frequent distance between fluorophores. Secondly, we developed a script to perform cluster analysis. This allowed us to find the most probable number of clusters (specifying some constraints) and to calculate their areas. To this end, we used the density-based spatial clustering of applications with noise (DBSCAN) method. DBSCAN is a data clustering algorithm that identifies high density clusters from low density clusters, and handles very well noise points as outliers. The combination of these algorithms has already been used by other authors for processing superresolution images (Zhang et al., 2016).

The NND program uses the KDTree algorithm (Scipy library, `scipy.spatial` module) to obtain a list of the distances for all the neighbors of each particle in the molecules list. It computes three analyses: 647 to 647, where the distance between each Alexa-647-labeled molecule and all of its Alexa647-labeled molecule neighbors is measured; Alexa-488 to Alexa-488, and Alexa-647 to Alexa-488. Then, only the distance of each particle to its nearest neighbor is saved (Fig. 4.10C). At this point we have three arrays, 647 to 647, 488 to 488 and 647 to 488, which contain the NND of each particle. NNDs are then distributed in a histogram to identify the most frequent distances between particles. The flowchart of the program is shown in Fig. 4.11. The script that performs the NND analysis is attached at **Appendix A**.

The other analysis carried out is a cluster analysis with the aim to identify, count and calculate the areas of all possible clusters formed. This second analysis uses the DBSCAN algorithm (scikit learn library, `sklearn.cluster` module), a data-clustering algorithm that finds core points of high density and expands clusters from them. Two parameters are required, eps (epsilon) and min_pts (minimum points). eps is the

Este documento incorpora firma electrónica, y es copia auténtica de un documento electrónico archivado por la ULL según la Ley 39/2015.
 Su autenticidad puede ser contrastada en la siguiente dirección <https://sede.ull.es/validacion/>

Identificador del documento: 1627512

Código de verificación: kOIBgUMu

Firmado por: Roger Gimeno Llobet UNIVERSIDAD DE LA LAGUNA	Fecha: 25/10/2018 11:00:30
Diego Álvarez de la Rosa Rodríguez UNIVERSIDAD DE LA LAGUNA	25/10/2018 11:52:58
Teresa Giráldez Fernández UNIVERSIDAD DE LA LAGUNA	25/10/2018 11:54:04
Ernesto Pereda de Pablo UNIVERSIDAD DE LA LAGUNA	29/10/2018 13:01:03

Near Neighbor Distance (NND)

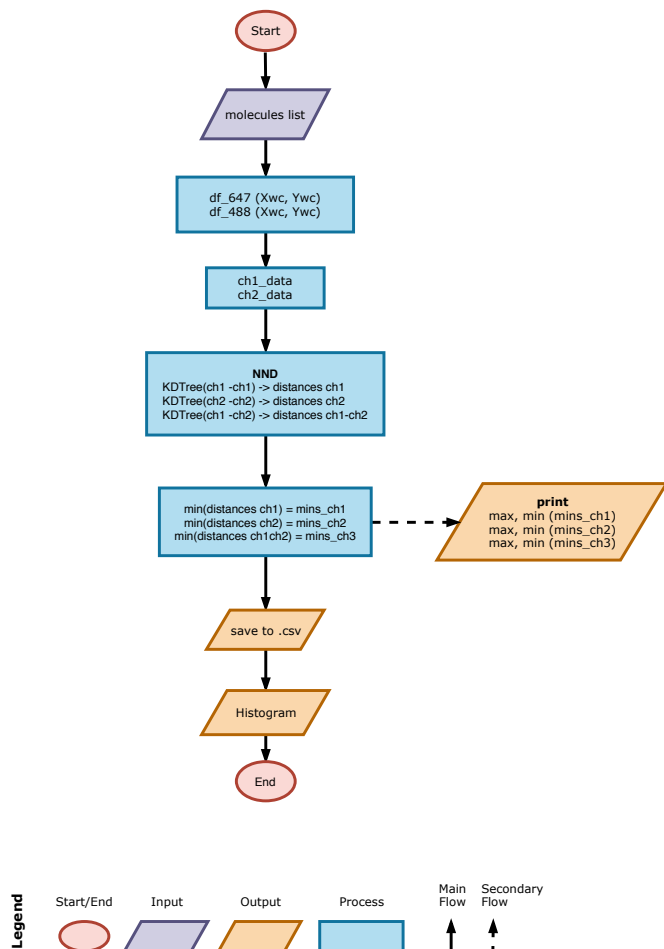


Figure 4.11: Flowchart of NND program

Este documento incorpora firma electrónica, y es copia auténtica de un documento electrónico archivado por la ULL según la Ley 39/2015.
 Su autenticidad puede ser contrastada en la siguiente dirección <https://sede.ull.es/validacion/>

Identificador del documento: 1627512

Código de verificación: kOIBgUMu

Firmado por: Roger Gimeno Llobet UNIVERSIDAD DE LA LAGUNA	Fecha: 25/10/2018 11:00:30
Diego Álvarez de la Rosa Rodríguez UNIVERSIDAD DE LA LAGUNA	25/10/2018 11:52:58
Teresa Giráldez Fernández UNIVERSIDAD DE LA LAGUNA	25/10/2018 11:54:04
Ernesto Pereda de Pablo UNIVERSIDAD DE LA LAGUNA	29/10/2018 13:01:03

maximum radius of the neighborhood of a point and can be inferred from the NND analysis, and *min_pts* are the minimum number of neighbors that have to be inside the *eps* radius. If a point has at least a number of neighbor points set by *min_pts* inside *eps* radius is counted as a core point of the cluster. Points that are within the *eps* radius of a core point but do not fulfill the *min_pts* requirement are counted as border points of the cluster. Finally, points that neither a border point nor a core point are noise (outliers) (Fig. 4.10D). The script that performs the Clusters analysis is attached at **Appendix B**.

The progress of the program can be followed either by the flowchart (Fig. 4.12) or the schematic representation of the variables involved (Fig. 4.13 and Fig. 4.14). This representation pretends to help in the operations performed in the different variables obtained during the process, and represents a simple example of five particles labeled wit Alexa-647 and five with Alexa-488 that forms one cluster of 647 only, one of 488 only and one of 647 with 488. The minimum points to form a cluster (*min_pts*) is set to three.

In practice, the first part of the Cluster program reads the .txt file outputted by the STORM Nikon software (molecules list), and splits the molecule list in 647-labeled particles, 488-labeled particles, and all particles (647 + 488), saving its X and Y corrected positions (Xwc, Ywc). Arrays containing the particles coordinates (2) are created and named ch1_data (647 molecules only), ch2_data (488 molecules only) and ch3_data (all molecules, 647 and 488). The number of particles for each array is printed (3). Then DBSCAN algorithm is applied to each array setting *eps* and *min_pts* values (4). The output are arrays where all the particles are related to clusters that are identified by a number, being -1 noise particles (not pertaining to any cluster) and 0, 1, 2, ..., the number that identifies the cluster (5). From these arrays the number of clusters (6) is calculated directly by the largest cluster identifier number. The number of clusters for each array is printed (7). The number of particles conforming each cluster is also calculated (8). Cluster identifiers obtained in (5) are applied to coordinates arrays (2) to generate new arrays (9) containing only particles forming clusters, sorted by identifier. To calculate the area of the clusters, the custom function Area has been defined at the beginning of the program, and it will be called in the next step (10). This function takes the positions of the vertices of the cluster given by the ConvexHull algorithm (scipy library, scipy.spatial module). The ConvexHull finds the smallest convex polygon that contains all the points that forms the cluster, identifying core points and vertices (10). The output are new arrays (11) containing the calculated areas of the clusters, for each channel (areas_ch1, areas_ch2, areas_ch3). Its important to note that areas_ch3 contains areas of clusters formed by 647-labeled molecules only, 488-labeled molecules only, and clusters formed by both. Clusters formed by 647 or 488-labeled molecules only have to be subtracted from areas_ch3 to obtain the correct number of 647-488 clusters. We found that the best way to address this was to identify clusters by number of particles and area, as a variation in any of them will be indicative of a 647-488 cluster. In this way new arrays were created (12) identifying the clusters by number of particles and area (chX_counts, areas_chX). Clusters of ch1 with same number of particles and area as ch3 were eliminated from ch3, and same as for ch2 with ch3 (13). To find these identical elements the Python's function intersection is used, that searches for common elements within arrays. Finally, a new array named ch3_new only containing 647-488 clusters was generated (14). At this points the values were stored in csv files and plotted in a histogram.

Este documento incorpora firma electrónica, y es copia auténtica de un documento electrónico archivado por la ULL según la Ley 39/2015.
 Su autenticidad puede ser contrastada en la siguiente dirección <https://sede.ull.es/validacion/>

Identificador del documento: 1627512

Código de verificación: KOIBgUMu

Firmado por:	Fecha:
Roger Gimeno Llobet UNIVERSIDAD DE LA LAGUNA	25/10/2018 11:00:30
Diego Álvarez de la Rosa Rodríguez UNIVERSIDAD DE LA LAGUNA	25/10/2018 11:52:58
Teresa Giráldez Fernández UNIVERSIDAD DE LA LAGUNA	25/10/2018 11:54:04
Ernesto Pereda de Pablo UNIVERSIDAD DE LA LAGUNA	29/10/2018 13:01:03

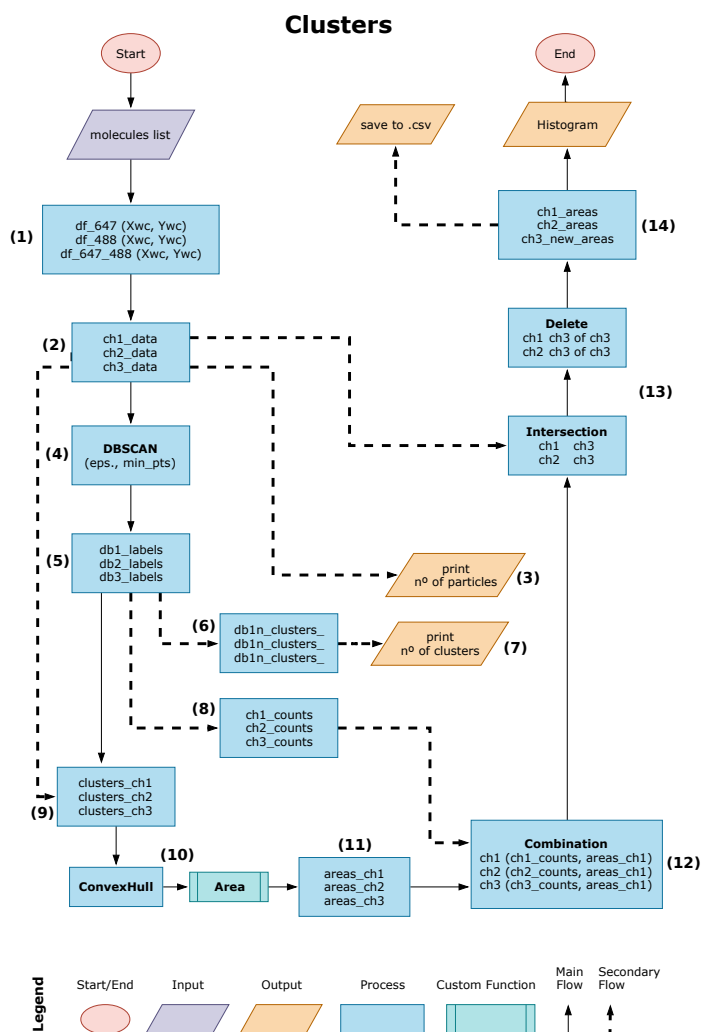


Figure 4.12: Flowchart of Clusters program. The numbers between parenthesis indicates steps of the program that are described in the text and in Fig. 4.13 and Fig. 4.14.

Este documento incorpora firma electrónica, y es copia auténtica de un documento electrónico archivado por la ULL según la Ley 39/2015.
 Su autenticidad puede ser contrastada en la siguiente dirección <https://sede.ull.es/validacion/>

Identificador del documento: 1627512

Código de verificación: KOIBgUMu

Firmado por: Roger Gimeno Llobet UNIVERSIDAD DE LA LAGUNA	Fecha: 25/10/2018 11:00:30
Diego Álvarez de la Rosa Rodríguez UNIVERSIDAD DE LA LAGUNA	25/10/2018 11:52:58
Teresa Giráldez Fernández UNIVERSIDAD DE LA LAGUNA	25/10/2018 11:54:04
Ernesto Pereda de Pablo UNIVERSIDAD DE LA LAGUNA	29/10/2018 13:01:03

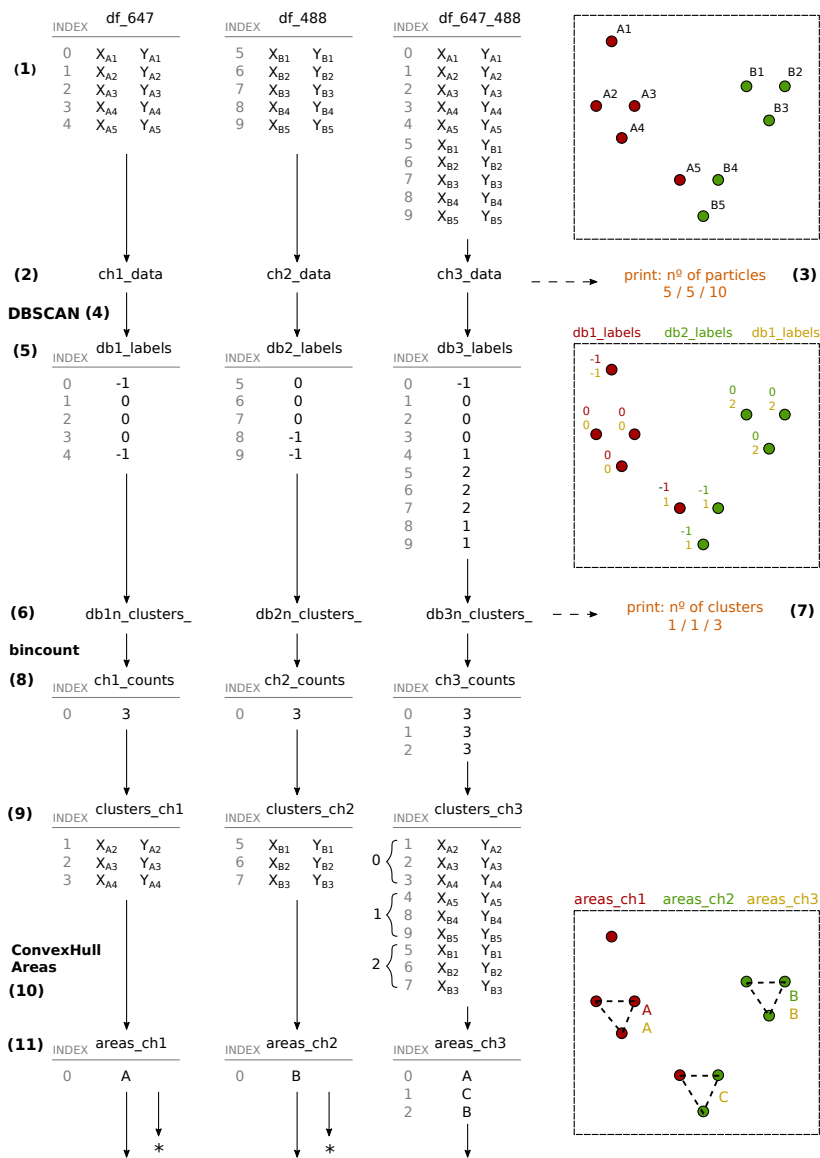


Figure 4.13: This figure continues in the next page.

Este documento incorpora firma electrónica, y es copia auténtica de un documento electrónico archivado por la ULL según la Ley 39/2015.
 Su autenticidad puede ser contrastada en la siguiente dirección <https://sede.ull.es/validacion/>

Identificador del documento: 1627512

Código de verificación: kOIBgUMU

Firmado por: Roger Gimeno Llobet UNIVERSIDAD DE LA LAGUNA	Fecha: 25/10/2018 11:00:30
Diego Álvarez de la Rosa Rodríguez UNIVERSIDAD DE LA LAGUNA	25/10/2018 11:52:58
Teresa Giráldez Fernández UNIVERSIDAD DE LA LAGUNA	25/10/2018 11:54:04
Ernesto Pereda de Pablo UNIVERSIDAD DE LA LAGUNA	29/10/2018 13:01:03

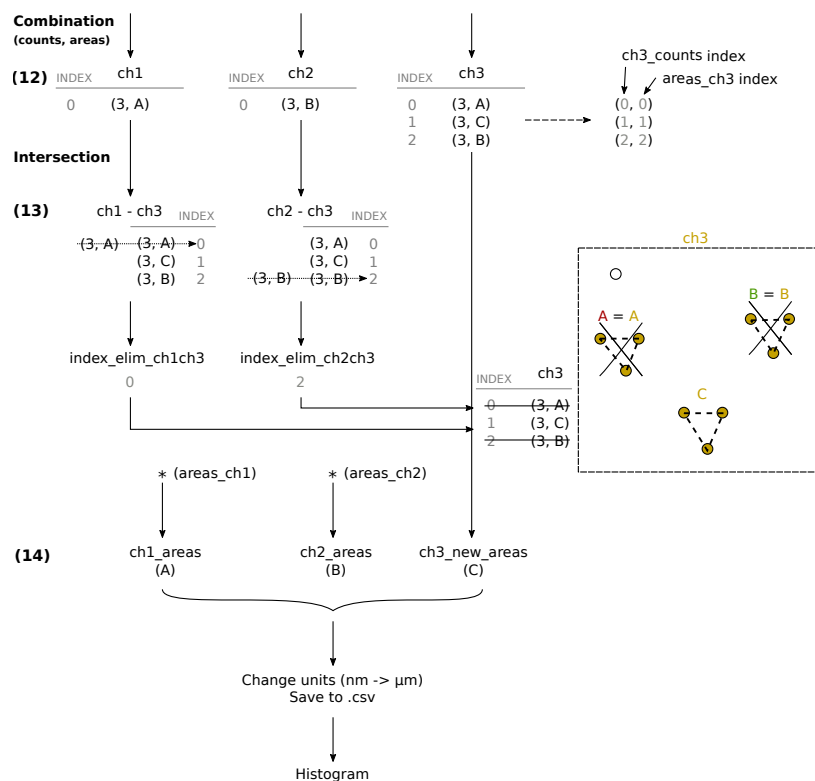


Figure 4.14: Description of the process for Clusters script, showing the operations in the variables for a simple example. The example consist in a field where five 647-labeled particles and five 488-labeled particles forms three clusters: one 647 only, one 488 only, and one composed by 647 and 488 particles. The numbers between parenthesis indicates steps of the program that are described in the text.

Este documento incorpora firma electrónica, y es copia auténtica de un documento electrónico archivado por la ULL según la Ley 39/2015.
 Su autenticidad puede ser contrastada en la siguiente dirección <https://sede.ull.es/validacion/>

Identificador del documento: 1627512

Código de verificación: KOIBgUMu

Firmado por: Roger Gimeno Llobet

UNIVERSIDAD DE LA LAGUNA

Fecha: 25/10/2018 11:00:30

Diego Álvarez de la Rosa Rodríguez
 UNIVERSIDAD DE LA LAGUNA

25/10/2018 11:52:58

Teresa Giráldez Fernández
 UNIVERSIDAD DE LA LAGUNA

25/10/2018 11:54:04

Ernesto Pereda de Pablo
 UNIVERSIDAD DE LA LAGUNA

29/10/2018 13:01:03

4.9.2 Controls for analysis scripts

control1: Simple configuration

We first checked the analysis scripts by creating very simple clusters, manually adding 647- and 488-labeled particles with (x,y) coordinates ranging from 0 to 9 (Fig. 4.15A), and setting the DBSCAN parameters eps and min_pts to obtain the desired number of clusters previously calculated. The particles are set in the plane in a way that changing the eps parameter alters the final number of clusters obtained (Fig. 4.15A vs Fig. 4.15E). We considered that a cluster would be constituted by minimum 3 particles fixing $min_samples$ to 3. If we set eps to 1, the furthest particles of 647 and 488 that are in the upper left corner and the middle right are not close enough to form a cluster between them (Fig. 4.15A, black arrows), and application of the algorithm will raise 3 clusters in 647 and 2 in 488 (Fig. 4.15B and C respectively). Clusters are connected with a dashed line, and particles that do not belong to any cluster are single dots. The final number of 647 and 488 clusters will be 2, containing 5 and 10 particles (Fig. 4.15D). Transparent clusters in 647 and 488 (Fig. 4.15D and H) are removed clusters that are only composed by 647 or 488 particles. Another situation will occur if we set eps to 2, because the furthest 647 and 488 particles in the upper left corner and the middle right will be within the eps value (Fig. 4.15E, black arrows). After running the algorithm we will obtain 2 clusters in 647, 2 in 488 and a final number of 2 clusters of 647 and 488 clusters, but now containing 6 and 17 particles. Now the single 488 dot counted before as noise is part of the upper left cluster, and the 647 only cluster in the upper right part removed before has joined the cluster below (Fig. 4.15H).

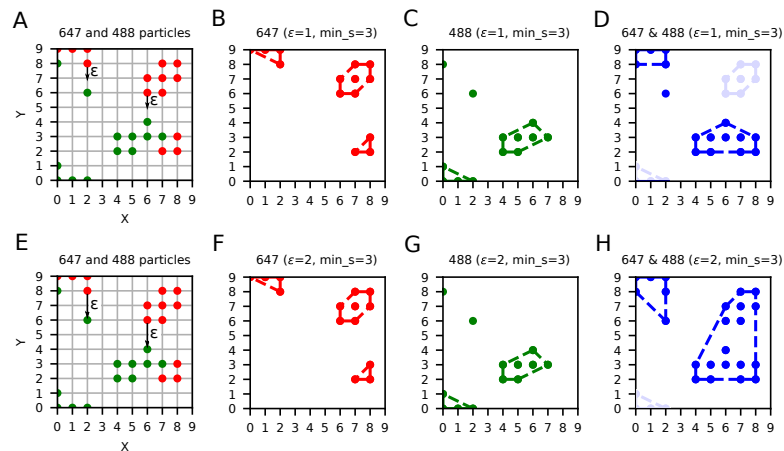


Figure 4.15: Control for STROM analysis scripts consisting in hand-written coordinates forming known clusters, in order to obtain the expected results. A) Field of coordinates; the distance eps (ϵ) value is set to 1 and the minimum points min_pts (min_s) to 3. B) Clusters found for the red labeled dots. C) Clusters found for the green labeled dots. D) Clusters formed by red-green dots (colored in blue); only red and only green are excluded (transparency). E) Same distribution of points but noe setting $eps = 2$. F) and G) same as for B) and C). H) With this values of eps , the upper left cluster reaches the green dot located at the bottom of the cluster, forming a new cluster. Similar situation for the upper right cluster, that reaches the bottom cluster, forming a new bigger cluster.

Este documento incorpora firma electrónica, y es copia auténtica de un documento electrónico archivado por la ULL según la Ley 39/2015.
 Su autenticidad puede ser contrastada en la siguiente dirección <https://sede.ull.es/validacion/>

Identificador del documento: 1627512

Código de verificación: kOIBgUMu

Firmado por: Roger Gimeno Llobet UNIVERSIDAD DE LA LAGUNA	Fecha: 25/10/2018 11:00:30
Diego Álvarez de la Rosa Rodríguez UNIVERSIDAD DE LA LAGUNA	25/10/2018 11:52:58
Teresa Giráldez Fernández UNIVERSIDAD DE LA LAGUNA	25/10/2018 11:54:04
Ernesto Pereda de Pablo UNIVERSIDAD DE LA LAGUNA	29/10/2018 13:01:03

control2: Rotation of a channel

The next control was to corroborate if the results obtained analyzing the dSTORM data were due to the formation of complexes between the labeled proteins and not due to random co-localization of the fluorophores. The over-expression of the target proteins in the cell and the possible immunostaining artifacts can cause the fluorophores to be close enough to be counted as clusters. An extended practice is to rotate the image of one channel, thus changing the relative position between labeled proteins without altering the co-expression or the labeling itself (Clifford M. Babbey, Nahid Ahkter, Exing Wang, Carlos Chih-Hsiung Chen, Dunn, and W., 2006; Kenneth W. Dunn, Malgorzata M. Kamocka and McDonald, 2011). We used one of the molecules list from the co-transfection of BK860cpG and Cav2.1 to generate the images of the localizations (Fig. 4.16A), where the BK860cpG is labeled with Alexa 488 (green dots) and Cav2.1 with Alexa 647 (red dots). The NND analysis gave a most frequent distant between BK860cpG and Cav2.1 of 60 nm, Fig. 4.16C) and the cluster analysis yielded 218 Cav2.1 clusters, 145 BK860cpG clusters and 271 BK860cpG-Cav2.1 clusters. A histogram representing the distribution the cluster's area (in μm^2) of each of the three kind of clusters (Cav2.1 only, BK860cpG only and clusters formed by BK860cpG and Cav2.1) related to the percentage of clusters in respect to the total amount of clusters (Cav2.1 plus BK860cpG plus BK860cpG-Cav2.1) is showed in Fig. 4.16D left. With the same molecule list, the positions of BK860cpG particles are modified rotating the field 90° clockwise and applying a vertical flip (Fig. 4.16B). This is the effect of performing a roll of the coordinates, and was accomplished with the *roll* function of the Python's numpy package. The new configuration of Cav2.1 and BK860cpG particles is analyzed again. In this case, the NND analysis gave a most frequent distant between BK860cpG and Cav2.1 of 150 nm with a second peak at 375 nm, with a substantial reduction in the number of counts (Fig. 4.16C). The cluster analysis yielded the same number of Cav2.1 alone and BK860cpG alone clusters, but now finding only 25 BK860cpG-Cav2.1 clusters. The associated histogram (Fig. 4.16D right) clearly shows that the number of clusters obtained in the original data was not the result of chance but a clear association between proteins.

4.9.3 BK860cpG construct colocalize with Cav2.1 channels in heterologous expression systems

We co-transfected HEK293T cells with BK860cpG and Cav2.1, and BK860cpG and Cav2.3. BK860cpG was labeled with Alexa 488 and Cav2.1 with Alexa 647. dSTORM imaging was carried out in Imaging Buffer (Table 3.2). dSTORM imaging of HEK293T visualized spatial association between BK860cpG and Cav2.1 (Fig. 4.17A). This situation was less frequent when BK860cpG was co-transfected with Cav2.3 (Fig. 4.17B). To quantify the data obtained, we used the two types of analysis previously described. NND analysis (Fig. 4.17C) revealed a colocalization consistent with a intimate assembly for BK860cpG and Cav2.1, with a sharp peak in the nearest neighbor localization distances of ~ 25 nm. For BK860cpG and Cav2.3 co-transfection a much broader peak was observed at ~ 50 nm. This results are in tune with the results obtained in other experiments co-transfecting wild-type BK with Cav2.1 (Fig. 4.17D), where the nearest neighbor localization distances were ~ 24 nm for BK-Cav2.1 and ~ 45 nm for BK-Cav2.3.

Cluster analysis was performed setting *eps* = 20 and *min_pts* = 10. The percentage of clusters in function of cluster area (in μm^2) is shown in Fig. 4.17E and

Este documento incorpora firma electrónica, y es copia auténtica de un documento electrónico archivado por la ULL según la Ley 39/2015.
 Su autenticidad puede ser contrastada en la siguiente dirección <https://sede.ull.es/validacion/>

Identificador del documento: 1627512

Código de verificación: kOIBgUMu

Firmado por:	Fecha:
Roger Gimeno Llobet UNIVERSIDAD DE LA LAGUNA	25/10/2018 11:00:30
Diego Álvarez de la Rosa Rodríguez UNIVERSIDAD DE LA LAGUNA	25/10/2018 11:52:58
Teresa Giráldez Fernández UNIVERSIDAD DE LA LAGUNA	25/10/2018 11:54:04
Ernesto Pereda de Pablo UNIVERSIDAD DE LA LAGUNA	29/10/2018 13:01:03

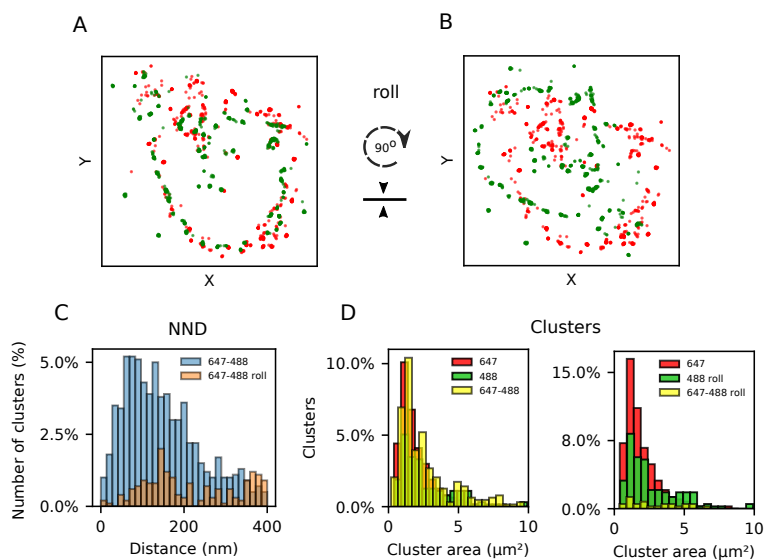


Figure 4.16: Control for STORM analysis scripts, consisting in the rotation of one of the images. A) Real STORM image of BK (488, green) and Cav (647, red) co-transfection. B) The BK image is rolled (90° rotation and flipped). C) NND analysis performed before (blue) and after (orange) the roll. Before the roll a sharp peak 60 nm was observed. After the roll the distribution is completely different, with smaller peaks in 150 and 375. D) The cluster analysis revealed a large number of clusters formed by 647 and 488 molecules in the original image. After the roll, the number of 647 only and 488 only clusters increased, as the number of 647-488 largely decreased. This kind of control indicates that the observed results in the original image are not due to a random distribution of points.

Este documento incorpora firma electrónica, y es copia auténtica de un documento electrónico archivado por la ULL según la Ley 39/2015.
 Su autenticidad puede ser contrastada en la siguiente dirección <https://sede.ull.es/validacion/>

Identificador del documento: 1627512

Código de verificación: KOIBgUMu

Firmado por: Roger Gimeno Llobet UNIVERSIDAD DE LA LAGUNA	Fecha: 25/10/2018 11:00:30
Diego Álvarez de la Rosa Rodríguez UNIVERSIDAD DE LA LAGUNA	25/10/2018 11:52:58
Teresa Giráldez Fernández UNIVERSIDAD DE LA LAGUNA	25/10/2018 11:54:04
Ernesto Pereda de Pablo UNIVERSIDAD DE LA LAGUNA	29/10/2018 13:01:03

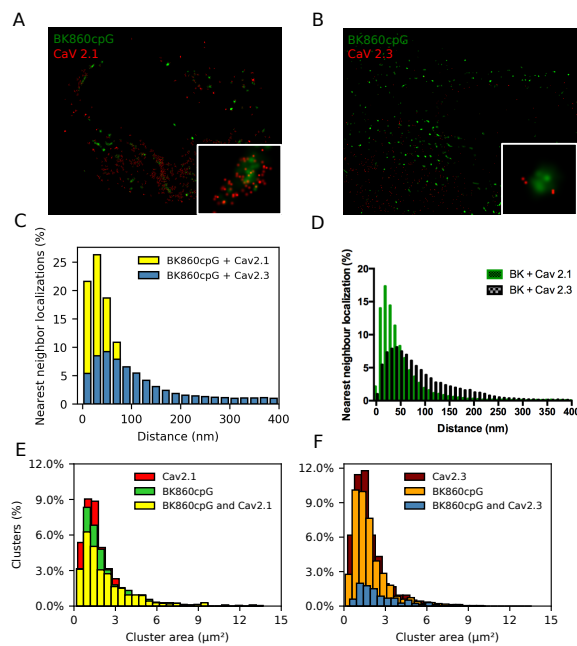


Figure 4.17: STORM experiments with BK860cpG and Cav2.1 or Cav2.3. Super-resolution images of co-transfection of BK860cpG and Cav2.1 (A) and BK860cpG and Cav2.3 (B) in HEK293T cells. c) NND analysis of BK860cpG with Cav2.1 (yellow) and BK860cpG with Cav2.3 (blue). D) NND analysis of wild-type BK with Cav2.1 (green) and wild-type BK with Cav2.3 (black). E) Cluster analysis of BK860cpG-Cav2.1 complexes. Clusters formed by Cav2.1 only are shown in red, by BK860cpG only in green, and by both BK860cpG and Cav2.1 in yellow. F) Clusters formed by Cav2.3 only are shown in maroon, by BK860cpG only in orange, and by both BK860cpG and Cav2.3 in blue.

F for the co-transfections of BK860cpG-Cav2.1 and BK860cpG-Cav2.3 respectively. BK860cpG-Cav2.1 have a similar amount of Cav2.1 (red) and BK860cpG (green) only clusters at ~9%. There is a considerable fraction of clusters formed by both BK860cpG and Cav2.1 (yellow) at ~6%. The peaks of the distributions points that the majority of clusters have ~1 µm² of area. On the other hand, the situation when BK860cpG is co-transfected with Cav2.3 (Fig. 4.17F) is quite different. The percentage of Cav2.3 (maroon) and BK860cpG (orange) only clusters is larger if compared to that of Fig. 4.17E (~12% in comparison to ~9%), indicating that there are less clusters formed by both, as can be seen from the dramatically reduced distribution of BK860cpG-Cav2.3 clusters (blue), near 1.5%. The obtained distributions strongly suggest that when BK860cpG is co-transfected with Cav2.1 both proteins localize in close proximity, with a distance between them of 25 nm, forming a considerable number of clusters with a cluster area of ~1 µm².

Este documento incorpora firma electrónica, y es copia auténtica de un documento electrónico archivado por la ULL según la Ley 39/2015.
 Su autenticidad puede ser contrastada en la siguiente dirección <https://sede.ull.es/validacion/>

Identificador del documento: 1627512

Código de verificación: KOIBgUMu

Firmado por: Roger Gimeno Llobet UNIVERSIDAD DE LA LAGUNA	Fecha: 25/10/2018 11:00:30
Diego Álvarez de la Rosa Rodríguez UNIVERSIDAD DE LA LAGUNA	25/10/2018 11:52:58
Teresa Giráldez Fernández UNIVERSIDAD DE LA LAGUNA	25/10/2018 11:54:04
Ernesto Pereda de Pablo UNIVERSIDAD DE LA LAGUNA	29/10/2018 13:01:03

4.10 Distance analysis for generation of additional BK-cpGFP Ca²⁺ sensors

A library of 22 functional BK fluorescent channels, with insertions of GFP variants in different places of the BK is available in our laboratory (Giraldez, Hughes, and Sigworth, 2005). Recently, structures of the full BK with bound (10 mM Ca²⁺ / 10 mM MgCa²⁺) and unbound (1 mM EDTA) Ca²⁺ have been resolved (Xiao Tao, Hite, and MacKinnon, 2017; Hite, Tao, and MacKinnon, 2017).

In this study we reasoned that the combination of our BK fluorescent constructs library with the recent extensive structural data could allow us to obtain novel BK-based Ca²⁺ sensors. We carefully studied the cryo-EM structures positioning our FP insertion sites previously obtained (Giraldez, Hughes, and Sigworth, 2005), hoping to make an educated guess to identify the best sites in BK to insert cpGFP. The idea was to identify regions undergoing major structural changes (thus ideal to insert a cpGFP) by quantifying the distance between sites in the Ca²⁺-bound and Ca²⁺-unbound structures. The sites studied were those obtained in our previous study, which were permissive for insertion of fluorescent proteins (Giraldez, Hughes, and Sigworth, 2005). For this purpose, we superimposed the bound/unbound Ca²⁺ structures and compared the distances within sites containing GFP insertions in the library (Fig. 4.18A). We used the software Chimera (UCSF) to superimpose the structures. From (Hite, Tao, and MacKinnon, 2017) we aligned the structures relative to their selectivity filters, pairing V277, G278 and F279 residues with the *match* command.

Fig. 4.18B shows the distance separating the specific residues C α in the Ca²⁺-bound and -unbound structures. It is important to note that the structures include large regions where the structure could not be resolved (Xiao Tao, Hite, and MacKinnon, 2017; Hite, Tao, and MacKinnon, 2017), including the regions containing the 860 and 667 sites studied in this Thesis. In Fig. 4.18B, residues which were solved in the structure are shown in blue. Sites corresponding to GFP insertions are labeled in red.

The existence of unsolved structural regions in the available structures made it impossible to calculate changes in distance between sites in constructs BK667cpG and BK860cpG, since the 667 and 860 positions were not resolved in the structures (blank spaces). However, we can calculate a rough estimate of the change in distance between the non-resolved sites by using the closest solved position. For the BK667cpG construct, that position is amino acid 685³. The change in distance between sites 685 for the Ca²⁺-unbound vs. Ca²⁺-bound structures is 8.7 Å. In the case of the BK860cpG, the closest structure-solved position is amino acid 884. The change in distance between the available structures is 6.3 Å. These calculated distances indicate larger rearrangements in the BK-667cpG construct than in the BK-860cpG, therefore predicting larger fluorescence intensity changes in the former. However, the results obtained in ionomycin-mediated Ca²⁺ loading experiments seem not to match our predictions. In fact, BK860cpG is the construct showing the larger change in fluorescence intensity. Although preliminary, this analysis shows that there is not a strict correlation of the distance a specific residue moves apart upon Ca²⁺ activation of BK with the structural rearrangements that are sensed by the cpGFP.

³Note that position numbers are from human BK (h). Resolved full BK structures are in the gastropod mollusk *Aplysia Californica* (ac). Correspondence of mentioned positions are h685 – ac707, h874 – ac884 and h965 – ac975.

Este documento incorpora firma electrónica, y es copia auténtica de un documento electrónico archivado por la ULL según la Ley 39/2015.
 Su autenticidad puede ser contrastada en la siguiente dirección <https://sede.ull.es/validacion/>

Identificador del documento: 1627512

Código de verificación: kOIBgUMu

Firmado por:	Fecha:
Roger Gimeno Llobet UNIVERSIDAD DE LA LAGUNA	25/10/2018 11:00:30
Diego Álvarez de la Rosa Rodríguez UNIVERSIDAD DE LA LAGUNA	25/10/2018 11:52:58
Teresa Giráldez Fernández UNIVERSIDAD DE LA LAGUNA	25/10/2018 11:54:04
Ernesto Pereda de Pablo UNIVERSIDAD DE LA LAGUNA	29/10/2018 13:01:03

4.11. The gating ring as a transferable Ca^{2+} -sensitive molecular module

63

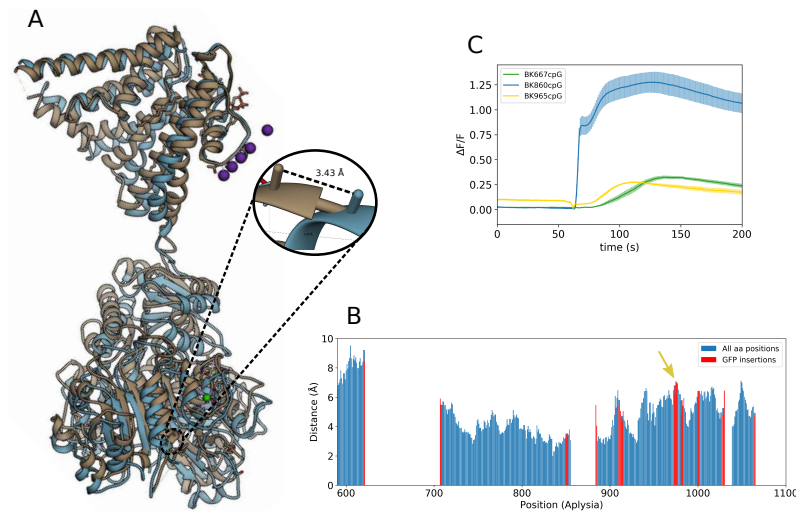


Figure 4.18: Study based on the resolved BK Cryo-EM structures to determine the best positions to insert the cpGFP. (A) The structures with bound/unbound Ca^{2+} were superimposed using Chimera. All the $C\alpha$ distances of the same residues between structures were calculated (insert). (B) Distance that moves each residue versus residue position. In blue all the residues, in red positions were we have our GFP variants insertions. Blank spaces are zones of the structure not resolved. Yellow arrow indicates residue 965, the candidate to generate the new construct, BK965cpG. (C) Ionomycin-mediated loading Ca^{2+} experiments to test the new construct. BK965cpG produced a similar response to BK667cpG.

To further confirm this idea, we studied the effect of inserting cpGFP into the 965 site, which showed a large distance change between sites in the Ca^{2+} -unbound vs. Ca^{2+} -bound structures, 7.3 Å (yellow arrow).

We subcloned the cpGFP into the existing construct BK965CFP (Giraldez, Hughes, and Sigworth, 2005), resulting in construct BK965cpG, where the cpGFP is inserted in the 965 amino acid position. Fig. 4.18C shows the fluorescent changes in response to ionomycin for BK965cpG, compared with BK860cpG and BK667cpG. BK965cpG showed a $\Delta F/F$ similar to BK667cpG, but with a slightly faster kinetics. Therefore, as will be further discussed in other sections, this approach (taking solely distance changes into consideration) cannot be used to predict useful insertion sites for sensor generation. More comprehensive analysis is needed, including other factors such as amino acid orientation or other environmental effects from neighboring residues, which may influence the rearrangements that eventually lead to measurable changes in cpGFP fluorescence.

4.11 The gating ring as a transferable Ca^{2+} -sensitive molecular module

In this study we have generated Ca^{2+} sensors based on the BK channel. Recent investigations carried out by our group have demonstrated that there are remarkably large rearrangements of the gating ring upon Ca^{2+} binding in intact BK channels, much larger than the rearrangements predicted by existing X-ray structures of the

Este documento incorpora firma electrónica, y es copia auténtica de un documento electrónico archivado por la ULL según la Ley 39/2015.
 Su autenticidad puede ser contrastada en la siguiente dirección <https://sede.ull.es/validacion/>

Identificador del documento: 1627512

Código de verificación: KOIBgUMu

Firmado por: Roger Gimeno Llobet UNIVERSIDAD DE LA LAGUNA	Fecha: 25/10/2018 11:00:30
Diego Álvarez de la Rosa Rodríguez UNIVERSIDAD DE LA LAGUNA	25/10/2018 11:52:58
Teresa Giráldez Fernández UNIVERSIDAD DE LA LAGUNA	25/10/2018 11:54:04
Ernesto Pereda de Pablo UNIVERSIDAD DE LA LAGUNA	29/10/2018 13:01:03

Table 4.5: Gating ring constructs of fluorescent BK-FRET pairs.

Constructs	Insertion site	GFP variant	FRET pair	Length (bp)
BKgr667C_j	667	CFP	BKgr667Y_j	2991
BKgr667Y_j	667	YFP	BKgr667C_j	2991
BKgr860C_j	860	CFP	BKgr860Y_j	2991
BKgr860Y_j	860	YFP	BKgr860C_j	2991
BKgr667C_o	667	CFP	BKgr667Y_o	2835
BKgr667Y_o	667	YFP	BKgr667C_o	2835
BKgr860C_o	860	CFP	BKgr860Y_o	2835
BKgr860Y_o	860	YFP	BKgr860C_o	2835

isolated gating ring (Miranda et al., 2013). The modular nature of this protein, including a gating ring structure containing all Ca^{2+} binding sites, led us to propose that the isolated gating ring may act as a Ca^{2+} -sensing module, which could be attached to other proteins, providing them with Ca^{2+} -sensitivity.

In this Thesis, we tested this hypothesis by generating two constructs based on the available information about the isolated gating ring. The first construct (BKgr667/860C/Y_j) was created based on the available crystal structure of the entire cytoplasmic region of the human BK channel in a Ca^{2+} -free state (Wu et al., 2010). This study of an isolated part of the gating ring provided the first glimpse of two possible gating-ring conformations of BK channels. The second construct generated in this Thesis (BKgr667/860C/Y_o) was done following the work by Javaherian *et al.*, in which they isolated the gating ring for biochemistry studies. All generated gating ring constructs with its FRET partners can be seen in Table 4.5. Specifically, this work functionally probed the metal-sensing properties of the human BK gating ring under physiologically relevant conditions (Javaherian et al., 2011). The authors demonstrated that the BK gating ring operates as a selective chemo-mechanical coupler that transduces the free energy of ligand binding into mechanical work that ultimately activates the channel. Both constructs generated in this Thesis (BKgr667/860C/Y_j and BKgr667/860C/Y_o) differed in their length, one containing a larger portion of the S6-RCK1 linker than the other (Fig. 3.3). In addition, our isolated BK gating ring included the cyan and yellow variants of the green fluorescent protein (CFP/YFP) inserted at residue 667 (located in the linker between RCK1 and RCK2), or at the 860 site (RCK2 domain).

4.11.1 FRET efficiency - Acceptor Photobleaching studies of isolated fluorescent gating rings

Heterotetramers formed by isolated gating rings with CFP or YFP insertions at the equivalent positions within the tetramers were co-transfected to ideally achieve a 3CFP:1YFO stoichiometry in HEK293T cells (Fig. 4.19A left and B left). In these experiments, FRET efficiency (E) (Fig. 4.19C) was obtained by the Acceptor Photobleaching (AB) technical approach. This technique consists on bleaching the acceptor fluorophore (Fig. 4.19B right) with a high intensity laser beam, and measuring the change between acceptor intensities before and after bleaching the acceptor (Fig. 4.19A). These experiments were performed in basal Ca^{2+} concentration conditions, without applying any stimuli. In these conditions, based on our previous

Este documento incorpora firma electrónica, y es copia auténtica de un documento electrónico archivado por la ULL según la Ley 39/2015.
 Su autenticidad puede ser contrastada en la siguiente dirección <https://sede.ull.es/validacion/>

Identificador del documento: 1627512

Código de verificación: kOIBgUMu

Firmado por:	Fecha:
Roger Gimeno Llobet UNIVERSIDAD DE LA LAGUNA	25/10/2018 11:00:30
Diego Álvarez de la Rosa Rodríguez UNIVERSIDAD DE LA LAGUNA	25/10/2018 11:52:58
Teresa Giráldez Fernández UNIVERSIDAD DE LA LAGUNA	25/10/2018 11:54:04
Ernesto Pereda de Pablo UNIVERSIDAD DE LA LAGUNA	29/10/2018 13:01:03

4.11. The gating ring as a transferable Ca^{2+} -sensitive molecular module

65

work (Miranda et al., 2013), we expected that constructs with CFP/YFP insertions at the 667 position would not produce FRET, since the 667 sites are too far apart. On the other hand, the fluorophores inserted at 860 positions should be close enough to produce FRET in basal Ca^{2+} conditions.

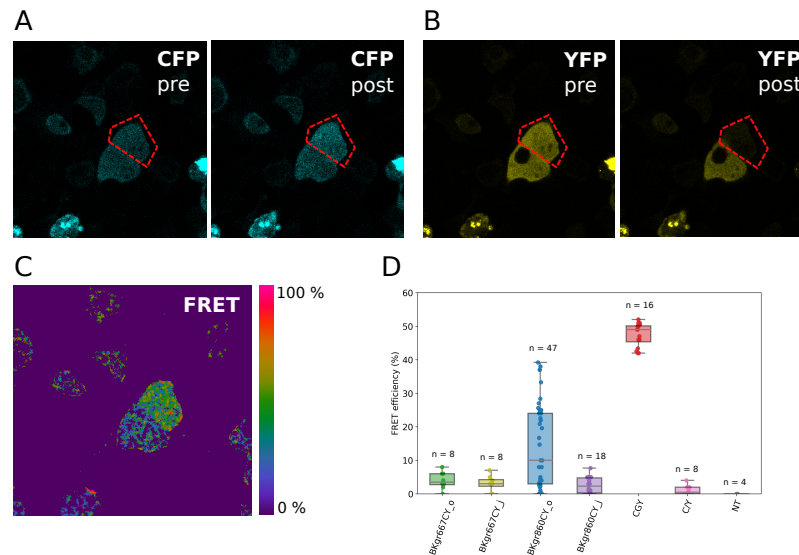


Figure 4.19: Acceptor Photobleaching experiments with gating ring construct BKgr860CY_o, carried out with a Leica SP8 confocal microscope. Transfection into HEK 293 cells was done co-transfecting constructs expressing CFP (BKgr860C_o) and constructs expressing YFP (BKgr860Y_o), with a stoichiometry of 3:1 of CFP:YFP. (A) Images of CFP detection before and after photobleaching. The red dashed polygon indicates the region selected for bleaching. Note the increase in fluorescence intensity in the bleached region. (B) Images of YFP detection before and after photobleaching. (C) FRET image with LUT of pseudocolors, ranging from 0% FRET efficiency (purple) to 100% FRET efficiency (pink). FRET efficiency of the ROI was 37%, nearly the maximum efficiency that CFP-YFP pair can reach. (D) FRET efficiency is showed for each isolated gating ring construct obtained using Acceptor Photobleaching technique. Constructs with the insertion in the 667 position didn't showed a considerable FRET efficiency as expected in this Ca^{2+} free state. BKgr860CY_o construct showed FRET efficiency about 14%. However, the asymmetric distribution of the results suggests that there is some point in the protein formation that leads to a non-working gating ring complex. In the other hand Jiang's 860 construct didn't showed a consistent FRET efficiency. It seems that the difference in the length of the aminoacidic chain is determinant in the gating ring formation. Controls are: not transfected cells (NT), simultaneous transfection of only ECFP and only EYFP plasmids (C/Y) and a positive FRET control CGY, a cytosolic plasmid formed by the ECFP and the EYFP linked by Glycines. n = 8 for BKgr667CY_o, n = 8 for BKgr667CY_j, n = 47 for BKgr860CY_o, n = 18 for BKgr860CY_j, n = 8 for C/Y and n = 16 for CGY. All plasmids have been transfected in HEK293 cells and FRET experiments in the confocal microscope Leica SP8 have been done after 24 hours.

Fig. 4.19D summarizes the FRET efficiencies obtained for the gating ring constructs and the controls used in this study. In non-transfected cells, E is near zero when the mean E value of the entire cell is computed. However, it is important to mention that the acceptor photobleaching method can introduce some artifacts in the determination of the FRET efficiency, probably due to some small movement of the sample between the pre-bleach and the post-bleach images. This can be observed in

Este documento incorpora firma electrónica, y es copia auténtica de un documento electrónico archivado por la ULL según la Ley 39/2015.
 Su autenticidad puede ser contrastada en la siguiente dirección <https://sede.ull.es/validacion/>

Identificador del documento: 1627512

Código de verificación: kOIBgUMu

Firmado por: Roger Gimeno Llobet UNIVERSIDAD DE LA LAGUNA	Fecha: 25/10/2018 11:00:30
Diego Álvarez de la Rosa Rodríguez UNIVERSIDAD DE LA LAGUNA	25/10/2018 11:52:58
Teresa Giráldez Fernández UNIVERSIDAD DE LA LAGUNA	25/10/2018 11:54:04
Ernesto Pereda de Pablo UNIVERSIDAD DE LA LAGUNA	29/10/2018 13:01:03

Fig. 4.19C, were cells that are not bleached (outside the red dashed-line area) display some FRET efficiency in the border or inside the cell (i.e. the red colored spot in the cell at the bottom of the image). A negative control consisting in the co-transfection of a CFP and YFP where fluorophores are not interacting was used (C/Y construct) rendering an E value of 1.12 ± 0.51 %.

Constructs with insertions in the 667 site, BKgr667CY_o and BKgr667CY_j showed slightly larger FRET efficiency values of $E = 4.00 \pm 0.91$ % and $E = 3.12 \pm 0.83$ % respectively. For construct BKgr667CY_o this difference was statistically significant ($P \leq 0.01$), indicating some degree of interaction between fluorophores.

The construct BKgr860CY_o showed a FRET efficiency value of $E = 14.01 \pm 1.83$ %. Surprisingly, construct BKgr860CY_j did not show FRET efficiency values significantly different from the C/Y negative control ($E = 2.52 \pm 0.55$ %). Interestingly, the BKgr860CY_o construct corresponds to the longer isolated gating ring construct studied by the Olcesse group (Javaherian et al., 2011), where functional experiments were carried out. However, the wide distribution of the results may suggest the existence of various protein conformations, probably including non-working gating ring complexes.

The major problem performing acceptor photobleaching in basal Ca^{2+} conditions as the method to quantify FRET between fluorophores is that we do not obtain information about the Ca^{2+} -bound configuration of the isolated gating rings. We designed an AB experiment to measure both Ca^{2+} -bound and unbound configurations of the isolated gating rings, by using ionomycin to increase the Ca^{2+} concentration in the cytosol. We performed AB in transfected cells in one half of the field (half left part of the coverslip); we then added 15 μ M ionomycin in the medium, and performed AB in the other half of the field (half right part) (**Fig. 4.20A**).

An schematic representation of the expected behavior of BKgr667CY_o,j and BKgr860CY_o,j constructs after the addition of ionomycin can be seen in **Fig. 4.20B**. The increase in the cytosolic $[Ca^{2+}]$ after addition of ionomycin will cause a structural rearrangement in the isolated gating rings. The fluorophores in the BKgr667 constructs will come closer and an increase in the FRET efficiency is expected. On the other hand, fluorophores in the BKgr860 constructs will move apart, causing a decrease in the FRET efficiency. In the scheme, sole emission of CFP represents a no-FRET situation, while emission of both CFP and YFP represents a FRET situation. The isolated gating ring constructs are represented as black cylinder cartoons with the inserted FRET pairs (cyan and yellow sphere cartoons representing CFP and YFP fluorophores). A black cross inside the cartoon represents the Ca^{2+} binding site Ca^{2+} bowl. Ca^{2+} ions are represented as orange dots (to simplify, the Ca^{2+} binding site in the RCK1 domain is not represented).

Fig. 4.20C shows the FRET efficiency obtained for each gating ring construct and the negative control C/Y obtained in these experiments. Isolated gating rings with FP insertions in the 667 site produce small increments in the E , as expected. However, these changes are not statistically significant. On the other hand, the construct BKgr860CY_o displayed a decrease in E after the addition of ionomycin. However, construct BKgr860CY_j did not show statistically significant changes in E . The negative control C/Y remained unchanged after ionomycin. Data is summarized in **Table 4.6**.

Este documento incorpora firma electrónica, y es copia auténtica de un documento electrónico archivado por la ULL según la Ley 39/2015.
 Su autenticidad puede ser contrastada en la siguiente dirección <https://sede.ull.es/validacion/>

Identificador del documento: 1627512

Código de verificación: kOIBgUMu

Firmado por:	Fecha:
Roger Gimeno Llobet UNIVERSIDAD DE LA LAGUNA	25/10/2018 11:00:30
Diego Álvarez de la Rosa Rodríguez UNIVERSIDAD DE LA LAGUNA	25/10/2018 11:52:58
Teresa Giráldez Fernández UNIVERSIDAD DE LA LAGUNA	25/10/2018 11:54:04
Ernesto Pereda de Pablo UNIVERSIDAD DE LA LAGUNA	29/10/2018 13:01:03

4.11. The gating ring as a transferable Ca^{2+} -sensitive molecular module

67

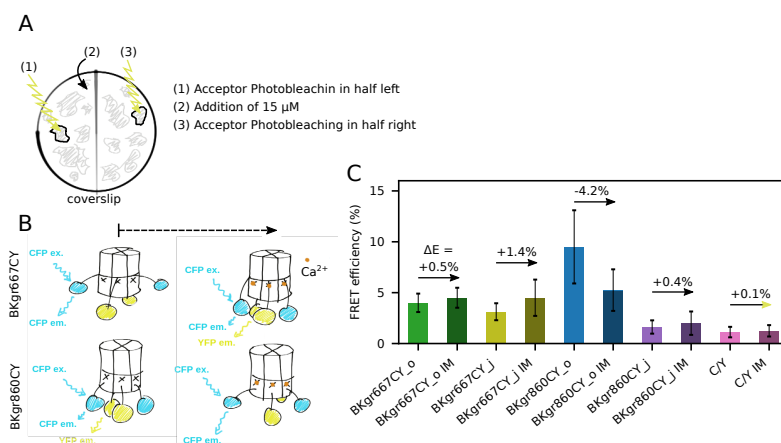


Figure 4.20: Acceptor Photobleaching experiments with gating ring constructs, where ionomycin is added between registries. (A) Schematic representation of a coverslip with transfected cells. The field is virtually divided in two parts (half left and half right). Acceptor photobleaching is performed first in basal conditions in the half left of the coverslip. Then 15 μ M ionomycin is added to the medium. After 30s, acceptor photobleaching is performed in the half right in order to avoid bleaching a bleached cell. (B) Schematic representation of the isolated gating ring constructs (black cylinder cartoons) with the inserted FRET pairs (cyan and yellow sphere cartoons representing CFP and YFP fluorophores). A black cross inside the cartoon represent the Ca^{2+} binding site Ca^{2+} bowl, and Ca^{2+} ions are represented as orange dots (to simplify, the Ca^{2+} binding site in the RCK1 domain is not represented). The dashed arrow indicates the expected behavior of BKgr667CY_oj and BKgr860CY_oj constructs with the addition of ionomycin. The increase in the cytosolic [Ca^{2+}] after addition of ionomycin will cause a structural rearrangement in the isolated gating rings. The fluorophores in the 667 constructs will come closer and an increase in the FRET efficiency is expected. On the other hand, fluorophores in the 860 constructs will move apart, causing a decrease in the FRET efficiency. In the scheme, emission of CFP only represents a no-FRET situation, while emission of both CFP and YFP represents a FRET situation. (C) FRET efficiency of each gating ring construct and the negative control C/Y for the basal Ca^{2+} situation before addition of ionomycin and the Ca^{2+} -binded situation (dark colors) after addition of ionomycin. The arrows between both situations represents the change in FRET efficiency (δE). Isolated gating rings with insertions in the 667 site have small increments in the E as expected. However the changes are not statistically significant. Construct BKgr860CY_o displayed a considerably decrease in the E after the addition of ionomycin, in tune with the expected results. Construct BKgr860CY_j showed a not statistically significant small increase in E . Negative control C/Y remained almost unchanged after ionomycin. Labels in the X axis identifies the situation before the ionomycin (names of the constructs), and the situation after ionomycin (names of the construct with IM). Bars and errors represent mean \pm SEM, and are 4.00 ± 0.91 % for BKgr667CY_o, 4.50 ± 0.98 % for BKgr667CY_o IM, 3.12 ± 0.83 % for BKgr667CY_j, 4.50 ± 1.78 % for BKgr667CY_j IM, 9.50 ± 3.59 % for BKgr860CY_o, 5.25 ± 2.04 % for BKgr860CY_o IM, 1.62 ± 0.65 % for BKgr860CY_j, 2.00 ± 1.15 % for BKgr860CY_j IM, 1.12 ± 0.51 % for C/Y, 1.25 ± 0.56 % for C/Y IM, and $n = 8$ for all the constructs.

Este documento incorpora firma electrónica, y es copia auténtica de un documento electrónico archivado por la ULL según la Ley 39/2015.
 Su autenticidad puede ser contrastada en la siguiente dirección <https://sede.ull.es/validacion/>

Identificador del documento: 1627512

Código de verificación: KOIBGUMU

Firmado por: Roger Gimeno Llobet UNIVERSIDAD DE LA LAGUNA	Fecha: 25/10/2018 11:00:30
Diego Álvarez de la Rosa Rodríguez UNIVERSIDAD DE LA LAGUNA	25/10/2018 11:52:58
Teresa Giráldez Fernández UNIVERSIDAD DE LA LAGUNA	25/10/2018 11:54:04
Ernesto Pereda de Pablo UNIVERSIDAD DE LA LAGUNA	29/10/2018 13:01:03

Table 4.6: FRET efficiencies (in %) of gating ring constructs and negative control C/Y applying Acceptor Photobleaching technique before and after (IM) addition of ionomycin. n= 8.

Constructs	E (%)	E (IM) (%)
BKgr667CY_o	4.00 ± 0.91	4.50 ± 0.98
BKgr667CY_j	3.12 ± 0.83	4.50 ± 1.78
BKgr860CY_o	9.50 ± 3.59	5.25 ± 2.04
BKgr860CY_j	1.62 ± 0.65	2.00 ± 1.15
C/Y	1.12 ± 0.51	1.25 ± 0.56

4.11.2 Lifetime measurement: Time-Correlated Single Photon Counting (TCSPC)

In this study we also aimed to explore another approximation to measure FRET using our constructs, based on the fluorescence lifetime (see introduction). A common problem of intensity-based methods to detect FRET is that can be influenced by fluorophore concentration due to different expression levels, background fluorescence and bleaching (Ahmed et al., 2016). The fluorescence lifetime of a fluorophore that is not affected by non-radiative processes is an intrinsic property, which can be altered by changes in the neighboring environment. FRET efficiencies can be precisely measured by monitoring the change in the fluorescence lifetime of the donor fluorophore, which is altered when donor and acceptor suffer variations in their relative distance.

In this study we have measured the fluorescence lifetimes of our gating ring constructs used a high-performance fluorescence spectrophotometer and the Time-Correlated Single Photon Counting (TCSPC) technique. All the lifetime decays are fitted to bi-exponentials. When FRET is occurring, the decay curves exhibit a bi-exponential behavior, composed by a first phase of shorter lifetime corresponding to the quenched donors, and a second phase of longer lifetime corresponding unquenched donors. In principle, for an isolated molecule like the CFP alone, the decay is mono-exponential, but the complex environment of the cell alters the decay times, and it is best fitted by a bi-exponential.

We used various controls in our experiments. Firstly, we transfected HEK293T cells with the CFP alone. Additionally, we transfected a positive control consisting on a construct where the CFP (donor) and a YFP (acceptor) are linked by a glycine linker, close enough to do FRET (Miranda et al., 2013). Fig. 4.21A shows the fluorescent lifetimes obtained for both constructs. We can appreciate that in the construct that FRET takes place (CGY), the fluorescence lifetime of the donor (τ_D) is notably lower than the CFP alone, with $\tau_1 = 0.60$ ns and $\tau_2 = 2.22$ ns for both exponentials, and $\tau_1 = 1.10$ ns and $\tau_2 = 3.37$ ns for the ECFP alone (Fig. 4.21B). Fluorescent lifetimes as well as fractional intensities can be seen in Table 4.7. Values for CGY are similar to those obtained by other authors (Staruschenko et al., 2004).

Fig. 4.21C shows results corresponding to TCSPC experiments using the constructs BKgr860CY in HEK293T cells. As explained in the Methods section, the lifetime of the donor was measured after re-suspending the cell preparation in 2 mM Ca^{2+} , and then again after adding ionomycin to the same cuvette. We expected a shorter lifetime in the first measurement, as the BKgr860CY construct is doing FRET

Este documento incorpora firma electrónica, y es copia auténtica de un documento electrónico archivado por la ULL según la Ley 39/2015.
 Su autenticidad puede ser contrastada en la siguiente dirección <https://sede.ull.es/validacion/>

Identificador del documento: 1627512

Código de verificación: kOIBgUMu

Firmado por: Roger Gimeno Llobet UNIVERSIDAD DE LA LAGUNA	Fecha: 25/10/2018 11:00:30
Diego Álvarez de la Rosa Rodríguez UNIVERSIDAD DE LA LAGUNA	25/10/2018 11:52:58
Teresa Giráldez Fernández UNIVERSIDAD DE LA LAGUNA	25/10/2018 11:54:04
Ernesto Pereda de Pablo UNIVERSIDAD DE LA LAGUNA	29/10/2018 13:01:03

4.11. The gating ring as a transferable Ca^{2+} -sensitive molecular module

69

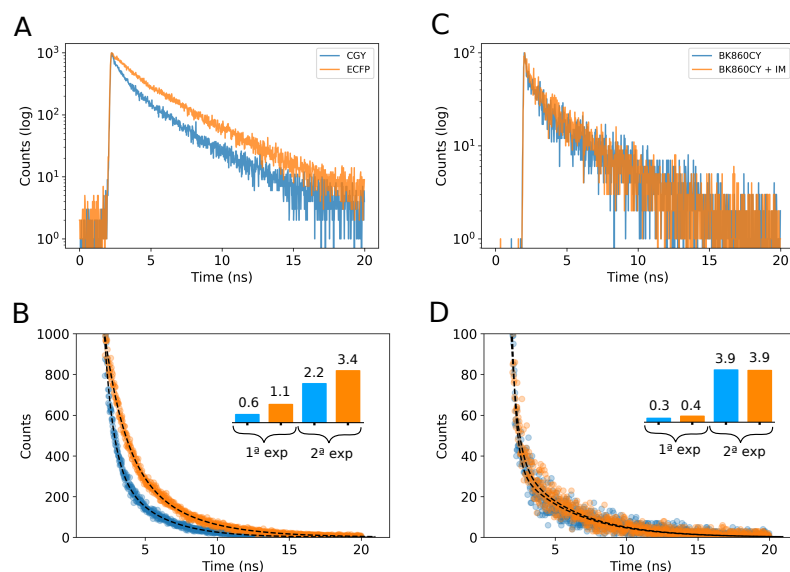


Figure 4.21: Time-correlated single photon counting experiments (TCSPC), carried out in a fluorescence spectrophotometer. (A) Fluorescence decay times for donor of CGY (blue) and CFP (orange) constructs. As expected, the donor molecule in the construct CGY that is doing FRET, have shorter lifetimes than the CFP alone (B). (C) Fluorescence decay times for donor of gating ring construct BKgr860CY, before (blue) and after (orange) the addition of ionomycin 15 μ M. (D) Due to a bad signal-to-noise ratio the exponentials could not be fitted properly and no apparent differences are seen. The decay times are fitted to bi-exponentials (Eq. 3.3).

in basal conditions. After the addition of the ionomycin, Ca^{2+} from the extracellular medium will permeate the membranes of the cells, binding to the BK and causing the separation of donor and acceptor molecules, increasing in this way the donor's lifetime. Unfortunately, due to the low signal of the sample, the decays could not be fitted accurately, being impossible to differentiate lifetimes adequately (Fig. 4.21D).

Table 4.7: Multi-exponential analysis of fluorescence intensity decays.

Constructs	D / DA	f_1 (%)	τ_1 (ns)	f_2 (%)	τ_2 (ns)	$\bar{\tau}$ (ns)	E (%)	r (nm)
ECFP	D	18.67	1.10	81.53	3.37	2.95		
CGY	DA	23.45	0.60	76.54	2.72	2.22	25	5.92

For the CGY construct, FRET efficiency (E) and distance between donor and acceptor fluorophores (r) are shown.

Este documento incorpora firma electrónica, y es copia auténtica de un documento electrónico archivado por la ULL según la Ley 39/2015.
 Su autenticidad puede ser contrastada en la siguiente dirección <https://sede.ull.es/validacion/>

Identificador del documento: 1627512

Código de verificación: KOIBgUMu

Firmado por: Roger Gimeno Llobet UNIVERSIDAD DE LA LAGUNA	Fecha: 25/10/2018 11:00:30
Diego Álvarez de la Rosa Rodríguez UNIVERSIDAD DE LA LAGUNA	25/10/2018 11:52:58
Teresa Giráldez Fernández UNIVERSIDAD DE LA LAGUNA	25/10/2018 11:54:04
Ernesto Pereda de Pablo UNIVERSIDAD DE LA LAGUNA	29/10/2018 13:01:03



Este documento incorpora firma electrónica, y es copia auténtica de un documento electrónico archivado por la ULL según la Ley 39/2015.
Su autenticidad puede ser contrastada en la siguiente dirección <https://sede.ull.es/validacion/>

Identificador del documento: 1627512

Código de verificación: kOIBgUMu

Firmado por: Roger Gimeno Llobet UNIVERSIDAD DE LA LAGUNA	Fecha: 25/10/2018 11:00:30
Diego Álvarez de la Rosa Rodríguez UNIVERSIDAD DE LA LAGUNA	25/10/2018 11:52:58
Teresa Giráldez Fernández UNIVERSIDAD DE LA LAGUNA	25/10/2018 11:54:04
Ernesto Pereda de Pablo UNIVERSIDAD DE LA LAGUNA	29/10/2018 13:01:03

Chapter 5

Discussion

There is a clear need to develop sensors able to report rapid Ca^{2+} concentration changes in subcellular nanodomains regulating neuronal excitability and neurotransmission. The BK channel is an ideal candidate as a Ca^{2+} sensor, since it naturally responds to physiological variations of this ion, restricted to the appropriate subcellular localizations. Previous work from our laboratory had developed fluorescently labeled BK channels that report Ca^{2+} changes as variation in FRET efficiency (Miranda et al., 2013), setting the ideal background for generating such tools. However, some improvements need to be made. On one hand, our constructs have the advantage of being GECl, thus warranting specific protein labeling. However, employing BK-based FRET Ca^{2+} sensors is not ideal. First, our genetically encoded (FP fusions) FRET-based constructs did not render high fluorescence levels when expressed in heterologous systems like HEK293T cells. CFP expression was very weak, even using a 3CFP:1YFP transfection stoichiometry. The limited signal intensity changes produced by FRET constructs makes it difficult to measure rapid variations in the Ca^{2+} concentrations in restricted subcellular domains where a good temporal and spatial resolution is needed (Tian et al., 2009). Secondly, if our future goal involves the expression of BK sensor *in vivo*, co-transfection (or co-infection) of the donor-labeled (CFP) and acceptor-labeled (YFP) BK subunits clearly reduces the experimental feasibility. In this context, fixing transfection quantities of donor and acceptor would not imply that the final donor/acceptor ratio is maintained in the BK tetramers, but rather a wide range of donor-acceptor proportions is present, generating a mixed FRET signal.

To overcome these issues, we took advantage of one of the most used and powerful single-wavelength fluorescent probes, the circularly permuted GFP (cpGFP). Circularly permuted fluorescent proteins (Baird, Zacharias, and Tsien, 1999) have been extensively used in combination with other Ca^{2+} -sensing proteins as Ca^{2+} indicators (Nagai et al., 2001). However, to implement a cpGFP in our constructs we have to take into account that the mechanism for which a cpGFP alters its fluorescence is totally different compared to FRET. The fluorescence of a cpGFP is modified by varying the positions of the N- and C-termini, i.e., by opening or closing the GFP barrel gap through movements of the amino acid chains linked to the N- and C-termini located at the barrel. Thus, cpGFP would mainly report structural changes within the same subunit. In contrast, changes in the fluorescence emission due to FRET are caused by the relative movement of donor and acceptor, which are located in equivalent positions of adjacent subunits within the tetramer. Therefore, FRET relays in an inter-subunit relative movement. Keeping this in mind, insertion of a cpGFP in the BK channel sequence is an empiric process, where the movements that caused that FRET pairs to move closer or apart from each other may or may not alter the distance between cpGFP linkers to produce the changes in the fluorescence intensity of the cpGFP. This is evidenced by the fact that our *in silico* study with BK

Este documento incorpora firma electrónica, y es copia auténtica de un documento electrónico archivado por la ULL según la Ley 39/2015.
Su autenticidad puede ser contrastada en la siguiente dirección <https://sede.ull.es/validacion/>

Identificador del documento: 1627512

Código de verificación: KOIBgUMu

Firmado por:	Fecha:
Roger Gimeno Llobet UNIVERSIDAD DE LA LAGUNA	25/10/2018 11:00:30
Diego Álvarez de la Rosa Rodríguez UNIVERSIDAD DE LA LAGUNA	25/10/2018 11:52:58
Teresa Giráldez Fernández UNIVERSIDAD DE LA LAGUNA	25/10/2018 11:54:04
Ernesto Pereda de Pablo UNIVERSIDAD DE LA LAGUNA	29/10/2018 13:01:03

structures in the open and closed conformations did not yield useful predictions regarding productive cpGFP insertion sites.

Our first attempt to test if our cpGFP-based constructs BK667cpG and BK860cpG were able to report changes in Ca^{2+} concentration varying the fluorescence signal consisted in increasing the intracellular $[\text{Ca}^{2+}]$ with ionomycin (Fig. 4.2). To achieve the maximum change in fluorescence we used an ionomycin concentration of 15 μM and a 5 mM extracellular Ca^{2+} solution. In response to ionomycin, construct BK667cpG construct showed a fluorescence increase of 40% and construct BK860cpG an increase of 140%. In comparison, a fully optimized Ca^{2+} sensor like Lck-GCaMP3 displayed a 700% increase. It is important to remark the myriad of optimizations that a GECI like GCaMP3 has suffered; in its beginnings (Nakai, Ohkura, and Imoto, 2001) former G-CaMP exhibited a increase in the fluorescence intensity of 400% in similar experiments (10 μM ionomycin, 2 mM $[\text{Ca}^{2+}]_e$, HEK293 cells). Our initial results, obtaining a construct that is showing a 140% fluorescence intensity increase previous to any optimization is very promising, with strong potential to become a useful Ca^{2+} sensor.

Although the experimental approximation is not the optimum to infer kinetics of the fluorescence responses -many factors like diffusion of ionomycin in the well have an impact on the final time, BK860cpG exhibits a faster response compared to Lck-GCaMP3 (τ and $t_{1/2}$, Fig. 4.2F and G).

In order to clarify the mechanism of the change in fluorescence obtained in ionomycin experiments, we designed a construct containing cytoplasmic cpGFP. In Ca^{2+} experiments with ionomycin repeating the same parameters (15 μM ionomycin and 5 mM extracellular $[\text{Ca}^{2+}]$), the isolated cpGFP displayed a $\Delta F/F$ of $118.95 \pm 1.77\%$ (Fig. 4.3C). This increase in the fluorescence intensity is due to deprotonation of the cpGFP by alkalization of the cytosol due to ionomycin (Müller et al., 2013), as this construct lacks any Ca^{2+} sensing domain. The increase in fluorescence is comparable to that of BK860cpG construct, and larger to that of BK667cpG construct. However, the fluorescence response did not exhibit a biphasic behavior like BK860cpG or Lck-GCaMP3, thus apparently the change in fluorescence observed in the first phase of construct BK860cpG can be attributable to the Ca^{2+} sensing mechanism of the BK channel (or a combination of both). Regarding BK667cpG construct, what could be the reason that its change in fluorescence intensity is smaller compared to that of the isolated cpGFP? A reasonable explanation is that the response of the BK667cpG to Ca^{2+} is a decrease in the fluorescence intensity, not an increase. The combination of a decrease in the fluorescence of BK667cpG to Ca^{2+} with the increase of the cpGFP by alkalization of the pH could lead to a overall reduced increment in the fluorescence.

Experiments with high doses of ionomycin are not adequate to elicit the real response to Ca^{2+} of BK-cpGFP constructs, as changes in the pH markedly interferes in the BK-mediated signal. To this end, experiments where precise changes in $[\text{Ca}^{2+}]$ are applied directly to the sensing mechanism of the constructs while controlling the pH are needed. Ca^{2+} - and pH-titrations are the initial steps to characterize the dependence to Ca^{2+} and pH of our constructs; after characterization, patch-clamp fluorometry (PCF) experiments were relevant because key factors such as $[\text{Ca}^{2+}]$, pH and membrane voltage are controlled.

Ideally, Ca^{2+} sensitivity from the BK-based Ca^{2+} sensors should arise from the specific BK Ca^{2+} binding sites. This would imply that the sensor would work within

Este documento incorpora firma electrónica, y es copia auténtica de un documento electrónico archivado por la ULL según la Ley 39/2015.
 Su autenticidad puede ser contrastada en la siguiente dirección <https://sede.ull.es/validacion/>

Identificador del documento: 1627512

Código de verificación: kOIBgUMu

Firmado por:	Fecha:
Roger Gimeno Llobet UNIVERSIDAD DE LA LAGUNA	25/10/2018 11:00:30
Diego Álvarez de la Rosa Rodríguez UNIVERSIDAD DE LA LAGUNA	25/10/2018 11:52:58
Teresa Giráldez Fernández UNIVERSIDAD DE LA LAGUNA	25/10/2018 11:54:04
Ernesto Pereda de Pablo UNIVERSIDAD DE LA LAGUNA	29/10/2018 13:01:03

the physiological range of Ca^{2+} concentrations typical of a Ca^{2+} nanodomain. We addressed this question by mutating the specific Ca^{2+} binding sites in the various BK-cpG constructs. Specifically, we designed four mutants for each BK cpGFP-based construct: a mutant of the Mg^{2+} and Ca^{2+} binding site in the transmembrane site (D99A), a mutant of the RCK1 binding site (D362/7A), a mutant of the RCK2 high-affinity site Ca^{2+} bowl (5D5A) and a mutant containing the three mutations. We repeated the Ca^{2+} -loading experiments with ionomycin but using the Ca^{2+} mutants (Fig. 4.4).

The most remarkable result is observed in construct BK860cpG, where all of its Ca^{2+} mutants showed a significantly reduction in the fluorescence intensity (Fig. 4.4C), as well as a critical slowdown in its kinetics. This result evidences that the mechanism which BK860cpG construct reported changes in the Ca^{2+} concentration is through Ca^{2+} binding in specific binding sites. Presumably, binding of Ca^{2+} ions induce structural rearrangements that are transmitted to the β -barrel by movement of the N- and C-termini of the cpGFP, leading to an increase in the fluorescence intensity. The remaining smaller change in fluorescence observed in the mutants seems to be an indicative that a distinct effect other than this mechanism explained above causes the increase in fluorescence, possibly due to direct effects of Ca^{2+} on the cpGFP or, alternatively, due to ionomycin-mediated changes in intracellular pH.

Interestingly, the second phase of the response of BK860cpG in ionomycin experiments shows some similarities with the response of BK667cpG and some of BK667cpG and BK860cpG mutants. Gutierrez et al. (Gutiérrez et al., 1999) described that application of high doses of ionomycin to LNCaP cells caused a biphasic response in the fluorescence ratio of fura-2. In a different experiment using thapsigargin (a sarco/endoplasmic reticulum Ca^{2+} ATPase (SERCA) inhibitor) and varying the extracellular Ca^{2+} concentration the authors determined that the first phase of the biphasic change in fluorescence was due to release of Ca^{2+} from intracellular stores and the second phase was due to the entrance of extracellular Ca^{2+} . It makes sense to attribute the first phase in the BK860cpG response to structural rearrangements upon Ca^{2+} binding in the BK, as the intracellular $[\text{Ca}^{2+}]$ is in the range of action of the channel. After this event, BK channels are saturated hence no increase in the fluorescence intensity of the cpGFP is possible through the BK mechanism. In the second phase the alkalization of the pH (due to the transport of H^+ ions to the extracellular medium by ionomycin (Müller et al., 2013) causes the deprotonation of the cpGFP fluorophore and an additional increase in the fluorescence signal. Since the response of BK667cpG is small and the responses of BK667cpG and BK860cpG Ca^{2+} mutants are also small or abolished, the increase in the fluorescence intensity detected with these constructs in ionomycin experiments can have the same explanation as with the second phase of the response of BK860cpG.

Many variables remain unknown in Ca^{2+} experiments with ionomycin. Which is the sensitivity to Ca^{2+} ions of constructs BK667cpG and BK860cpG and how are its fluorescence responses? Which sensitivity to pH has these constructs and of what magnitude? First, the generation of a control construct based on a cpGFP expressed alone, to test if the change in the environment of the fluorophore after addition of ionomycin can lead to changes in the fluorescence apart from the structural changes in the β -barrel gap caused by the new N- and C-termini. The other strategy is to vary the Ca^{2+} concentration and pH in a controlled way. For this we used an approach that consists in the generation of fragments of plasmatic membrane (microsomes) with the attached fluorescent BK channels in suspension, allowing us to vary the Ca^{2+} concentration and the pH of the medium with precision. The method that we

Este documento incorpora firma electrónica, y es copia auténtica de un documento electrónico archivado por la ULL según la Ley 39/2015.
 Su autenticidad puede ser contrastada en la siguiente dirección <https://sede.ull.es/validacion/>

Identificador del documento: 1627512

Código de verificación: KOIBgUMu

Firmado por:	Fecha:
Roger Gimeno Llobet UNIVERSIDAD DE LA LAGUNA	25/10/2018 11:00:30
Diego Álvarez de la Rosa Rodríguez UNIVERSIDAD DE LA LAGUNA	25/10/2018 11:52:58
Teresa Giráldez Fernández UNIVERSIDAD DE LA LAGUNA	25/10/2018 11:54:04
Ernesto Pereda de Pablo UNIVERSIDAD DE LA LAGUNA	29/10/2018 13:01:03

used to have the channels in contact with the medium is the creation of “microsomes” from transfected cells, disrupting the cells and isolating them from cell debris by differential centrifugation. After cell disruption, plasmatic membranes with the attached labeled BK channels formed vesicle-like aggregates that we named microsomes¹. The fraction of microsomes with channels enclosed inside are permeated to Ca²⁺ and H⁺ ions adding ionomycin in the solution before the experiment.

Physiological variations of Ca²⁺ (ranging from Ca²⁺ free to 1 mM Ca²⁺) induced opposite responses of BK667cpG and BK860cpG (Fig. 4.5A). While fluorescence of BK860cpG construct increase with increasing Ca²⁺ concentrations ($K_d = 235$ nM, $n_H = 2.1$), BK667cpG construct displays a small decrease in the fluorescence signal for increasing Ca²⁺ concentrations ($K_d = 427$ nM, $n_H = 7.3$). Hill coefficient (n_H) for BK channel is known to range from 1.5 to 6 (Cui, Yang, and Lee, 2009). This coefficient is a measure of cooperative association in binding processes, being a positive cooperativity indicative of the number of binding sites. An $n_H = 2.1$ for BK860cpG suggests that the observed fluorescence signal is reporting binding of the nearest binding site, the Ca²⁺ bowl. For construct BK667cpG, a $n_H = 7.3$ can imply that the fluorescence signal observed is reporting both RCK1 and RCK2 binding sites. This is consistent, as the cpGFP in this construct is inserted in the linker between RCK1 and RCK2 domains. Apparently the true response of construct BK667cpG (a decrease in fluorescence after Ca²⁺ binding) in Ca²⁺ experiments with ionomycin was masked due to an artifact increase in the fluorescence, maybe related to the cpGFP itself as mentioned before. However, it is remarkable the fact that responses of Bk667cpG and BK860cpG are opposite. This result is in agreement with previous experiments with BK667CY and BK860CY constructs, where using patch-clamp fluorometry the fluorescence signals were opposite (Miranda et al., 2013).

Regarding to BK667cpG construct, we have to take into account the dependence in the fluorescence signal that showed preliminary BK667CY construct with voltage (Miranda et al., 2013). As reported, some Ca²⁺-driven conformational changes that are sensitive to voltage are detected by fluorophores inserted at the 667 site. Our approximation with the microsomes lacks voltage information and control. One assumption is that transmembrane voltage in microsomes is near zero, because when the microsome self-assembled, the medium that remained at the inner part of the microsome was the same of the outside. This bias in the voltage can be the reason why BK667cpG construct exhibits such a small decrease in the fluorescence intensity.

We have to take into account the strong pH-dependence of cpGFP based constructs. The small BK667cpG signal is unidentifiable if the fluorescent signal varies due to pH. In the case of BK860cpG construct, the composition of both signals (due to Ca²⁺ binding to BK and due to deprotonation of cpGFP) can be seen. A tight control of the pH will be crucial. In this sense co-transfection with a genetically encoded pH sensor (GEPI, i.e. superecliptic pHluorin, (Lin and Schnitzer, 2016)) can be convenient.

In relation with the microsomes procedure that we used, it has to be mentioned that the apparent Ca²⁺ affinity and Hill slope values of Lck-GCaMP3 ($K_d = 153$ nM and $n_H = 3.5$) differ from the values obtained in (Shigetomi et al., 2010). The variation in the values obtained could be due to the different methods employed. Shigetomi *et al.* used an *in vivo* procedure consisting in permeabilize the transfected cells with Triton X-100 and subsequent addition of buffered solutions.

¹The term microsomes is usually used to describe the artifactual vesicles formed *in vitro* from the endoplasmic reticulum after disruption of eukaryotic cells.

Este documento incorpora firma electrónica, y es copia auténtica de un documento electrónico archivado por la ULL según la Ley 39/2015.
 Su autenticidad puede ser contrastada en la siguiente dirección <https://sede.ull.es/validacion/>

Identificador del documento: 1627512

Código de verificación: kOIBgUMu

Firmado por:	Fecha:
Roger Gimeno Llobet UNIVERSIDAD DE LA LAGUNA	25/10/2018 11:00:30
Diego Álvarez de la Rosa Rodríguez UNIVERSIDAD DE LA LAGUNA	25/10/2018 11:52:58
Teresa Giráldez Fernández UNIVERSIDAD DE LA LAGUNA	25/10/2018 11:54:04
Ernesto Pereda de Pablo UNIVERSIDAD DE LA LAGUNA	29/10/2018 13:01:03

Using patch-clamp fluorometry (PCF) we have measured in inside-out patches changes in the fluorescence intensity related to Ca^{2+} binding while controlling the membrane potential (Fig. 4.6). PCF experiments supported what we have obtained in Ca^{2+} -titrations: BK667cpG and BK860cpG exhibit opposite responses during activation of the channel. It is interesting to note that while the $\Delta F/F$ of BK860cpG is similar to that obtained in Ca^{2+} -titrations (0.30 in PCF, 0.31 in Ca^{2+} -titrations), values for BK667cpG significantly differs (-0.20 in PCF, -0.03 in Ca^{2+} -titrations). As previously described (Miranda et al., 2013), BK construct with GFP variants inserted in the 860 position (BK860CY) reported BK activity induced by Ca^{2+} binding, while insertions in the 667 position (BK667CY) reported BK activity induced by Ca^{2+} binding and voltage.

The data obtained in PCF experiments contrasted with Ca^{2+} -titrations suggests that, while in the BK860cpG construct the reported changes in fluorescence are only due to Ca^{2+} binding, in the BK667cpG construct the shift of the membrane potential to +100 mV is sensed in the 667 position, and these structural rearrangements potentiate the ones caused by the binding of Ca^{2+} ions, increasing the separation between the linkers of the cpGFP and causing a reduction in the fluorescence intensity.

We have to take into account that our sensor is indeed a ionic channel. A relevant problem when over-expressing ionic channels is that the ionic balance of the cell can be altered; for example, overexpression of voltage-gated K^+ channel Kv1.1 in the murine CNS lead to a dysregulation of the rectifier K^+ currents altering the action potentials and causing a hyperexcitable network response (Sutherland et al., 1999). Hence it will be useful to have a non-conducting BK Ca^{2+} sensor adapted to report Ca^{2+} dynamics without altering the electrical balance of the cell. It has been described (Wang and Brenner, 2006; Carrasquel-Ursulaez et al., 2015) that the mutation F315A located in the S6 segment (pore domain) have critical effects in the channel's conductance. The first aspect to highlight is that transfected HEK293T cells with pore mutant constructs BK667cpG-F315A and BK860cpG-F315A is that the distribution of the channel is clearly located in the plasmatic membrane (Fig. 4.7A), a part of distributed in internal reservoirs. Apparently, mutated channels can accumulate in the membrane as are not causing a dysregulation the that evoke the cell to maintain the homeostasis removing the channels from the membrane. Curiously, in Ca^{2+} experiments with ionomycin, the mutated construct BK860cpG-F315A did not show the increase in the fluorescence intensity that showed the non-mutated construct BK860cpG. Both mutated constructs displayed changes in the fluorescence similar to that of BK667cpG, suggesting that the part in the response in BK860cpG-F315A regarding to BK binding is annulled with F315A mutation. This result is interesting because it has been argued (Wu et al., 2009) that the changes in voltage and Ca^{2+} sensitivity that causes this mutation evidence that the mutated residue can take part in the allosteric transmission between the voltage sensor domain (VSD) and the pore gate domain (PGD). Since the Ca^{2+} sensing domain is allosterically coupled to the VSD and the PGD (Horrigan and Aldrich, 2002), it could be a link between this mutation and the Ca^{2+} sensing mechanism, as shown with the abolished BK860cpG typical biphasic response that BK860cpG-F315A displayed. Electrophysiological experiments (Fig. 4.7D) showed G-V curves significantly shifted to positive voltages, indicating that K^+ conduction is abolished at physiological Ca^{2+} concentrations and changes in the membrane potential.

To support ionomycin-mediated experiments with information about membrane voltage and current, we repeated these experiments in an electrophysiological setup.

Este documento incorpora firma electrónica, y es copia auténtica de un documento electrónico archivado por la ULL según la Ley 39/2015.
 Su autenticidad puede ser contrastada en la siguiente dirección <https://sede.ull.es/validacion/>

Identificador del documento: 1627512

Código de verificación: KOIBgUMu

Firmado por:	Fecha:
Roger Gimeno Llobet UNIVERSIDAD DE LA LAGUNA	25/10/2018 11:00:30
Diego Álvarez de la Rosa Rodríguez UNIVERSIDAD DE LA LAGUNA	25/10/2018 11:52:58
Teresa Giráldez Fernández UNIVERSIDAD DE LA LAGUNA	25/10/2018 11:54:04
Ernesto Pereda de Pablo UNIVERSIDAD DE LA LAGUNA	29/10/2018 13:01:03

Whole cell configuration was used to measure changes in the membrane or currents of all the cell, while fluorescence emission was simultaneously recorded. Initially, hiperpolarizing currents caused by the activation of BK channels after application of ionomycin were linked to the increase in the fluorescense intensity in both BK667cpG and BK860cpG constructs (Fig. 4.8). Nevertheless, although addition of the K⁺ channel blocker paxiline caused the depletion of the hiperpolarizing currents, increases in the fluorescense intensity were still seen in both constructs. These depolarizing currents, probably due to the entrance of extracellular Ca²⁺ were observed in this situation, suggests that the electroneutral transport caused by ionomycin (two Ca²⁺ ions to the intracelular side for one H⁺ to the extracelular side) causes the alkalization of the cell and the subsequent increase in the fluorescense of the cpGFP by deprotonation. One point for we do not have explication yet, is that the fluorescent signals obtained for BK667cpG and BK860cpG do not match with values obtained in previous experiments (Fig. 4.2); while the increase in BK667cpG is larger than obtained in previous ionomycin experiments, for BK860cpG the increase do not reach the what previously obtained.

The validation of our sensors BK667cpG and BK860cpG to internal Ca²⁺ sources utilizing carbachol did not yield the expected signals (Fig. 4.9). Release of Ca²⁺ from internal stores after carbachol application increase the cytosolic Ca²⁺ concentration 0.7 - 1 μM (Mayerhofer et al., 1992; Mountjoy et al., 2001). Taking into account the results obtained in Ca²⁺-titrations (Table 4.3), we expected to obtain changes in the fluorescense intensity up to ~0.23 for BK860cpG and ~2.79 for Lck-GCaMP3. The obtained changes are far from the expected values (ΔF/F = 0.05 ± 0.01 for BK860cpG and ΔF/F = 0.08 ± 0.01 for Lck-GCaMP3). Studies carried out with a earlier version of GCaMP3, G-CaMP (Nakai, Ohkura, and Imoto, 2001), revealed a ΔF/F = 0.8 after application of carbachol in HEK293 cells. Although Lck-GCaMP3 construct has been modified to localize at the membrane, not a huge difference in the ΔF/F is expected for sensing Ca²⁺ from internal stores (i.e. for GCaMP3 application of 100μM ATP led to a ΔF/F = 3.2 (Chen et al., 2012), and for Lck-GCaMP3 application of 30μM ATP led to a ΔF/F = 2.7). The fact that both Lck-GCaMP3 and BK860cpG had such small responses suggests that the problem could be related to carbachol. We are planning to repeat these experiments in the future but with verified stocks of carbachol.

One fundamental question of our work was if the BK860cpG sensor was able to couple with Cav channels forming Ca²⁺ nanodomains. In our experiments we tested the sensor with Cav2.1 channel, because it is known that BK channels and Cav2.1 channels are spatially and functionally coupled forming nanodomains in neurons and when reconstituted in heterologous expression systems (Contet et al., 2016; Berkefeld et al., 2006; Fakler and Adelman, 2008). As a negative control, we used Cav2.3 channels for the co-expression with BK860cpG sensor as it has been described that do not couple with BK channels (Berkefeld et al., 2006). To analyze the data obtained with the dSTORM technique we developed our own programs. Although there are specialized software to process SMLM data in the web (i.e. a repository, mainly focused in localization tasks, can be found in www.epfl.ch/smlm/), most of them are not free or are written in proprietary programming languages like

Este documento incorpora firma electrónica, y es copia auténtica de un documento electrónico archivado por la ULL según la Ley 39/2015.
 Su autenticidad puede ser contrastada en la siguiente dirección <https://sede.ull.es/validacion/>

Identificador del documento: 1627512

Código de verificación: KOIBgUMu

Firmado por:	Fecha:
Roger Gimeno Llobet UNIVERSIDAD DE LA LAGUNA	25/10/2018 11:00:30
Diego Álvarez de la Rosa Rodríguez UNIVERSIDAD DE LA LAGUNA	25/10/2018 11:52:58
Teresa Giráldez Fernández UNIVERSIDAD DE LA LAGUNA	25/10/2018 11:54:04
Ernesto Pereda de Pablo UNIVERSIDAD DE LA LAGUNA	29/10/2018 13:01:03

MATLAB (Mathworks). We developed our programs in Python programming language (Python Software Foundation), open-source and with a strong community-based developmental model to be accessible to anyone. These post-processing programs focus on two tasks to quantify the data obtained from dSTORM: a nearest-neighbor localization distance analysis to determine the most common distance between labeled-proteins, and a clustering analysis to characterize the spatial association of these proteins. The results obtained (Fig. 4.17) suggests that our sensor BK860cpG forms nanodomains with one of its Ca^{2+} effectors, Cav2.1 channels, situation that can not be reproduced with our negative control Cav2.3. The NND and clusters analysis (Fig. 4.17C and D) showed that BK860cpG-Cav2.1 complexes, when co-transfected in HEK293T cells, forms a substantial number of spatially restricted clusters of $\sim 1 \mu\text{m}^2$, where its constituents are separated $\sim 25\text{nm}$ between them, results compatible with Ca^{2+} nanodomains. With the co-transfection of BK860cpG-Cav2.3 we do not obtain such tight coupling.

The recent publication of BK full cryo-EM structures with bound (10 mM Ca^{2+} / 10 mM Mg^{2+}) and unbound (1 mM EDTA) Ca^{2+} (Tao2017; Hite, Tao, and MacKinnon, 2017) permitted us explore our BK fluorescent constructs library (Giraldez, Hughes, and Sigworth, 2005) to obtain new candidates to Ca^{2+} sensors. The approximation that we used to infer the best sites in the BK to insert a cpGFP was straightforward; quantify how does residues move between the Ca^{2+} bound/unbound configurations. From the positions that we had GFP insertions we selected site 965, because of the resolved residues it suffered the largest movement (Fig. 4.18B, yellow arrow). Unfortunately positions 667 and 860 were not resolved in the structure. Our first attempt to check the potential of the new construct BK965cpG did not provide the expected response. BK965cpG exhibited a change in the fluorescence intensity after the addition of ionomycin comparable at BK667cpG (Fig. 4.18B). As we have previously demonstrated, this change in the fluorescence is due to the effect of alkalization over the cpGFP itself. We were looking at a response that in magnitude exceeded that of BK860cpG. From this unsuccessful analysis we can extract some elements: 1) This study its simplistic; other variables involved in the rearrangements of a structure such as rotations are not taken into account. 2) Although the study of a protein structure has contributed to important findings and improvements (Akerboom et al., 2009), in many cases it is an empirical process (Ast et al., 2017). 3) The resolved cryo-EM structure may have been fixed in a state that it is not the most adequate. It is possible that in intermediate steps of the full rearrangement the movement of some residues is larger. Having a photography of the initial state (Ca^{2+} free) and the possible final state (10 mM Ca^{2+}) may not provide all the necessary information.

After the publication of the resolved structure of the cytosolic Ca^{2+} -sensitive domain of the BK channel by Wu et al. (Wu et al., 2010), studies carried out by Javaherian et al. (Javaherian et al., 2011) with a slightly shorter version of isolated cytosolic domain demonstrated that the isolated gating ring suffers conformational changes upon Ca^{2+} binding. Therefore, the isolated gating ring is a self-assembled structure that preserves the molecular mechanisms capable of transduce the Ca^{2+} signal into structural rearrangements. From previous work carried out in the laboratory (Miranda et al., 2013), BK channels with GFP variants inserted in specific sites reported changes in Ca^{2+} concentration via changes in FRET due to structural rearrangements. The study used constructs had GFP variants inserted in two positions of the gating ring (position 667 between RCK1 and RCK2, and 860 in RCK2 near the

Este documento incorpora firma electrónica, y es copia auténtica de un documento electrónico archivado por la ULL según la Ley 39/2015.
 Su autenticidad puede ser contrastada en la siguiente dirección <https://sede.ull.es/validacion/>

Identificador del documento: 1627512

Código de verificación: KOIBGUMu

Firmado por:	Fecha:
Roger Gimeno Llobet UNIVERSIDAD DE LA LAGUNA	25/10/2018 11:00:30
Diego Álvarez de la Rosa Rodríguez UNIVERSIDAD DE LA LAGUNA	25/10/2018 11:52:58
Teresa Giráldez Fernández UNIVERSIDAD DE LA LAGUNA	25/10/2018 11:54:04
Ernesto Pereda de Pablo UNIVERSIDAD DE LA LAGUNA	29/10/2018 13:01:03

Ca²⁺ bowl). With this in mind, we hypothesized that isolated gating rings of our labeled constructs could be employed as transferable modules that could be attached to a specific protein of interest, being able to report changes in the Ca²⁺ concentration of the protein environment by changes in fluorescence. Furthermore, we could advance in the knowledge of the unclear molecular and biophysical processes of BK Ca²⁺ modulation by studying isolated gating rings.

The first experimental approach was to corroborate if the labeled gating ring structures were constituted correctly (Fig. 4.19). To this end we used a technique, Acceptor Photobleaching (AB) FRET, which allowed us to obtain information of the formation of the structure and the relative position of the inserted fluorophores. As it was published in previous work (Miranda et al., 2013), BK constructs with the fluorescent proteins inserted in site 667 (between RCK1 and RCK2 domains) showed no FRET efficiency (*E*) in basal Ca²⁺ conditions (free Ca²⁺), but reporting an increase in *E* when Ca²⁺ concentration was increased. On the other hand, BK constructs with the fluorescent proteins inserted in site 860 (in the RCK2, near the Ca²⁺ bowl) showed a basal (*E*) in free Ca²⁺, and decreased the *E* when Ca²⁺ concentration was increased. Taking this into account, applying the AB technique in transfected cells and in physiologic Ca²⁺ concentrations in the cytosol, we expected to obtain no *E* for 667 gating ring constructs and a considerable *E* for 860 constructs. Interestingly, BKgr860CY_j did not show a significant *E*, while BKgr860CY_o did, even though showing a wide spread in *E* values. This is an interesting result, because (Wu et al., 2010) based construct was employed in structural studies, while (Javaherian et al., 2011) based construct was employed in functional studies. One drawback of crystallographic studies is the non-physiological environment where proteins are studied. Another, is that the arrangement of the resolved structure may only be reporting one possible conformation of the protein, but maybe are the intermediate conformation the ones that are more relevant in terms of function. On the other hand, the isolated gating ring structure from (Javaherian et al., 2011) has been tested in functional studies, where structural rearrangements have been confirmed with physiological changes of cations (Ca²⁺ and Mg²⁺). It appears that the extra 18 amino acids that the j construct has make a difference in terms of basal gating ring conformation. In any rate, taking into account the wide spread of *E* of construct BKgr860CY_o, it is possible that the correct folding of the isolated gating ring does not occur in some cases. Interestingly, in the gating ring constructs with the insertions in the 667 site both constructs showed a small FRET efficiency above the negative control, consisting in soluble CFP and a YFP transfected together. With this construct no *E* is expected, because both are separate proteins that move freely and are not interacting specifically. The higher value of *E* in construct BKgr667CY_o was statistically significant compared to C/Y (*E* = 4.00 ± 0.91 % for BKgr667CY_o, *E* = 1.12 ± 0.51 % for C/Y, *P* = 0.01). This small amount of *E* may indicate that the isolated gating ring structure in basal Ca²⁺ concentrations may be rearranged in such a way that the fluorophores are closer than in the full BK protein.

The next step was to perform an experiment that would provide us information about the structural rearrangements of the isolated gating rings in the presence of Ca²⁺ ions (Fig. 4.20). We planned to continue using the AB technique but changing the intracellular [Ca²⁺] at some point during the experiment with the application of ionomycin. For construct BKgr860CY_o, the decrease in the *E* after addition of ionomycin (from *E* = 9.50 ± 3.60 % to *E* = 5.25 ± 2.04 %, Δ*E* = -4.2 %) was the proof that this isolated gating ring is functional and is able to detect changes in the Ca²⁺ concentration. However the widespread in its *E* could mean that the protein is not always folding correctly.

Este documento incorpora firma electrónica, y es copia auténtica de un documento electrónico archivado por la ULL según la Ley 39/2015.
 Su autenticidad puede ser contrastada en la siguiente dirección <https://sede.ull.es/validacion/>

Identificador del documento: 1627512

Código de verificación: kOIBgUMU

Firmado por:	Fecha:
Roger Gimeno Llobet UNIVERSIDAD DE LA LAGUNA	25/10/2018 11:00:30
Diego Álvarez de la Rosa Rodríguez UNIVERSIDAD DE LA LAGUNA	25/10/2018 11:52:58
Teresa Giráldez Fernández UNIVERSIDAD DE LA LAGUNA	25/10/2018 11:54:04
Ernesto Pereda de Pablo UNIVERSIDAD DE LA LAGUNA	29/10/2018 13:01:03

Although intensity-based FRET studies have been extensively used to report interactions between fluorescent labeled proteins, some artifacts could appear when measuring FRET efficiencies. During a FRET experiment, the fluorescent proteins can change its fluorescence intensity not only due to energy transfer but also due to specific photo-physical properties such as photo-conversion or photobleaching (Tramier et al., 2002). In contrast, determination of donor fluorescent lifetimes has considerable advantages over FRET techniques. Fluorescent lifetime is not affected by the possible artifacts that lead to changes in the fluorescent intensity because it is not a intensity-based method to detect FRET. To overcome these issues and support the results obtained with FRET experiments with ionomycin (Fig. 4.20), we attempted to measure the FRET phenomena in our BKgr860CY_o construct by the changes in the fluorescent lifetime of the donor molecule (Fig. 4.21). To simulate the non-FRET and FRET states of the donor molecule in the BKgr860CY_o construct, we first measured the lifetime of a CFP (expressed alone in the cell), and then we measured the CFP lifetime of a tandem construct formed by a CFP and a YFP linked by glycine residues in a fixed position (CGY), a construct where the fluorescent proteins are in an intramolecular FRET situation (Fig. 4.21A). Although the fluorescence decay lifetime of single molecules of CFP can be fitted to a mono-exponential (Tramier et al., 2002), we found that a bi-exponential was a better fit, in agreement with previous studies (Duncan et al., 2004). Lifetime measurements of the donor molecule of the CGY construct yielded shorter lifetimes when quenched in the presence of the acceptor molecule (Fig. 4.21B). The average lifetime for ECFP alone (τ_D) was 2.95 ns, and the average lifetime for the CFP linked with the YFP, CGY (τ_{DA}) was 2.22 ns. These values match with values of ECFP and CGY obtained elsewhere ($\tau_{ECFP} = 2.9$ ns and $\tau_{CGY} = 2.3$ ns, (Fujiwara and Cieslik, 2006)). With the obtained lifetimes FRET efficiency in the CGY construct is $E = 0.25$ and the distance r between the donor and the acceptor in the CGY construct is $r = 5.92$ nm. We assumed $R_0 = 4.92$ nm (Patterson, Piston, and Barisas, 2000) in Eq. 3.6. Unfortunately, donor fluorescent lifetimes determined for the BKgr860CY_o construct in basal Ca^{2+} conditions (without ionomycin, FRET positive in AB experiments) and after Ca^{2+} binding (addition of ionomycin, no-FRET situation in AB experiments) were un-resolvable due to the bad signal-to-noise ratio (Fig. 4.21C) that made impossible a proper fit of the lifetime decays (Fig. 4.21D).

Results obtained came to the conclusion that generated BK667cpG and BK860cpG constructs exhibit fluorescent responses that are Ca^{2+} -dependent, in physiological $[Ca^{2+}]$. We have to take into account that the pH-dependence for these constructs is large, due to the circularly permuted GFP (cpGFP). pH have to be tightly controlled in order to discern responses of constructs due to Ca^{2+} binding. In this sense, fluorescent signals due to Ca^{2+} binding for BK667cpG are too small; we will focus our next steps in construct BK860cpG. The fluorescent responses to Ca^{2+} displayed by BK860cpG are promising, since no optimizations have been made in this construct yet. Moreover, this construct form complexes with Cav2.1 channels in a similar way that wild-type BK channels do. We have demonstrated this coupling with superresolution experiments, contrasting the obtained results with a known negative association with Cav2.3 channels. Construct BK860cpG provides an excellent starting point to develop a sensor capable to report changes in Ca^{2+} dynamics in nanodomains.

Este documento incorpora firma electrónica, y es copia auténtica de un documento electrónico archivado por la ULL según la Ley 39/2015.
 Su autenticidad puede ser contrastada en la siguiente dirección <https://sede.ull.es/validacion/>

Identificador del documento: 1627512

Código de verificación: kOIBgUMu

Firmado por:	Fecha:
Roger Gimeno Llobet UNIVERSIDAD DE LA LAGUNA	25/10/2018 11:00:30
Diego Álvarez de la Rosa Rodríguez UNIVERSIDAD DE LA LAGUNA	25/10/2018 11:52:58
Teresa Giráldez Fernández UNIVERSIDAD DE LA LAGUNA	25/10/2018 11:54:04
Ernesto Pereda de Pablo UNIVERSIDAD DE LA LAGUNA	29/10/2018 13:01:03



Este documento incorpora firma electrónica, y es copia auténtica de un documento electrónico archivado por la ULL según la Ley 39/2015.
Su autenticidad puede ser contrastada en la siguiente dirección <https://sede.ull.es/validacion/>

Identificador del documento: 1627512

Código de verificación: kOIBgUMu

Firmado por:	Fecha:
Roger Gimeno Llobet UNIVERSIDAD DE LA LAGUNA	25/10/2018 11:00:30
Diego Álvarez de la Rosa Rodríguez UNIVERSIDAD DE LA LAGUNA	25/10/2018 11:52:58
Teresa Giráldez Fernández UNIVERSIDAD DE LA LAGUNA	25/10/2018 11:54:04
Ernesto Pereda de Pablo UNIVERSIDAD DE LA LAGUNA	29/10/2018 13:01:03

Chapter 6

Conclusions

- Fluorescence signals observed from BK667cpG and BK860cpG sensors are Ca^{2+} -dependent.
- Both BK667cpG and BK860cpG sensors respond to physiological $[\text{Ca}^{2+}]$.
- Changes in the pH can mask the fluorescent signals of sensors due to Ca^{2+} binding.
- The generated sensors form complexes with voltage-dependent Ca^{2+} channels similar to those formed with BK channels.
- Construct BK860cpG have potential to become a Ca^{2+} sensor in Ca^{2+} nanodomains.

Este documento incorpora firma electrónica, y es copia auténtica de un documento electrónico archivado por la ULL según la Ley 39/2015.
Su autenticidad puede ser contrastada en la siguiente dirección <https://sede.ull.es/validacion/>

Identificador del documento: 1627512

Código de verificación: KOIBgUMu

Firmado por: Roger Gimeno Llobet UNIVERSIDAD DE LA LAGUNA	Fecha: 25/10/2018 11:00:30
Diego Álvarez de la Rosa Rodríguez UNIVERSIDAD DE LA LAGUNA	25/10/2018 11:52:58
Teresa Giráldez Fernández UNIVERSIDAD DE LA LAGUNA	25/10/2018 11:54:04
Ernesto Pereda de Pablo UNIVERSIDAD DE LA LAGUNA	29/10/2018 13:01:03



Este documento incorpora firma electrónica, y es copia auténtica de un documento electrónico archivado por la ULL según la Ley 39/2015.
Su autenticidad puede ser contrastada en la siguiente dirección <https://sede.ull.es/validacion/>

Identificador del documento: 1627512

Código de verificación: kOIBgUMu

Firmado por:	Fecha:
Roger Gimeno Llobet UNIVERSIDAD DE LA LAGUNA	25/10/2018 11:00:30
Diego Álvarez de la Rosa Rodríguez UNIVERSIDAD DE LA LAGUNA	25/10/2018 11:52:58
Teresa Giráldez Fernández UNIVERSIDAD DE LA LAGUNA	25/10/2018 11:54:04
Ernesto Pereda de Pablo UNIVERSIDAD DE LA LAGUNA	29/10/2018 13:01:03

Appendix A

NND program code

Este documento incorpora firma electrónica, y es copia auténtica de un documento electrónico archivado por la ULL según la Ley 39/2015.
Su autenticidad puede ser contrastada en la siguiente dirección <https://sede.ull.es/validacion/>

Identificador del documento: 1627512

Código de verificación: kOIBgUMu

Firmado por:	Fecha:
Roger Gimeno Llobet UNIVERSIDAD DE LA LAGUNA	25/10/2018 11:00:30
Diego Álvarez de la Rosa Rodríguez UNIVERSIDAD DE LA LAGUNA	25/10/2018 11:52:58
Teresa Giráldez Fernández UNIVERSIDAD DE LA LAGUNA	25/10/2018 11:54:04
Ernesto Pereda de Pablo UNIVERSIDAD DE LA LAGUNA	29/10/2018 13:01:03

```
'''
Cálculo de la distancia mínima de cada partícula con su vecino más cercano (nearest
neighbor distance, NND) para 647, 488 y 647-488.
-----
Instrucciones:
Poner en una misma carpeta los archivos de molecule lists .txt y este script.
Se crearan 3 archivos .csv con los NND para cada partícula de todos los molecule
lists del 647, el 488 y el 647 con el 488. Los archivos se nombran como
'archivo'_NND_647.csv, 'archivo'_NND_488.csv y 'archivo'_NND_647-488.csv respectivamente.
El histograma generado se guarda como 'archivo'_NND_hist.pdf
'''

#===MODIFICAR=====
# Nombre archivos csv
archivo = 'hola'

# Histograma
Bins = 15
label647 = 'Cav2.1'
label488 = 'BK'
label647_488 = 'Cav2.1 + BK'
#=====

# Cargar módulos-----
import os
import pandas as pd
from scipy import spatial
import numpy as np
import matplotlib.pyplot as plt
import scipy.stats as stats
from matplotlib.ticker import FuncFormatter

# Leer archivos-----
list_ml = (glob.glob("*.txt"))

# Extraer coordenadas X, Y corregidas de la lista de moléculas, separadas por canal
mins_ch1 = []
mins_ch2 = []
mins_ch3 = []

for item in list_ml:
    print(item)
    df = pd.read_csv(item, sep=" ")
    df_647 = df.loc[df['Channel Name'] == 647]
    df_647 = df_647[['Xwc', 'Ywc']].copy()
    df_488 = df.loc[df['Channel Name'] == 488]
    df_488 = df_488[['Xwc', 'Ywc']].copy()

    # Valores 647 -> ch1, 488 -> ch2
    ch1_data = df_647.values
    ch2_data = df_488.values

    # NND-----
    # ch1: 647
    for i in range(len(ch1_data)):
        llista = [ch1_data[i]]
        distance, index = spatial.KDTree(llista).query(ch1_data)
        distance = distance[distance != 0]
        mins_ch1.append(min(distance))
```

Figure A.1: Nearest Neighbor Distance program (page1/2)

Este documento incorpora firma electrónica, y es copia auténtica de un documento electrónico archivado por la ULL según la Ley 39/2015.
Su autenticidad puede ser contrastada en la siguiente dirección <https://sede.ull.es/validacion/>

Identificador del documento: 1627512

Código de verificación: KOIBgUMu

Firmado por: Roger Gimeno Llobet UNIVERSIDAD DE LA LAGUNA	Fecha: 25/10/2018 11:00:30
Diego Álvarez de la Rosa Rodríguez UNIVERSIDAD DE LA LAGUNA	25/10/2018 11:52:58
Teresa Giráldez Fernández UNIVERSIDAD DE LA LAGUNA	25/10/2018 11:54:04
Ernesto Pereda de Pablo UNIVERSIDAD DE LA LAGUNA	29/10/2018 13:01:03

```
# ch2: 488
for i in range(len(ch2_data)):
    llista = [ch2_data[i]]
    distance,index = spatial.KDTree(llista).query(ch2_data)
    distance = distance[distance != 0]
    mins_ch2.append(min(distance))

# ch3: 647+488
for i in range(len(ch1_data)):
    llista = [ch1_data[i]]
    distance,index = spatial.KDTree(llista).query(ch2_data)
    mins_ch3.append(min(distance))

print('Valor mínimo partículas 647:', max(mins_ch1))
print('Valor máximo partículas 647:', max(mins_ch1))
print('Valor mínimo partículas 488:', max(mins_ch2))
print('Valor máximo partículas 488:', max(mins_ch2))
print('Valor mínimo partículas 647 con 488:', max(mins_ch3))
print('Valor máximo partículas 647 con 488:', max(mins_ch3))

# Guardar a csv-----
np.savetxt(archivo+"_NND_647.csv", mins_ch1, delimiter=",")
np.savetxt(archivo+"_NND_488.csv", mins_ch2, delimiter=",")
np.savetxt(archivo+"_NND_647-488.csv", mins_ch3, delimiter=",")

# Histograma-----
total = mins_ch1+mins_ch2+mins_ch3
plt.hist(mins_ch1, bins=Bins, alpha=0.5, label=label647,
         weights=np.ones_like(mins_ch1) / len(total))
plt.hist(mins_ch2, bins=Bins, alpha=0.5, label=label488 ,
         weights=np.ones_like(mins_ch2) / len(total))
plt.hist(mins_ch3, bins=Bins, alpha=0.5, label=label647_488,
         weights=np.ones_like(mins_ch3) / len(total))

plt.xlabel('Distance (nm)')
plt.ylabel('Number of counts (%)')
formatter = FuncFormatter(lambda y, _: str(y * 100) + '%')
plt.gca().yaxis.set_major_formatter(formatter)
plt.legend()
plt.savefig(archivo+'_NND_hist.pdf', bbox_inches='tight')
plt.show()
```

Figure A.2: Nearest Neighbor Distance program (page2/2)

Este documento incorpora firma electrónica, y es copia auténtica de un documento electrónico archivado por la ULL según la Ley 39/2015.
 Su autenticidad puede ser contrastada en la siguiente dirección <https://sede.ull.es/validacion/>

Identificador del documento: 1627512

Código de verificación: KOIBgUMu

Firmado por: Roger Gimeno Llobet UNIVERSIDAD DE LA LAGUNA	Fecha: 25/10/2018 11:00:30
Diego Álvarez de la Rosa Rodríguez UNIVERSIDAD DE LA LAGUNA	25/10/2018 11:52:58
Teresa Giráldez Fernández UNIVERSIDAD DE LA LAGUNA	25/10/2018 11:54:04
Ernesto Pereda de Pablo UNIVERSIDAD DE LA LAGUNA	29/10/2018 13:01:03



Este documento incorpora firma electrónica, y es copia auténtica de un documento electrónico archivado por la ULL según la Ley 39/2015.
Su autenticidad puede ser contrastada en la siguiente dirección <https://sede.ull.es/validacion/>

Identificador del documento: 1627512

Código de verificación: kOIBgUMu

Firmado por:	Fecha:
Roger Gimeno Llobet UNIVERSIDAD DE LA LAGUNA	25/10/2018 11:00:30
Diego Álvarez de la Rosa Rodríguez UNIVERSIDAD DE LA LAGUNA	25/10/2018 11:52:58
Teresa Giráldez Fernández UNIVERSIDAD DE LA LAGUNA	25/10/2018 11:54:04
Ernesto Pereda de Pablo UNIVERSIDAD DE LA LAGUNA	29/10/2018 13:01:03

Appendix B

Clusters program code

Este documento incorpora firma electrónica, y es copia auténtica de un documento electrónico archivado por la ULL según la Ley 39/2015.
Su autenticidad puede ser contrastada en la siguiente dirección <https://sede.ull.es/validacion/>

Identificador del documento: 1627512

Código de verificación: kOIBgUMu

Firmado por:	Fecha:
Roger Gimeno Llobet UNIVERSIDAD DE LA LAGUNA	25/10/2018 11:00:30
Diego Álvarez de la Rosa Rodríguez UNIVERSIDAD DE LA LAGUNA	25/10/2018 11:52:58
Teresa Giráldez Fernández UNIVERSIDAD DE LA LAGUNA	25/10/2018 11:54:04
Ernesto Pereda de Pablo UNIVERSIDAD DE LA LAGUNA	29/10/2018 13:01:03

```
'''
Cálculo de la cantidad y tamaño de clusters de marcaje 647, 488 y combinación 647-488
-----
Instrucciones:
Poner en una misma carpeta los archivos de molecule lists .txt y este script.
Se crearan 3 archivos .csv con todas las areas de todos los molecule lists del 647,
el 488 y el 647 con el 488. Los archivos se nombran como 'archivo'_areas_647.csv,
'archivo'_areas_488.csv y 'archivo'_areas_647-488.csv respectivamente. El histograma
generado se guarda como 'archivo'_areas__hist.pdf
'''

#===MODIFICAR=====
# Parametros DBSCAN
epsilon = 1
minimum_samples = 3

# Nombre archivos csv
archivo = 'hola'

# Histograma
Bins = 15
label647 = 'Cav2.1'
label488 = 'BK'
label647_488 = 'Cav2.1 + BK'
#=====

# Cargar módulos-----
import os
import glob
import pandas as pd
import numpy as np
import matplotlib.pyplot as plt
from sklearn.cluster import DBSCAN
import itertools
from scipy.spatial import ConvexHull
from matplotlib.ticker import FuncFormatter

# Definir funciones-----
def Area(vertices):
    n = len(vertices) # of corners
    a = 0.0
    for i in range(n):
        j = (i + 1) % n
        a += abs(vertices[i][0] * vertices[j][1] - vertices[j][0] * vertices[i][1])
    result = a / 2.0
    return result

# Leer archivos-----
list_ml = (glob.glob("*.txt"))

# Extraer coordenadas X, Y corregidas de la lista de moléculas, separadas por canal
ch1_areas = []
ch2_areas = []
ch3_areas = []
ch3_new_areas = []

for item in list_ml:
    print(item)
    df = pd.read_csv(item, sep=" ")
```

Figure B.1: Clusters program (page1/4)

Este documento incorpora firma electrónica, y es copia auténtica de un documento electrónico archivado por la ULL según la Ley 39/2015.
Su autenticidad puede ser contrastada en la siguiente dirección <https://sede.ull.es/validacion/>

Identificador del documento: 1627512

Código de verificación: KOIBgUMu

Firmado por: Roger Gimeno Llobet UNIVERSIDAD DE LA LAGUNA	Fecha: 25/10/2018 11:00:30
Diego Álvarez de la Rosa Rodríguez UNIVERSIDAD DE LA LAGUNA	25/10/2018 11:52:58
Teresa Giráldez Fernández UNIVERSIDAD DE LA LAGUNA	25/10/2018 11:54:04
Ernesto Pereda de Pablo UNIVERSIDAD DE LA LAGUNA	29/10/2018 13:01:03

```

df_647 = df.loc[df['Channel Name'] == 647]
df_647 = df_647[['Xwc', 'Ywc']].copy()
df_488 = df.loc[df['Channel Name'] == 488]
df_488 = df_488[['Xwc', 'Ywc']].copy()
df_647_488 = df[['Xwc', 'Ywc']].copy()

# Valores 647 -> ch1, 488 -> ch2, 647+488 -> ch3
ch1_data = df_647.values
ch2_data = df_488.values
ch3_data = df_647_488.values

#DBSCAN-----
# Ch1: 647
print('Number of particles 647:', len(ch1_data))
db1 = DBSCAN(eps=epsilon, min_samples=minimum_samples,
metric='euclidean').fit(ch1_data)
db1_labels = db1.labels_
db1n_clusters_ = len(set(db1_labels)) - (1 if -1 in db1_labels else 0)
print('Number of clusters in 647: %d' % db1n_clusters_)
labels_ch1 = db1.labels_
ch1_counts = np.bincount(labels_ch1[labels_ch1>=0])

# Ch2: 488
print('Number of particles 488:', len(ch2_data))
db2 = DBSCAN(eps=epsilon, min_samples=minimum_samples,
metric='euclidean').fit(ch2_data)
db2_labels = db2.labels_
db2n_clusters_ = len(set(db2_labels)) - (1 if -1 in db2_labels else 0)
print('Number of clusters in 488: %d' % db2n_clusters_)
labels_ch2 = db2.labels_
ch2_counts = np.bincount(labels_ch2[labels_ch2>=0])

# ch3: 647+488
print('Number of particles 647 + 488:', len(ch3_data))
db3 = DBSCAN(eps=epsilon, min_samples=minimum_samples,
metric='euclidean').fit(ch3_data)
db3_labels = db3.labels_
db3n_clusters_ = len(set(db3_labels)) - (1 if -1 in db3_labels else 0)
labels_ch3 = db3.labels_
ch3_counts = np.bincount(labels_ch3[labels_ch3>=0])

# Cálculo de las áreas de los clusters-----
# ch1
clusters_ch1 = [ch1_data[db1_labels == i] for i in range(db1n_clusters_)]
areas_ch1 = []
for i,item in enumerate(clusters_ch1):
    points = np.array(clusters_ch1[i])
    hull = ConvexHull(points)
    A = hull.points
    B = hull.vertices
    ixgrid = np.ix_(B)
    AA = A[ixgrid]
    areas_ch1.append(Area(AA))

# ch2
clusters_ch2 = [ch2_data[db2_labels == i] for i in range(db2n_clusters_)]
areas_ch2 = []
for i,item in enumerate(clusters_ch2):
    points = np.array(clusters_ch2[i])

```

Figure B.2: Clusters program (page2/4)

Este documento incorpora firma electrónica, y es copia auténtica de un documento electrónico archivado por la ULL según la Ley 39/2015.
 Su autenticidad puede ser contrastada en la siguiente dirección <https://sede.ull.es/validacion/>

Identificador del documento: 1627512

Código de verificación: KOIBgUMu

Firmado por: Roger Gimeno Llobet UNIVERSIDAD DE LA LAGUNA	Fecha: 25/10/2018 11:00:30
Diego Álvarez de la Rosa Rodríguez UNIVERSIDAD DE LA LAGUNA	25/10/2018 11:52:58
Teresa Giráldez Fernández UNIVERSIDAD DE LA LAGUNA	25/10/2018 11:54:04
Ernesto Pereda de Pablo UNIVERSIDAD DE LA LAGUNA	29/10/2018 13:01:03

```

hull = ConvexHull(points)
A = hull.points
B = hull.vertices
ixgrid = np.ix_(B)
AA = A[ixgrid]
areas_ch2.append(Area(AA))

# ch1 ch2
clusters_ch3 = [ch3_data[db3_labels == i] for i in range(db3n_clusters_)]
areas_ch3 = []
for i,item in enumerate(clusters_ch3):
    points = np.array(clusters_ch3[i])
    hull = ConvexHull(points)
    A = hull.points
    B = hull.vertices
    ixgrid = np.ix_(B)
    AA = A[ixgrid]
    areas_ch3.append(Area(AA))

# Nueva identificación de cada cluster por (nº partículas, área)-----
xch1 = ch1_counts
ych1 = areas_ch1
xch2 = ch2_counts
ych2 = areas_ch2
xch3 = ch3_counts
ych3 = areas_ch3

ch1 = []
for combination in itertools.zip_longest(xch1, ych1):
    ch1.append(combination)
ch2 = []
for combination in itertools.zip_longest(xch2, ych2):
    ch2.append(combination)
ch3 = []
for combination in itertools.zip_longest(xch3, ych3):
    ch3.append(combination)

# Eliminar de ch3 (647+488) los clusters que sean identicos en ch1 (647) y ch2 (488)-
# el nuevo ch3 con las substraciones será ch3_new
delete_ch1ch3 = list(set(ch1).intersection(ch3))
delete_ch2ch3 = list(set(ch2).intersection(ch3))

index_elim_ch1ch3 = []
for item in delete_ch1ch3:
    index_elim_ch1ch3.append(ch3.index(item))
for index in sorted(index_elim_ch1ch3, reverse=True):
    del ch3[index]

index_elim_ch2ch3 = []
for item in delete_ch2ch3:
    index_elim_ch2ch3.append(ch3.index(item))
for index in sorted(index_elim_ch2ch3, reverse=True):
    del ch3[index]

# Nuevo ch3 (647+488) que sólo contiene clusters formados por ch1 (647) con ch2 (488)
xch3_new = [x[0] for x in ch3]
ych3_new = [x[1] for x in ch3]
print('Number of clusters in 647 + 488: ', len(ych3_new))

```

Figure B.3: Clusters program (page3/4)

Este documento incorpora firma electrónica, y es copia auténtica de un documento electrónico archivado por la ULL según la Ley 39/2015.
 Su autenticidad puede ser contrastada en la siguiente dirección <https://sede.ull.es/validacion/>

Identificador del documento: 1627512

Código de verificación: kOIBgUMu

Firmado por: Roger Gimeno Llobet UNIVERSIDAD DE LA LAGUNA	Fecha: 25/10/2018 11:00:30
Diego Álvarez de la Rosa Rodríguez UNIVERSIDAD DE LA LAGUNA	25/10/2018 11:52:58
Teresa Giráldez Fernández UNIVERSIDAD DE LA LAGUNA	25/10/2018 11:54:04
Ernesto Pereda de Pablo UNIVERSIDAD DE LA LAGUNA	29/10/2018 13:01:03


```

# Vectores que contienen sólo las áreas
ch1_areas.extend(ych1)
ch2_areas.extend(ych2)
ch3_new_areas.extend(ych3_new)

# Cambiar unidades de las áreas de nm a um y guardar a archivos csv-----
ch1_areas[:] = [x / 1000000 for x in ch1_areas]
ch2_areas[:] = [x / 1000000 for x in ch2_areas]
ch3_new_areas[:] = [x / 1000000 for x in ch3_new_areas]

np.savetxt(archivo+"_areas_647.csv", ch1_areas, delimiter=",")
np.savetxt(archivo+"_areas_488.csv", ch2_areas, delimiter=",")
np.savetxt(archivo+"_areas_647-488.csv", ch3_new_areas, delimiter=",")

# Histograma-----
areas = ch1_areas+ch2_areas+ch3_new_areas

plt.hist(ch1_areas, bins=Bins, fc='red', alpha=0.5, label=label647,
         weights=np.ones_like(ch1_areas) / len(areas))

plt.hist(ch2_areas, bins=Bins, fc='green', alpha=0.5, label=label488,
         weights=np.ones_like(ch2_areas) / len(areas))

plt.hist(ch3_new_areas, bins=Bins, fc='yellow', alpha=0.5, label=label647_488,
         weights=np.ones_like(ch3_new_areas) / len(areas))

formatter = FuncFormatter(lambda y, _: str(y * 100) + '%')
plt.gca().yaxis.set_major_formatter(formatter)
plt.xlabel('Cluster area (µm²)', fontsize=14)
plt.ylabel('Clusters (%)', fontsize=14)
plt.legend()
plt.savefig(archivo'_areas_hist.pdf', bbox_inches='tight')
plt.show()

```

Figure B.4: Clusters program (page4/4)

Este documento incorpora firma electrónica, y es copia auténtica de un documento electrónico archivado por la ULL según la Ley 39/2015.
 Su autenticidad puede ser contrastada en la siguiente dirección <https://sede.ull.es/validacion/>

Identificador del documento: 1627512

Código de verificación: kOIBgUMu

Firmado por: Roger Gimeno Llobet UNIVERSIDAD DE LA LAGUNA	Fecha: 25/10/2018 11:00:30
Diego Álvarez de la Rosa Rodríguez UNIVERSIDAD DE LA LAGUNA	25/10/2018 11:52:58
Teresa Giráldez Fernández UNIVERSIDAD DE LA LAGUNA	25/10/2018 11:54:04
Ernesto Pereda de Pablo UNIVERSIDAD DE LA LAGUNA	29/10/2018 13:01:03



Este documento incorpora firma electrónica, y es copia auténtica de un documento electrónico archivado por la ULL según la Ley 39/2015.
Su autenticidad puede ser contrastada en la siguiente dirección <https://sede.ull.es/validacion/>

Identificador del documento: 1627512

Código de verificación: kOIBgUMu

Firmado por:	Fecha:
Roger Gimeno Llobet UNIVERSIDAD DE LA LAGUNA	25/10/2018 11:00:30
Diego Álvarez de la Rosa Rodríguez UNIVERSIDAD DE LA LAGUNA	25/10/2018 11:52:58
Teresa Giráldez Fernández UNIVERSIDAD DE LA LAGUNA	25/10/2018 11:54:04
Ernesto Pereda de Pablo UNIVERSIDAD DE LA LAGUNA	29/10/2018 13:01:03

Bibliography

- Ahmed, Sohail et al. (2016). "Practical Manual For Fluorescence Microscopy Techniques". In: *PicoQuant GmbH*. URL: https://www.picoquant.com/images/uploads/page/files/17319/4{_}td{_}flim.pdf.
- Ai, Hui Wang (2015). "Fluorescent-protein-based probes: General principles and practices". In: *Analytical and Bioanalytical Chemistry* 407.1, pp. 9–15. ISSN: 16182650. DOI: [10.1007/s00216-014-8236-3](https://doi.org/10.1007/s00216-014-8236-3).
- Akerboom, J. et al. (2012). "Optimization of a GCaMP Calcium Indicator for Neural Activity Imaging". In: *Journal of Neuroscience* 32.40, pp. 13819–13840. ISSN: 0270-6474. DOI: [10.1523/JNEUROSCI.2601-12.2012](https://doi.org/10.1523/JNEUROSCI.2601-12.2012). URL: <http://www.jneurosci.org/cgi/doi/10.1523/JNEUROSCI.2601-12.2012>.
- Akerboom, Jasper et al. (2009). "Crystal structures of the GCaMP calcium sensor reveal the mechanism of fluorescence signal change and aid rational design". In: *Journal of Biological Chemistry* 284.10, pp. 6455–6464. ISSN: 00219258. DOI: [10.1074/jbc.M807657200](https://doi.org/10.1074/jbc.M807657200).
- Ast, Cindy et al. (2017). "Ratiometric Matryoshka biosensors from a nested cassette of green- and orange-emitting fluorescent proteins". In: *Nature Communications* 8.1. ISSN: 20411723. DOI: [10.1038/s41467-017-00400-2](https://doi.org/10.1038/s41467-017-00400-2).
- Augustine, George J., Fidel Santamaria, and Keiko Tanaka (2003). "Local calcium signaling in neurons". In: *Neuron* 40.2, pp. 331–346. ISSN: 08966273. DOI: [10.1016/S0896-6273\(03\)00639-1](https://doi.org/10.1016/S0896-6273(03)00639-1).
- Baird, G. S., D. A. Zacharias, and R. Y. Tsien (1999). "Circular permutation and receptor insertion within green fluorescent proteins". In: *Proceedings of the National Academy of Sciences* 96.20, pp. 11241–11246. ISSN: 0027-8424. DOI: [10.1073/pnas.96.20.11241](https://doi.org/10.1073/pnas.96.20.11241). URL: <http://www.pnas.org/cgi/doi/10.1073/pnas.96.20.11241>.
- Berkefeld, Henrike et al. (2006). "BKCa-Cav channel complexes mediate rapid and localized Ca²⁺-activated K⁺ signaling". In: *Science* 314.5799, pp. 615–620. ISSN: 00368075. DOI: [10.1126/science.1132915](https://doi.org/10.1126/science.1132915).
- Bock, Tobias and Greg J. Stuart (2016). "The Impact of BK Channels on Cellular Excitability Depends on their Subcellular Location". In: *Frontiers in Cellular Neuroscience* 10.August, pp. 1–8. ISSN: 1662-5102. DOI: [10.3389/fncel.2016.00206](https://doi.org/10.3389/fncel.2016.00206). URL: <http://journal.frontiersin.org/Article/10.3389/fncel.2016.00206/abstract>.
- Bose, T, A Cieřlar-Pobuda, and E Wiechec (2015). "Role of ion channels in regulating Ca²⁺ homeostasis during the interplay between immune and cancer cells". In: *Cell Death and Disease* 6.2, e1648. ISSN: 2041-4889. DOI: [10.1038/cddis.2015.23](https://doi.org/10.1038/cddis.2015.23). URL: <http://www.nature.com/doi/10.1038/cddis.2015.23>.
- Brini, M. et al. (1995). *Transfected aequorin in the measurement of cytosolic Ca²⁺ concentration ([Ca²⁺]_i)*. A critical evaluation. DOI: [10.1074/jbc.270.17.9896](https://doi.org/10.1074/jbc.270.17.9896). arXiv: [arXiv:1011.1669v3](https://arxiv.org/abs/1011.1669v3).
- Campbell, Tessa N. and Francis Y.M. Choy (2001). "The effect of pH on Green Fluorescent Protein: a brief review". In: *Molecular Biology Today* 2, pp. 1–4. ISSN: 9781908230331.

Este documento incorpora firma electrónica, y es copia auténtica de un documento electrónico archivado por la ULL según la Ley 39/2015.
Su autenticidad puede ser contrastada en la siguiente dirección <https://sede.ull.es/validacion/>

Identificador del documento: 1627512

Código de verificación: kOIBgUMu

Firmado por: Roger Gimeno Llobet UNIVERSIDAD DE LA LAGUNA	Fecha: 25/10/2018 11:00:30
Diego Álvarez de la Rosa Rodríguez UNIVERSIDAD DE LA LAGUNA	25/10/2018 11:52:58
Teresa Giráldez Fernández UNIVERSIDAD DE LA LAGUNA	25/10/2018 11:54:04
Ernesto Pereda de Pablo UNIVERSIDAD DE LA LAGUNA	29/10/2018 13:01:03

- Carrasquel-Ursulaez, Willy et al. (2015). "Hydrophobic interaction between contiguous residues in the S6 transmembrane segment acts as a stimuli integration node in the BK channel". In: *The Journal of General Physiology* 145.1, pp. 61–74. ISSN: 0022-1295. DOI: [10.1085/jgp.201411194](https://doi.org/10.1085/jgp.201411194). URL: <http://www.jgp.org/lookup/doi/10.1085/jgp.201411194>.
- Chen, Qian et al. (2012). "Imaging Neural Activity Using Thy1-GCaMP Transgenic Mice". In: *Neuron* 76.2, pp. 297–308. ISSN: 08966273. DOI: [10.1016/j.neuron.2012.07.011](https://doi.org/10.1016/j.neuron.2012.07.011). arXiv: NIHMS150003. URL: <http://dx.doi.org/10.1016/j.neuron.2012.07.011>.
- Chen, Tsai-Wen et al. (2013). "Ultrasensitive fluorescent proteins for imaging neuronal activity". In: *Nature* 499.7458, pp. 295–300. ISSN: 0028-0836. DOI: [10.1038/nature12354](https://doi.org/10.1038/nature12354). arXiv: [arXiv: 1011.1669v3](https://arxiv.org/abs/1011.1669v3). URL: <http://www.nature.com/doi/10.1038/nature12354>.
- Clapham, David E. (2007). "Calcium Signaling". In: *Cell* 131.6, pp. 1047–1058. ISSN: 00928674. DOI: [10.1016/j.cell.2007.11.028](https://doi.org/10.1016/j.cell.2007.11.028). arXiv: NIHMS150003.
- Clifford M. Babbey, Nahid Ahktar, Exing Wang, Carlos Chih-Hsiung Chen, Barth D. Grant, Dunn, and Kenneth W. (2006). "Rab10 Regulates Membrane Transport through Early Endosomes of Polarized Madin-Darby Canine Kidney Cells". In: *Molecular Biology of the Cell* 17, pp. 3156–3175. ISSN: 00166731. DOI: [10.1091/mbc.E05](https://doi.org/10.1091/mbc.E05).
- Contet, C et al. (2016). "BK channel in the CNS". In: *Int Rev Neurobiol*, pp. 281–342. DOI: [10.1016/bs.irn.2016.04.001](https://doi.org/10.1016/bs.irn.2016.04.001). BK.
- Contreras, Gustavo F. et al. (2013). "A BK (Slo1) channel journey from molecule to physiology". In: *Channels* 7.6, pp. 442–458. ISSN: 19336950. DOI: [10.4161/chan.26242](https://doi.org/10.4161/chan.26242).
- Cui, J., H. Yang, and U. S. Lee (2009). "Molecular mechanisms of BK channel activation". In: *Cellular and Molecular Life Sciences* 66.5, pp. 852–875. ISSN: 1420682X. DOI: [10.1007/s00018-008-8609-x](https://doi.org/10.1007/s00018-008-8609-x). arXiv: NIHMS150003.
- Cui, Jianmin (2010). "BK-type calcium-activated potassium channels: Coupling of metal ions and voltage sensing". In: *Journal of Physiology* 588.23, pp. 4651–4658. ISSN: 00223751. DOI: [10.1113/jphysiol.2010.194514](https://doi.org/10.1113/jphysiol.2010.194514).
- Dong, Zheng et al. (2006). "Calcium in Cell Injury and Death". In: *Annual Review of Pathology: Mechanisms of Disease* 1.1, pp. 405–434. ISSN: 1553-4006. DOI: [10.1146/annurev.pathol.1.110304.100218](https://doi.org/10.1146/annurev.pathol.1.110304.100218). URL: <http://www.annualreviews.org/doi/10.1146/annurev.pathol.1.110304.100218>.
- Duncan, R. R. et al. (2004). "Multi-dimensional time-correlated single photon counting (TCSPC) fluorescence lifetime imaging microscopy (FLIM) to detect FRET in cells". In: *Journal of Microscopy* 215.1, pp. 1–12. ISSN: 00222720. DOI: [10.1111/j.0022-2720.2004.01343.x](https://doi.org/10.1111/j.0022-2720.2004.01343.x).
- Eggermann, Emmanuel et al. (2012). "Nanodomain coupling between Ca²⁺ channels and sensors of exocytosis at fast mammalian synapses". In: *Nature Reviews Neuroscience* 13.1, pp. 7–21. ISSN: 1471003X. DOI: [10.1038/nrn3125](https://doi.org/10.1038/nrn3125). arXiv: NIHMS150003.
- Engbers, Jordan D. T. et al. (2013). "Signal processing by T-type calcium channel interactions in the cerebellum". In: *Frontiers in Cellular Neuroscience* 7. November, pp. 1–15. ISSN: 1662-5102. DOI: [10.3389/fncel.2013.00230](https://doi.org/10.3389/fncel.2013.00230). URL: <http://journal.frontiersin.org/article/10.3389/fncel.2013.00230/abstract>.
- Erdahl, Warren L. et al. (1994). "Ca²⁺ Transport Properties of Ionophores A23187, lonomycin, and 4-BrA23187 in a Well Defined Model System". In: *Biophysical Journal* 66. May, pp. 1678–1693. ISSN: 00063495. DOI: [10.1016/S0006-3495\(94\)80959-2](https://doi.org/10.1016/S0006-3495(94)80959-2).

Este documento incorpora firma electrónica, y es copia auténtica de un documento electrónico archivado por la ULL según la Ley 39/2015.
 Su autenticidad puede ser contrastada en la siguiente dirección <https://sede.ull.es/validacion/>

Identificador del documento: 1627512

Código de verificación: kOIBgUMu

Firmado por:	Fecha:
Roger Gimeno Llobet UNIVERSIDAD DE LA LAGUNA	25/10/2018 11:00:30
Diego Álvarez de la Rosa Rodríguez UNIVERSIDAD DE LA LAGUNA	25/10/2018 11:52:58
Teresa Giráldez Fernández UNIVERSIDAD DE LA LAGUNA	25/10/2018 11:54:04
Ernesto Pereda de Pablo UNIVERSIDAD DE LA LAGUNA	29/10/2018 13:01:03

- Fakler, Bernd and John P. Adelman (2008). "Control of KCa Channels by Calcium Nano/Microdomains". In: *Neuron* 59.6, pp. 873–881. ISSN: 08966273. DOI: 10.1016/j.neuron.2008.09.001.
- Frommer, Wolf B., Michael W. Davidson, and Robert E. Campbell (2009). "Genetically encoded biosensors based on engineered fluorescent proteins". In: *Chemical Society Reviews* 38.10, pp. 2833–2841. ISSN: 03060012. DOI: 10.1039/b907749a.
- Fujiwara, Masanobu and William Cieslik (2006). "Fluorescence Lifetime Imaging Microscopy: Two-Dimensional Distribution Measurement of Fluorescence Lifetime". In: *Methods in Enzymology* 414.06, pp. 633–642. ISSN: 00766879. DOI: 10.1016/S0076-6879(06)14033-1.
- Giraldez, Teresa, Thomas E Hughes, and Fred J Sigworth (2005). "Generation of Functional Fluorescent BK Channels by Random Insertion of GFP Variants". In: *The Journal of General Physiology* 126.5, pp. 429–438. ISSN: 0022-1295. DOI: 10.1085/jgp.200509368. URL: <http://www.jgp.org/cgi/doi/10.1085/jgp.200509368><http://www.jgp.org/lookup/doi/10.1085/jgp.200509368>.
- Giraldez, Teresa and Brad S. Rothberg (2017). "Understanding the conformational motions of RCK gating rings". In: *The Journal of General Physiology* 149.4, pp. 431–441. ISSN: 0022-1295. DOI: 10.1085/jgp.201611726. URL: <http://www.jgp.org/lookup/doi/10.1085/jgp.201611726>.
- Gleichmann, Marc and Mark P. Mattson (2011). "Neuronal Calcium Homeostasis and Dysregulation". In: *Antioxidants & Redox Signaling* 14.7, pp. 1261–1273. ISSN: 1523-0864. DOI: 10.1089/ars.2010.3386. URL: <http://www.liebertonline.com/doi/abs/10.1089/ars.2010.3386>.
- Grienberger, Christine and Arthur Konnerth (2012). "Imaging Calcium in Neurons". In: *Neuron* 73.5, pp. 862–885. ISSN: 08966273. DOI: 10.1016/j.neuron.2012.02.011. URL: <http://dx.doi.org/10.1016/j.neuron.2012.02.011>.
- Gutiérrez, Andrés A. et al. (1999). "Activation of a Ca²⁺-permeable cation channel by two different inducers of apoptosis in a human prostatic cancer cell line". In: *The Journal of Physiology* 517.1, pp. 95–107. ISSN: 00223751. DOI: 10.1111/j.1469-7793.1999.0095z.x. URL: <http://doi.wiley.com/10.1111/j.1469-7793.1999.0095z.x>.
- Hirono, M. et al. (2015). "BK Channels Localize to the Paranodal Junction and Regulate Action Potentials in Myelinated Axons of Cerebellar Purkinje Cells". In: *Journal of Neuroscience* 35.18, pp. 7082–7094. ISSN: 0270-6474. DOI: 10.1523/JNEUROSCI.3778-14.2015. URL: <http://www.jneurosci.org/cgi/doi/10.1523/JNEUROSCI.3778-14.2015>.
- Hite, Richard K., Xiao Tao, and Roderick MacKinnon (2017). "Structural basis for gating the high conductance Ca²⁺-activated K⁺ channel". In: *Nature* 541.7635, pp. 52–57. ISSN: 2045-2322. DOI: 10.1016/j.semcan.2015.04.010. Targeting. arXiv: 15334406.
- Hogan, Patrick G. and Anjana Rao (2015). "Store-operated calcium entry: Mechanisms and modulation". In: *Biochemical and Biophysical Research Communications* 460.1, pp. 40–49. ISSN: 10902104. DOI: 10.1016/j.bbrc.2015.02.110. URL: <http://dx.doi.org/10.1016/j.bbrc.2015.02.110>.
- Horrigan, Frank T and Richard W Aldrich (2002). "Coupling between voltage sensor activation, Ca²⁺ binding and channel opening in large conductance (BK) potassium channels." In: *The Journal of general physiology* 120.3, pp. 267–305. ISSN: 0022-1295. DOI: 10.1085/jgp.20028605. URL: <http://www.ncbi.nlm.nih.gov/pubmed/12198087><http://www.pubmedcentral.nih.gov/articlerender.fcgi?artid=PMC2229516>.

Este documento incorpora firma electrónica, y es copia auténtica de un documento electrónico archivado por la ULL según la Ley 39/2015.
 Su autenticidad puede ser contrastada en la siguiente dirección <https://sede.ull.es/validacion/>

Identificador del documento: 1627512

Código de verificación: kOIBgUMu

Firmado por:	Fecha:
Roger Gimeno Llobet UNIVERSIDAD DE LA LAGUNA	25/10/2018 11:00:30
Diego Álvarez de la Rosa Rodríguez UNIVERSIDAD DE LA LAGUNA	25/10/2018 11:52:58
Teresa Giráldez Fernández UNIVERSIDAD DE LA LAGUNA	25/10/2018 11:54:04
Ernesto Pereda de Pablo UNIVERSIDAD DE LA LAGUNA	29/10/2018 13:01:03

- Javaherian, Anoosh D. et al. (2011). "Metal-driven operation of the human large-conductance voltage- and Ca²⁺-dependent potassium channel (BK) gating ring apparatus". In: *Journal of Biological Chemistry* 286.23, pp. 20701–20709. ISSN: 00219258. DOI: 10.1074/jbc.M111.235234.
- Jensen, Ellen and David J. Crossman (2014). "Technical review: Types of imaging-direct STORM". In: *Anatomical Record* 297.12, pp. 2227–2231. ISSN: 19328494. DOI: 10.1002/ar.22960.
- Jiang, Tianyu, Lupei Du, and Minyong Li (2016). "Lighting up bioluminescence with coelenterazine: Strategies and applications". In: *Photochemical and Photobiological Sciences* 15.4, pp. 466–480. ISSN: 14749092. DOI: 10.1039/c5pp00456j.
- Kenneth W. Dunn, Malgorzata M. Kamocka and John H. McDonald (2011). "A practical guide to evaluating colocalization in biological microscopy Kenneth". In: *Am J Physiol Cell Physiol* 300: 300.314, pp. C723–C742. ISSN: 0363-6143. DOI: 10.1152/ajpcell.00462.2010..
- Kshatri, Aravind S., Alberto Gonzalez-Hernandez, and Teresa Giraldez (2018). "Physiological Roles and Therapeutic Potential of Ca²⁺ Activated Potassium Channels in the Nervous System". In: *Frontiers in Molecular Neuroscience* 11.July, pp. 1–18. ISSN: 1662-5099. DOI: 10.3389/fnmol.2018.00258. URL: <https://www.frontiersin.org/article/10.3389/fnmol.2018.00258/full>.
- Kulik, Ákos et al. (2004). "Immunocytochemical localization of the $\alpha 1A$ subunit of the P/Q-type calcium channel in the rat cerebellum". In: *Eur J Neurosci* 19.February, pp. 2169–2178. DOI: 10.1111/j.1460-9568.2004.03319.x. URL: http://www.ncbi.nlm.nih.gov/entrez/query.fcgi?cmd=Retrieve&db=PubMed&dopt=Citation&list_uids=15090043.
- Lakowicz, Joseph R. (2011). *Principles of Fluorescence Spectroscopy*. ISBN: 3540236988. DOI: 10.1007/b102213.
- Latorre, Ramon and Christopher Miller (1983). "Conduction and selectivity in potassium channels". In: *The Journal of Membrane Biology* 71.1-2, pp. 11–30. ISSN: 00222631. DOI: 10.1007/BF01870671.
- Latorre, Ramon et al. (2017). "Molecular Determinants of BK Channel Functional Diversity and Functioning". In: *Physiological Reviews* 97.1, pp. 39–87. ISSN: 0031-9333. DOI: 10.1152/physrev.00001.2016. URL: <http://physrev.physiology.org/lookup/doi/10.1152/physrev.00001.2016>.
- Liang, Xiquan et al. (2012). "A method for multi-site-directed mutagenesis based on homologous recombination". In: *Analytical Biochemistry* 427.1, pp. 99–101. ISSN: 00032697. DOI: 10.1016/j.ab.2012.05.002.
- Lin, Michael Z. and Mark J. Schnitzer (2016). "Genetically encoded indicators of neuronal activity". In: *Nature Neuroscience* 19.9, pp. 1142–1153. ISSN: 15461726. DOI: 10.1038/nn.4359.
- Marrion, N V and S J Tavalin (1998). "Selective activation of Ca²⁺-activated K⁺ channels by co-localized Ca²⁺ channels in hippocampal neurons." In: *Nature* 395.6705, pp. 900–905. ISSN: 0028-0836. DOI: 10.1038/27674. URL: <http://eutils.ncbi.nlm.nih.gov/entrez/eutils/efetch.fcgi?dbfrom=pubmed&id=9804423&retmode=ref&cmd=prlinks&http://www.nature.com/nature/journal/v395/n6705/pdf/395900a0.pdf>.
- Mayerhofer, a et al. (1992). "Carbachol increases intracellular free calcium concentrations in human granulosa-lutein cells". In: *J Endocrinol* 135.1, pp. 153–159. ISSN: 0022-0795.
- Miranda, Pablo, Teresa Giraldez, and Miguel Holmgren (2016). "Interactions of divalent cations with calcium binding sites of BK channels reveal independent motions within the gating ring". In: *Proceedings of the National Academy of Sciences*

Este documento incorpora firma electrónica, y es copia auténtica de un documento electrónico archivado por la ULL según la Ley 39/2015.
 Su autenticidad puede ser contrastada en la siguiente dirección <https://sede.ull.es/validacion/>

Identificador del documento: 1627512

Código de verificación: kOIBgUMU

Firmado por:	Fecha:
Roger Gimeno Llobet UNIVERSIDAD DE LA LAGUNA	25/10/2018 11:00:30
Diego Álvarez de la Rosa Rodríguez UNIVERSIDAD DE LA LAGUNA	25/10/2018 11:52:58
Teresa Giráldez Fernández UNIVERSIDAD DE LA LAGUNA	25/10/2018 11:54:04
Ernesto Pereda de Pablo UNIVERSIDAD DE LA LAGUNA	29/10/2018 13:01:03

- 113.49, pp. 14055–14060. ISSN: 0027-8424. DOI: [10.1073/pnas.1611415113](https://doi.org/10.1073/pnas.1611415113). URL: <http://www.pnas.org/lookup/doi/10.1073/pnas.1611415113>.
- Miranda, Pablo et al. (2013). "State-dependent FRET reports calcium- and voltage-dependent gating-ring motions in BK channels." In: *Proceedings of the National Academy of Sciences of the United States of America* 110.13, pp. 5217–22. ISSN: 1091-6490. DOI: [10.1073/pnas.1219611110](https://doi.org/10.1073/pnas.1219611110). URL: <http://www.pnas.org/content/110/13/5217>.
- Miyawaki, a et al. (1997). "Fluorescent indicators for Ca²⁺ based on green fluorescent proteins and calmodulin." In: *Nature* 388.6645, pp. 882–887. ISSN: 0028-0836. DOI: [10.1038/42264](https://doi.org/10.1038/42264).
- Mountjoy, Kathleen G et al. (2001). "Melanocortin receptor-mediated mobilization of intracellular free calcium in HEK293 cells." In: *Physiological genomics* 5.1, pp. 11–9. ISSN: 1531-2267. DOI: [5/1/11\[pii\]](https://doi.org/10.1159/000011111). URL: <http://www.ncbi.nlm.nih.gov/pubmed/11161002>.
- Müller, Margit S. et al. (2013). "Complex actions of ionomycin in cultured cerebellar astrocytes affecting both calcium-induced calcium release and store-operated calcium entry". In: *Neurochemical Research* 38.6, pp. 1260–1265. ISSN: 03643190. DOI: [10.1007/s11064-013-1021-4](https://doi.org/10.1007/s11064-013-1021-4).
- Nadler, Dana C. et al. (2016). "Rapid construction of metabolite biosensors using domain-insertion profiling". In: *Nature Communications* 7, pp. 1–11. ISSN: 20411723. DOI: [10.1038/ncomms12266](https://doi.org/10.1038/ncomms12266). URL: <http://dx.doi.org/10.1038/ncomms12266>.
- Nagai, T. et al. (2001). "Circularly permuted green fluorescent proteins engineered to sense Ca²⁺". In: *Proceedings of the National Academy of Sciences* 98.6, pp. 3197–3202. ISSN: 0027-8424. DOI: [10.1073/pnas.051636098](https://doi.org/10.1073/pnas.051636098). URL: <http://www.pnas.org/cgi/doi/10.1073/pnas.051636098>.
- Nahidiazar, Leila et al. (2016). "Optimizing imaging conditions for demanding multi-color super resolution localization microscopy". In: *PLoS ONE* 11.7, pp. 1–18. ISSN: 19326203. DOI: [10.1371/journal.pone.0158884](https://doi.org/10.1371/journal.pone.0158884).
- Nakai, J, M Ohkura, and K Imoto (2001). "A high signal-to-noise Ca(2+) probe composed of a single green fluorescent protein." In: *Nature biotechnology* 19.2, pp. 137–41. ISSN: 1087-0156. DOI: [10.1038/84397](https://doi.org/10.1038/84397). URL: <http://www.ncbi.nlm.nih.gov/pubmed/11175727>.
- Neher, Erwin (1998). "Vesicle Pools and Ca²⁺ Microdomains: New Tools for Understanding Their Roles in Neurotransmitter Release". In: *Neuron* 20.3, pp. 389–399. ISSN: 08966273. DOI: [10.1016/S0896-6273\(00\)80983-6](https://doi.org/10.1016/S0896-6273(00)80983-6). URL: <http://linkinghub.elsevier.com/retrieve/pii/S0896627300809836>.
- Obermair, Gerald J et al. (2004). "Differential targeting of the L-type Ca²⁺ channel α_1 ". In: *Neuroscience* 19. December 2003. DOI: [10.1111/j.1460-9568.2004.03272.x](https://doi.org/10.1111/j.1460-9568.2004.03272.x).
- Ohkura, Masamichi et al. (2005). "Genetically encoded bright Ca²⁺ probe applicable for dynamic Ca²⁺ imaging of dendritic spines". In: *Analytical Chemistry* 77.18, pp. 5861–5869. ISSN: 00032700. DOI: [10.1021/ac0506837](https://doi.org/10.1021/ac0506837).
- Patterson, George H., David W. Piston, and B. George Barisas (2000). "Forster distances between green fluorescent protein pairs". In: *Analytical Biochemistry* 284.2, pp. 438–440. ISSN: 00032697. DOI: [10.1006/abio.2000.4708](https://doi.org/10.1006/abio.2000.4708).
- Prakriya, M and C J Lingle (1999). "BK channel activation by brief depolarizations requires Ca²⁺ influx through L- and Q-type Ca²⁺ channels in rat chromaffin cells." In: *Journal of Neurophysiology* 81.5, pp. 2267–2278. ISSN: 0022-3077. DOI: [10.1038/367072a0](https://doi.org/10.1038/367072a0). URL: <http://eutils.ncbi.nlm.nih.gov/entrez/eutils/elink.fcgi?dbfrom=pubmed{\&}id=10322065{\&}retmode=ref{\&}cmd=prlinks{\&}5Cnhttp://jn.physiology.org/content/jn/81/5/2267.full.pdf>.

Este documento incorpora firma electrónica, y es copia auténtica de un documento electrónico archivado por la ULL según la Ley 39/2015.
 Su autenticidad puede ser contrastada en la siguiente dirección <https://sede.ull.es/validacion/>

Identificador del documento: 1627512

Código de verificación: KOIBgUMu

Firmado por:	Fecha:
Roger Gimeno Llobet UNIVERSIDAD DE LA LAGUNA	25/10/2018 11:00:30
Diego Álvarez de la Rosa Rodríguez UNIVERSIDAD DE LA LAGUNA	25/10/2018 11:52:58
Teresa Giráldez Fernández UNIVERSIDAD DE LA LAGUNA	25/10/2018 11:54:04
Ernesto Pereda de Pablo UNIVERSIDAD DE LA LAGUNA	29/10/2018 13:01:03

- Rose, Tobias et al. (2014). "Putting a finishing touch on GECIs". In: *Frontiers in Molecular Neuroscience* 7.November, pp. 1–15. ISSN: 1662-5099. DOI: 10.3389/fnmol.2014.00088. URL: <http://journal.frontiersin.org/article/10.3389/fnmol.2014.00088/abstract>.
- Schreiber, Matthew and Lawrence Salkoff (1997). "A novel calcium-sensing domain in the BK channel". In: *Biophysical Journal* 73.3, pp. 1355–1363. ISSN: 00063495. DOI: 10.1016/S0006-3495(97)78168-2. URL: <http://www.ncbi.nlm.nih.gov/pubmed/9284303><http://www.pubmedcentral.nih.gov/articlerender.fcgi?artid=PMC1181035>.
- Schreiber, Matthew, Alex Yuan, and Lawrence Salkoff (1999). "Transplantable sites confer calcium sensitivity to BK channels". In: *Nature Neuroscience* 2.5, pp. 416–421. ISSN: 10976256. DOI: 10.1038/8077.
- Shigetomi, Eiji, Sebastian Kracun, and Baljit S. Khakh (2010). "Monitoring astrocyte calcium microdomains with improved membrane targeted GCaMP reporters". In: *Neuron Glia Biology* 6.03, pp. 183–191. ISSN: 1740-925X. DOI: 10.1017/S1740925X10000219. URL: http://www.journals.cambridge.org/abstract/_S1740925X10000219.
- Shigetomi, Eiji, Sandip Patel, and Baljit S. Khakh (2016). "Probing the Complexities of Astrocyte Calcium Signaling". In: *Trends in Cell Biology* 26.4, pp. 300–312. ISSN: 18793088. DOI: 10.1016/j.tcb.2016.01.003. arXiv: 15334406. URL: <http://dx.doi.org/10.1016/j.tcb.2016.01.003>.
- Shigetomi, Eiji et al. (2010). "A genetically targeted optical sensor to monitor calcium signals in astrocyte processes". In: *Nature Neuroscience* 13.6, pp. 759–766. ISSN: 10976256. DOI: 10.1038/nn.2557. arXiv: NIHMS150003. URL: <http://dx.doi.org/10.1038/nn.2557>.
- Shimomura, Osamu, Frank H. Johnson, and Yo Saiga (1962). "Extraction, Purification and Properties of Aequorin, a Bioluminescent Protein from the Luminous Hydromedusa, Aequorea". In: *Journal of Cellular and Comparative Physiology* 59.3, pp. 223–239. ISSN: 0095-9898. DOI: 10.1002/jcp.1030590302. URL: <http://doi.wiley.com/10.1002/jcp.1030590302>.
- Staruschenko, Alexander et al. (2004). "Fluorescence resonance energy transfer analysis of subunit stoichiometry of the epithelial Na⁺ channel." In: *The Journal of biological chemistry* 279.26, pp. 27729–34. ISSN: 0021-9258. DOI: 10.1074/jbc.M404169200. URL: <http://www.ncbi.nlm.nih.gov/pubmed/15096495>.
- Stryer, L (1978). "Fluorescence Energy Transfer as a Spectroscopic Ruler". In: *Annual Review of Biochemistry* 47.1, pp. 819–846. ISSN: 0066-4154. DOI: 10.1146/annurev.bi.47.070178.004131. arXiv: arXiv:1011.1669v3. URL: <http://www.annualreviews.org/doi/10.1146/annurev.bi.47.070178.004131>.
- Sun, Xiaolu, Xiang Q Gu, and Gabriel G Haddad (2003). "Calcium influx via L- and N-type calcium channels activates a transient large-conductance Ca²⁺-activated K⁺ current in mouse neocortical pyramidal neurons." In: *Journal of Neuroscience* 23.9, pp. 3639–3648. ISSN: 1529-2401. URL: <http://eutils.ncbi.nlm.nih.gov/entrez/eutils/elink.fcgi?dbfrom=pubmed{\&}id=12736335{\&}retmode=ref{\&}cmd=prlinks{\%}5Cnhttp://www.jneurosci.org/content/23/9/3639.full.pdf>.
- Sutherland, D J, Z Pujic, and G J Goodhill (2014). "Calcium signaling in axon guidance". In: *Trends in neurosciences* 37.8, pp. 424–432. ISSN: 1878-108X; 0166-2236. DOI: 10.1016/j.tins.2014.05.008; 10.1016/j.tins.2014.05.008.
- Sutherland, M L et al. (1999). "Overexpression of a Shaker-type potassium channel in mammalian central nervous system dysregulates native potassium channel gene expression." In: *Proceedings of the National Academy of Sciences of the United States of America* 96.5, pp. 2451–5. ISSN: 0027-8424. DOI: 10.1073/pnas.96.5.2451. URL:

Este documento incorpora firma electrónica, y es copia auténtica de un documento electrónico archivado por la ULL según la Ley 39/2015.
 Su autenticidad puede ser contrastada en la siguiente dirección <https://sede.ull.es/validacion/>

Identificador del documento: 1627512

Código de verificación: KOIBgUMU

Firmado por:	Fecha:
Roger Gimeno Llobet UNIVERSIDAD DE LA LAGUNA	25/10/2018 11:00:30
Diego Álvarez de la Rosa Rodríguez UNIVERSIDAD DE LA LAGUNA	25/10/2018 11:52:58
Teresa Giráldez Fernández UNIVERSIDAD DE LA LAGUNA	25/10/2018 11:54:04
Ernesto Pereda de Pablo UNIVERSIDAD DE LA LAGUNA	29/10/2018 13:01:03

- <http://www.pubmedcentral.nih.gov/articlerender.fcgi?artid=26805&tool=pmcentrez&rendertype=abstract>.
- Tadross, M. R., R. W. Tsien, and D. T. Yue (2013). "Ca²⁺ channel nanodomains boost local Ca²⁺ amplitude". In: *Proceedings of the National Academy of Sciences* 110.39, pp. 15794–15799. ISSN: 0027-8424. DOI: 10.1073/pnas.1313898110. URL: <http://www.pnas.org/cgi/doi/10.1073/pnas.1313898110>.
- Tallini, Y. N. et al. (2006). "Imaging cellular signals in the heart in vivo: Cardiac expression of the high-signal Ca²⁺ indicator GCaMP2". In: *Proceedings of the National Academy of Sciences* 103.12, pp. 4753–4758. ISSN: 0027-8424. DOI: 10.1073/pnas.0509378103. URL: <http://www.pnas.org/cgi/doi/10.1073/pnas.0509378103>.
- Tian, Lin et al. (2009). "Imaging neural activity in worms, flies and mice with improved GCaMP calcium indicators". In: *Nature Methods* 6.12, pp. 875–881. ISSN: 1548-7091. DOI: 10.1038/nmeth.1398. URL: <http://www.nature.com/doi/10.1038/nmeth.1398>.
- Tramier, Marc et al. (2002). "Picosecond-hetero-FRET microscopy to probe protein-protein interactions in live cells". In: *Biophysical Journal* 83.6, pp. 3570–3577. ISSN: 00063495. DOI: 10.1016/S0006-3495(02)75357-5.
- Tsien, Roger Y (1980). "New Calcium Indicators and Buffers with High Selectivity against Magnesium and Protons: Design, Synthesis, and Properties of Prototype Structures". In: *Biochemistry* 19.1966, pp. 2396–2404.
- (1998). "the Green Fluorescent". In: *Proteins* 67.11, pp. 509–44. ISSN: 00664154. DOI: 10.1146/annurev.biochem.67.1.509. URL: <http://www.ncbi.nlm.nih.gov/pubmed/9759496>.
- Vivas, Oscar et al. (2017). "Proximal clustering between BK and Ca V 1.3 channels promotes functional coupling and BK channel activation at low voltage". In: *eLife* 6, pp. 1–18. ISSN: 2050-084X. DOI: 10.7554/eLife.28029. URL: <http://elifesciences.org/lookup/doi/10.7554/eLife.28029>.
- Wang, Bin and Robert Brenner (2006). "An S6 Mutation in BK Channels Reveals β 1 Subunit Effects on Intrinsic and Voltage-dependent Gating". In: *The Journal of General Physiology* 128.6, pp. 731–744. ISSN: 0022-1295. DOI: 10.1085/jgp.200609596. URL: <http://www.jgp.org/lookup/doi/10.1085/jgp.200609596>.
- Wang, Lu-Yang and George J. Augustine (2015). "Presynaptic nanodomains: a tale of two synapses". In: *Frontiers in Cellular Neuroscience* 8.January, pp. 1–10. ISSN: 1662-5102. DOI: 10.3389/fncel.2014.00455. URL: <http://journal.frontiersin.org/article/10.3389/fncel.2014.00455/abstract>.
- Webb, Sarah E., Eric Karplus, and Andrew L. Miller (2015). "Retrospective on the development of aequorin and aequorin-based imaging to visualize changes in intracellular free [Ca²⁺]"'. In: *Molecular Reproduction and Development* 82.7-8, pp. 563–586. ISSN: 10982795. DOI: 10.1002/mrd.22298.
- Webb, Sarah E. and Andrew L. Miller (2012). "Aequorin-based genetic approaches to visualize Ca²⁺ signaling in developing animal systems". In: *Biochimica et Biophysica Acta - General Subjects* 1820.8, pp. 1160–1168. ISSN: 03044165. DOI: 10.1016/j.bbagen.2011.12.008. URL: <http://dx.doi.org/10.1016/j.bbagen.2011.12.008>.
- Whitaker, Michael (2010). "Genetically-encoded probes for measurement of intracellular calcium". In: *Methods in cell biology* 99, pp. 153–182. ISSN: 0091-679X. DOI: 10.1016/B978-0-12-374841-6.00006-2. Genetically-encoded.
- Whitt, Joshua P, Beth A McNally, and Andrea L Meredith (2017). "Differential contribution of Ca²⁺ sources to day and night BK current activation in the circadian clock." In: *The Journal of general physiology*, jgp.201711945. ISSN: 1540-7748. DOI:

Este documento incorpora firma electrónica, y es copia auténtica de un documento electrónico archivado por la ULL según la Ley 39/2015.
 Su autenticidad puede ser contrastada en la siguiente dirección <https://sede.ull.es/validacion/>

Identificador del documento: 1627512

Código de verificación: KOIBgUMu

Firmado por:	Fecha:
Roger Gimeno Llobet UNIVERSIDAD DE LA LAGUNA	25/10/2018 11:00:30
Diego Álvarez de la Rosa Rodríguez UNIVERSIDAD DE LA LAGUNA	25/10/2018 11:52:58
Teresa Giráldez Fernández UNIVERSIDAD DE LA LAGUNA	25/10/2018 11:54:04
Ernesto Pereda de Pablo UNIVERSIDAD DE LA LAGUNA	29/10/2018 13:01:03

- 10.1085/jgp.201711945. URL: <http://www.ncbi.nlm.nih.gov/pubmed/29237755>
<http://jgp.rupress.org/content/early/2017/12/12/jgp.201711945>.
- Wu, L G et al. (1999). "Calcium channel types with distinct presynaptic localization couple differentially to transmitter release in single calyx-type synapses." In: *The Journal of neuroscience : the official journal of the Society for Neuroscience* 19.2, pp. 726–736. ISSN: 0270-6474. DOI: 1999/01/0900:01.
- Wu, Ying et al. (2009). "Intersubunit coupling in the pore of BK channels". In: *Journal of Biological Chemistry* 284.35, pp. 23353–23363. ISSN: 00219258. DOI: 10.1074/jbc.M109.027789.
- Wu, Yunkun et al. (2010). "Structure of the gating ring from the human large-conductance Ca(2+)-gated K(+) channel." In: *Nature* 466.7304, pp. 393–7. ISSN: 1476-4687. DOI: 10.1038/nature09252. URL: <http://www.pubmedcentral.nih.gov/articlerender.fcgi?artid=2910425&tool=pmcentrez&rendertype=abstract>.
- Xia, Xiao-Ming, Xuhui Zeng, and Christopher J Lingle (2002). "Multiple regulatory sites in large-conductance calcium-activated potassium channels." In: *Nature* 418.6900, pp. 880–4. ISSN: 0028-0836. DOI: 10.1038/nature00956. URL: <http://www.ncbi.nlm.nih.gov/pubmed/12192411>.
- Xiao Tao, Richard K. Hite, and Roderick MacKinnon (2017). "Cryo-EM structure of the open high conductance Ca²⁺-activated K⁺ channel". In: *Nature* 541.7635, pp. 46–51. DOI: 10.1016/j.cogdev.2010.08.003. Personal.
- Zhang, Guohui et al. (2010). "Ion sensing in the RCK1 domain of BK channels." In: *Proceedings of the National Academy of Sciences of the United States of America* 107.43, pp. 18700–5. ISSN: 1091-6490. DOI: 10.1073/pnas.1010124107. URL: <http://www.ncbi.nlm.nih.gov/pubmed/20937866>
<http://www.pubmedcentral.nih.gov/articlerender.fcgi?artid=PMC2972974>.
- Zhang, Jie et al. (2016). "Clustering and Functional Coupling of Diverse Ion Channels and Signaling Proteins Revealed by Super-resolution STORM Microscopy in Neurons". In: *Neuron*. DOI: 10.1016/j.neuron.2016.09.014.
- Zhang, Jiyuan et al. (2018). "Glutamate-activated BK channel complexes formed with NMDA receptors". In: *Proceedings of the National Academy of Sciences*, p. 201802567. ISSN: 0027-8424. DOI: 10.1073/pnas.1802567115. URL: <http://www.pnas.org/lookup/doi/10.1073/pnas.1802567115>.

Este documento incorpora firma electrónica, y es copia auténtica de un documento electrónico archivado por la ULL según la Ley 39/2015.
Su autenticidad puede ser contrastada en la siguiente dirección <https://sede.ull.es/validacion/>

Identificador del documento: 1627512

Código de verificación: kOIBgUMU

Firmado por:	Fecha:
Roger Gimeno Llobet UNIVERSIDAD DE LA LAGUNA	25/10/2018 11:00:30
Diego Álvarez de la Rosa Rodríguez UNIVERSIDAD DE LA LAGUNA	25/10/2018 11:52:58
Teresa Giráldez Fernández UNIVERSIDAD DE LA LAGUNA	25/10/2018 11:54:04
Ernesto Pereda de Pablo UNIVERSIDAD DE LA LAGUNA	29/10/2018 13:01:03